UNIVERSIDAD DE CHILE
FACULTAD DE CIENCIAS FISICAS Y MATEMATICAS
DEPARTAMENTO DE INGENIERÍA DE MINAS

SEISMIC PARAMETERS OF SPACE – TIME CLUSTERED MINING – INDUCED AFTERSHOCK SEQUENCES APPLIED TO SEISMIC HAZARD IN MINING

TESIS PARA OPTAR AL GRADO DE
DOCTOR EN INGENIERÍA DE MINAS

RODRIGO ANDRÉS ESTAY HUIDOBRO

PROFESOR GUIA:
JAVIER VALLEJOS MASSA

MIEMBROS DE LA COMISION:
CESAR PARDO MELLA
DENISSE PASTÉN GUZMÁN
BRIAN TOWNLEY CALLEJAS

SANTIAGO DE CHILE
2018

RESUMEN DE LA TESIS PARA OPTAR AL GRADO DE
Doctor en Ingeniería de Minas
POR: Rodrigo Andrés Estay Huidobro
FECHA: Octubre, 2018
PROF. GUÍA: Javier Vallejos Massa.

Resumen

Una característica común en la minería que se realiza en roca competetente es la sismicidad inducida. Esta es resultado de los cambios en los esfuerzos y el fallamiento de la roca alrededor de las excavaciones mineras. Posterior a un evento sísmico, existe un aumento en los niveles de sismicidad que gradualmente decaen con el tiempo, conocido como una secuencia de réplicas. Restringir el acceso a las áreas de la mina por el tiempo suficiente que permita que ocurra este decaimiento de los eventos sísmicos es el enfoque principal de los protocolos de re – entrada.

Las propiedades estadísticas de las secuencias de réplicas pueden ser estudiadas mediante tres relaciones o leyes sísmicas: (1) Ley de Gutenberg – Richter, (2) Ley de Omori Modificada (MOL) para el decaimiento temporal de la sismicidad, y (3) Ley de Båth para la magnitud de la réplica de mayor magnitud.

Esta tesis contiene tres partes principales: estimación y correlaciones de los parámetros de las leyes sísmicas para secuencias de réplicas inducidas por la minería, desarrollo de protocolos de re – entrada en el espacio – tiempo – magnitud y el reconocimiento y comportamiento temporal de secuencias de réplicas usando un aglomeramiento espacio – tiempo.

En la primera parte, se aplicaron las tres leyes sísmicas, además del modelo estocástico de Reasenberg – Jones, para estudiar los parámetros de 11 secuencias sísmicas inducidas por la minería en cuatro minas en Ontario, Canadá. Para proporcionar directrices para el desarrollo del protocolo de re – entrada, se estudió y aplicó la dependencia de esto parámetros con la magnitud del evento sísmico principal de la secuencia sísmica.

Los resultados obtenidos son coincidentes con los que diferentes autores han estimado en sismicidad tectónica. Sin embargo, aparecen algunas "diferencias de escala", especialmente con el valor *b* de Gutenberg – Richter y el valor *p* de la ley modificada de Omori, encontrando que, en promedio, hay diferencias de +0.35 y -0.2 respectivamente entre los resultados de la sismicidad inducida y tectónica.

La segunda parte corresponde al desarrollo de un protocolo estocástico de re –entrada en el espacio – tiempo – magnitud, utilizando las relaciones entre los parámetros sísmicos inducidos y la magnitud del evento principal. Se define un radio de exclusión y una relación entre el tiempo de máxima curvatura y la magnitud del evento principal. Esto permite construir curvas de decaimiento sísmico, proporcionando información sobre los patrones de decaimiento de una secuencia en curso. Finalmente, se propone un rango de probabilidad de ocurrencia de la réplica de mayor magnitud, basado en el modelo de probabilidad de Reasenberg – Jones.

La última parte consiste en analizar el comportamiento del agrupamiento de la sismicidad inducida por la minería a través del tiempo y el espacio. Usando el criterio estadístico de Akaike para seleccionar los parámetros del aglomeramiento espacio – tiempo, fue posible identificar una secuencia de réplicas asociada a un evento principal con magnitud $Mw = 0.7$. Además, se encontró que la distancia espacio – tiempo aparentemente disminuye su valor antes de que ocurra un evento principal, para luego retornar a su valor normal.

Todos los hallazgos anteriores proporcionan una aproximación a pautas concisas y bien justificadas para el desarrollo del protocolo de re – entrada.

Abstract

A common characteristic of deep mines in hard rock is induced seismicity. This results from stress changes and rock failure around mining excavations. Following large seismic events, there is an increase in the levels of seismicity which gradually decays with time, which is known as an aftershock sequence. Restricting the access to areas of a mine for enough time to allow this decay of seismic events is the main approach in re – entry strategies.

The statistical properties of aftershock sequences can be studied with three scaling relations or seismic law: (1) Gutenberg – Richter's frequency magnitude, (2) the Modified Omori's law (MOL) for the seismicity's temporal decay, and (3) Båth´s law for the magnitude of the largest aftershock.

This thesis has three main parts: estimation and correlations of mining – induced aftershock sequences parameters, development of a space – time – magnitude re – entry protocol, and the recognition and time behavior of aftershock sequences using space – time clustering.

In the first part, the three scaling relations, in addition to the stochastic Reasenberg – Jones model are applied to study the characteristic parameters of 11 large magnitude mining – induced aftershock sequences in four mines in Ontario, Canada. To provide guidelines for re – entry protocol development the dependence of the scaling relation parameters on the magnitude of the main seismic event of the aftershock sequence is studied.

The results obtained are according to those that different authors have estimated in tectonic seismicity. Nevertheless, some "scale differences" appears, especially with the Gutenberg – Richter's *b – value* and the Modified Omori´s law *p – value*, finding that, in average, there are differences of +0.35 and -0.2 respectively between the results of induced and tectonic seismicity.

The second part corresponds to the development of a stochastic space – time – magnitude re – entry protocol, using the relations between the seismic induced parameters and the magnitude of the main event. An exclusion radius is defined and the time of maximum curvature relation with mainshock event are established. This enables to build the seismic decay curves, providing information on the decay patterns of an on-going sequence. Finally, a probability range of the occurrence of the largest aftershock is proposed, based on the Reasenberg – Jones probability model.

The last part consists in analyze the behaviour of clustering in time and space for mining – induced seismicity. Using the Akaike's statistical criterion to select the space – time clustering parameters, it was possible to identify an aftershock sequence associate to a main event with magnitude $Mw = 0.7$. Also, it was found that the space – time distance apparently decreases its value before the occurrence of a main shock to, later, return to its normal value.

All the previous findings provide an approximation to concise and well – justified guidelines for re – entry protocol development.

Table of Contents

1.Introduction 1
1.1. Thesis proposal and objectives 2
1.2. Thesis structure 3
2. State of the art and definitions 5
2.1. Seismic magnitudes 6
2.2. Magnitude of completeness 7
2.2.1. Maximum Curvature (MaxC) 8
2.2.2. Goodness of Fit (GoF) 8
2.3. Seismic laws 9
2.3.1. Gutenberg – Richter's law (GR) 9
2.3.2. Modified Omori's law (MOL) parameters. 11
2.3.3. Båth's law 13
2.3.4. Reasenberg – Jones probability model 15
2.4. Space and Space – Time clustering 16
2.5. The Akaike Information Criterion (AIC) 18
3. Sources of aftershock sequences 19
4. Aftershock sequences magnitudes and filtering 24
4.1. Estimate of Moment (M_w) and Local (M_l) magnitude from Nuttli magnitude (M_n) 24
4.2. Location error and magnitude of completeness filtering 25
4.3. Space hierarchical Clustering 32
5. Seismic parameters of mining – induced aftershock sequences 34
5.1. Gutenberg – Richter's law 34
5.2. Modified Omori's law 38
5.3. Båth's law 40
5.4. Reasenberg – Jones model 41
5.5. Comparison between mining – induced and tectonic seismic parameters of aftershock sequences 42
6. Re-entry protocol development 50
6.1. Methodology 51
6.2. Exclusion zone 52
6.3. Time of maximum curvature (T_{MC}) 54

6.4. Largest aftershock probability 56
7. Space – Time clustering in mining – induced seismicity application 58
7.1. Seismic data 58
7.2. Selection of *C* and *D* values 59
7.3. Cluster selection and behaviour through time 60
8. General discussions 63
9. Conclusions 65
Bibliography 67
Appendix A - Fisher information matrix 76
Appendix B – Clustered seismicity per sequence 79
Appendix C – Error propagation 83
C.1. T_{MC} estimation error propagation 84

Index of Tables

Table 1. Brief description of the thesis chapters. 3

Table 2. Rockburst mechanism proposed by Ortlepp (1992) 6

Table 3. List of analyzed aftershock sequences (Seq) following large magnitude events collected from Ontario mines, Canada 19

Table 4. Conversion of Nuttli (M_n) magnitude to Moment ($M_{w,m}$) and Local (M_L) magnitude. ... 25

Table 5. Results of optimal R^2 for each combination of seismic parameters obtained by applying methodology presented in Figure 13 31

Table 6. Number of events in each seismic sequence after the magnitude of completeness filtering. 32

Table 7. Number of events in the sequences after filtering and hierarchical clustering 33

Table 8. MOL's parameters for each aftershock sequence. 40

Table 9. Results of ΔM and its modified form, ΔM^* 40

Table 10. Summary of some researches that estimates the Gutenberg-Richter's, Omori's and Reasenberg – Jones's parameters for tectonic aftershock sequences from different regions 44

Table 11. Coefficients, intercepts and correlation, ρ, between seismic parameters of the Ontario's mining induced and tectonic aftershock sequences 45

Table 12. *p – values* for Italy and New Zealand for each type of focal mechanism 50

Table 13. Regression equations and coefficient of adjustment (R^2) for each option of the exclusion zone radius 53

Table 14. Gutenberg – Richter's adjustment for the best and worst results of the Space – time clustering 61

Index of Figures

Figure 1. Example of the frequency of events indicator..... 1

Figure 2. Schematic view of aftershocks and potential foreshocks and their effect on the number of events in time 5

Figure 3. Scheme that shows the goal of clustering. 16

Figure 4. Example of agglomerative hierarchical clustering and its dendrogram..... 17

Figure 5. (a) Location of Kidd Creek and Macassa mines. (b) Location of the mines around the Sudbury Igneous Complex 20

Figure 6. Geology of Sudbury Igneous Complex..... 20

Figure 7. A cross-section of the underground workings of the Copper Cliff Mine 21

Figure 8. Cross section of the Creighton Mine..... 22

Figure 9. Longitudinal (W–E) section of the McCreedy East and Coleman deposits..... 22

Figure 10. (a) Kidd Creek Mine ore bodies looking East from surface to 3110 meters (10200 ft). (b) Stratigraphy and lithology in Kidd Creek Mine 23

Figure 11. Goodness of Fit, R_{GoF}, for each sequence. 26

Figure 12. Methodology diagram to estimate *Mc**..... 30

Figure 13. Magnitude of completeness, *Mc*, for each sequence..... 31

Figure 14. Frequency – magnitude distribution of each aftershock sequence in analysis before filtering and its respective Gutenberg – Richter adjustment after filtering. 34

Figure 15. Dependence of *b-value* on the main shock magnitude, $M_{w,m}$ for each filtered and clustered sequence 37

Figure 16. Dependence of the MOL parameters (a) *p-value* (b) *K-value* and (c) *c-value* with the main shock magnitude..... 39

Figure 17. Comparison between the *a'* and *b* parameters estimated for mining induced (Ontario) and tectonic aftershock sequences. 46

Figure 18. Comparison between the b values of Gutenberg – Richter's law and the *p – values* of the Modified Omori's law for Ontario mining induced and tectonic aftershock sequences 46

Figure 19. Comparison between *p* vs *b* parameters from Ontario's induced and Japan aftershock sequences..... 47

Figure 20. Comparison between *p* and *log(c)* parameters of the Modified Omori's law for Ontario Italy and New Zealand aftershock sequences. 48

Figure 21. *p-values* as a function of the main shocks in local magnitude for the mining induced aftershock sequences (Ontario Mines) and California catalogue from years 1932 to 2003. 49

Figure 22. Faulting zones defined by: (a) Modified from Chiarabba et al (2005). (b) Modified from Stirling et al (2002) 50

Figure 23. Methodology and results obtained in this section. 52

Figure 24. Spherical radiuses as a function of the main shock magnitude of the main event. 53

Figure 25. Correlation between the time of maximum curvature, T_{MC}, and the magnitude of the main event. 54

Figure 26. Events per hour as a function of time and magnitude after a main event applied to sequence 15 with $M_{w,m} = 2.6$ 56

Figure 27. Application of Reasenberg – Jones probability model 57

Figure 28. Frequency – magnitude distribution of induced seismicity in the Chilean mine for the year 2012. 59

Figure 29. Variations of AIC_{total} for some of the *C* and *D* values. 60

Figure 30. Frequency – magnitude distribution for clustered and not clustered events and *C = 0 [m/hr], D = 400 [m]* 61

Figure 31. Clustered mining induced seismicity for some values of *C* and *D* 62

Figure 32. Variation of 8-hours – moving average d_{ST}, 8 hours after and before the main shock (*dt = 0*) 62

1. Introduction

Immediately following large seismic events or blasts in seismically active mines, there is a short – term increase of the levels of seismicity which gradually decays to background levels. The complete phenomenon is knowing as an aftershock sequence. During this time of elevated seismicity, the risk of aftershocks with sufficiently high magnitude to cause damage increases, putting the workers at risk. Therefore, the policy adopted by mines is to restrict access to the affected areas for a space - time period, known as exclusion zone. This is the re – entry protocol (Vallejos & McKinnon 2009a, 2009b, 2010a, 2010b, 2011; Vallejos, 2010).

Recently, studies have been carried out to evaluate the statistical performance of some seismic indicators, such as the frequency of events, the probabilistic indicator, the space – clustering indicator or the multifractal analysis, among others (Vallejos et al, 2012; Estay, 2014; Pastén et al., 2015). The seismic indicators are helpful to monitor the rock mass response due to mining operations, using different parameters obtained from the induced seismicity recorded by seismic monitoring system installed at the mine. The objective is to generate an alert situation when abnormal levels of seismicity are identified that could indicate an uncontrolled response of the rock mass (Figure 1).

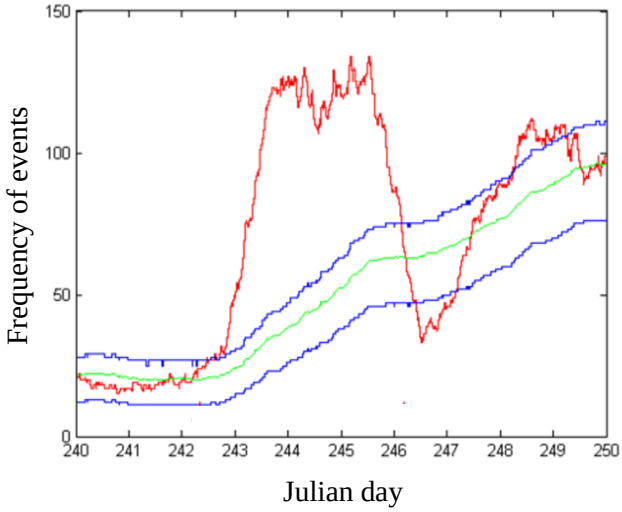

Figure 1. Example of the frequency of events indicator. Blue lines correspond to the upper and lower bounds that define the normal range of the seismicity indicator. If the indicator is beyond these bounds, a seismic alert is generated. The green line corresponds to the weekly average of the indicator (Estay, 2014).

Some of the most used indicators are:

- Frequency of events indicator (Dunlop & Gaete, 1997; Vallejos et al., 2012).
- Generic rate of Seismic Moment (Shcherbakov, 2010; Estay, 2014).
- Space – clustering (Malek & Leslie, 2006).
- Probabilistic (Benjamin, 1968; Estay, 2014).

- Using Epidemic Type Aftershock Sequence (ETAS) model (Ogata, 1988, 1989, 1999, 2001).
- Multifractal análisis (Pastén et al., 2015)

This thesis explores three fundamental aspects of mining induced seismicity.

First, correlations between the seismic parameters of mining – induced seismicity and the magnitude of the main event, to be applied in re – entry protocols. To accomplish this, three scaling relations are studied: (1) Gutenberg – Richter frequency magnitude (Richter, 1958), (2) the modified Omori's law (MOL) for the temporal decay (Utsu et al, 1995), and (3) Båth´s law for the magnitude of the largest aftershock (Båth, 1965). The stochastic model of Reasenberg – Jones (Reasenberg & Jones, 1989, 1994) is also included in the analysis to define the probability of occurrence of a large aftershock. The patterns of aftershock sequences described by these scaling laws and their implications for re – entry assessment is addressed and discussed (chapter 5).

Secondly, using the scaling relations, a stochastic space – time – magnitude re – entry protocol is developed (chapter 0).

Finally, it is analyzed the behaviour of the space – time clustering through time and space in mining – induced seismicity (chapter 7) using the Akaike's statistical criterion (subsection 2.5).

1.1. Thesis proposal and objectives

There are varied methodologies that have been developed and applied to understand the phenomenon and behavior of seismicity, especially at a local, regional and global tectonic level.

In this thesis, it is expected to use the seismic laws that have been mainly developed in tectonic seismicity and apply them in mining – induced seismicity data to apply a re – entry protocol in which the magnitude, space and time of an aftershock sequence, are involved.

The main goal of this thesis is to recognize patterns of behavior of the parameters of the seismic laws, to apply them in a space – time – magnitude re – entry protocols using mining – induced seismicity aftershock sequences.

For doing this, it is expected to achieve the following goals:

1. Estimate the aftershock sequences parameters for mining induced and tectonic seismic records.
2. Define and implement a methodology of space and space – time parametric clustering.

3. Compare and analyze the results of seismic induced parameters with those from tectonic seismicity, checking whether there is any effect on the change of seismicity scale.

By achieving these goals this thesis aims to increase the current understanding of mining – induced seismicity and be a contribution in the definition and application of new methodologies of re – entry protocols.

1.2. Thesis structure

In the table below are summarized the chapters and contents of the thesis.

Table 1. Brief description of the thesis chapters.

Chapter	Title	Summary
2	State of the art	A review of literature about seismological concepts, seismic laws and the definition of the criteria used in the thesis.
3	Sources of aftershock sequences	A description of the geology and monitoring system of the mines where the seismic sequences where acquired.
4	Aftershock sequences magnitudes and filtering	Estimation of Moment and local magnitude from Nuttli magnitude and explanation of the filtering by magnitude of completeness and space – clustering.
5	Seismic parameters of mining – induced aftershock sequences	The seismic laws used in this thesis are explained and each parameter is defined for the seismic sequences.
6	Comparison between mining – induced and tectonic seismicity	Comparison and search of correlations/scale effects between the Ontario seismic sequences of this thesis and researches of other authors about seismic parameters applied in tectonic seismicity.
7	Re – entry protocol development	Development of the space – time – magnitude re – entry protocol, applying the parameters of the seismic laws defined in chapter 4.
8	Space – time clustering application	Application of the space – time clustering methodology with mining – induced seismicity of a Chilean mine. Definition of parameters of the clustering, cluster selection and behaviour of the space – time distance after and before the main shock magnitude.
9	General discussions	
10	Conclusions	

References	
Appendix A	Fisher information matrix development
Appendix B	Figures of the space – clustered seismic sequences.
Appendix C	Error analysis for Time of Maximum Curvature.

2. State of the art and definitions

Cook (1964a) describes a seismic event as the release of energy that propagates through a medium through elastic waves and that is produced by the rupture, or failure, of the rock. These waves are recorded by a seismic monitoring system, composed, mainly, by geophones, accelerometers and GPS.

Through these signals we can calculate the location of the earthquake, in addition to the size of the seismogenic source, the seismic parameters and the failure mechanism.

Duplancic (2002) describes different methodologies for locating a seismic event and the different sources of error, which will not be detailed because it is not part of the objectives sought in this research, ergo, we will consider that the seismic events are well located.

The induced seismicity corresponds to those seismic events that are produced by some external agent. This study will be focused on the seismicity induced by the productive process of mining, such as blasting and extraction of ore. This seismicity is the result of changes in the stress field and the failure of the rock around the excavations that these processes generate.

Once the blast or an event of large magnitude has occurred, there is a period in which the levels of seismicity increase (aftershocks), both in its frequency and magnitude. This process, until normal levels of seismicity (background level) are reached, is what is known as an aftershock sequence (Figure 2). A simple definition of background seismicity is given by Nishikawa & Ide (2015) as the frequency of seismic events, excluding aftershocks.

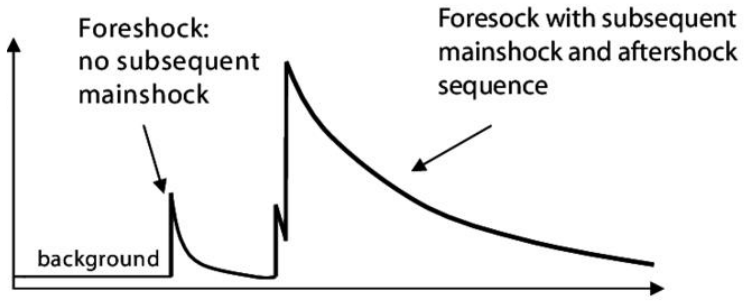

Figure 2. Schematic view of aftershocks and potential foreshocks and their effect on the number of events in time. Background level correspond to normal level of seismicity, i. e., frequency of seismic events, excluding aftershocks (modified from Gerstenberger et al., 2004).

During the process described above, it may happen that some of the seismic events cause damage to facilities, equipment and personnel, due to violent expulsions of rocky material, which is referred to as rockburst.

A rockburst is considered when a seismic event result in visible rockmass damage. This happens generally with large seismic events. Ortlepp (1992) define five mechanisms of rockburst damaging (Table 2).

Table 2. Rockburst mechanism proposed by Ortlepp (1992)

Rockburst type	Postulated source mechanism
Strain – bursting	Superficial spalling with violent ejection of fragments.
Buckling	Outward expulsion of larger slabs pre – existing parallel to opening.
Pillar or face crush	Collapse of stope pillar, or violent expulsion of rock from tunnel face.
Shear rupture	Violent propagation of shear fracture through intact rockmass.
Fault – slip	Violent renewed movement on existing fault.

In 1996, Kaiser et al. identified three basic types of rockburst damage: rock bulking, rock ejection and rock falls. In the first one, the rockmass increases in volume due to fracturing, and ejection of rocks may occur. In the second one, kinetic energy is transferred to rock blocks, causing its ejection. And in the third case, the rockburst generates a vibration in the rockmass, causing the falling of previously stable blocks.

This risk of a rockburst is higher due to the deepening of mining and, with this, the severity and frequency of the rockbursts (Obert & Duval, 1967; Cook, 1976; Hudyma & Potvin, 2004). An example of this is what happens with the new El Teniente Mine level in Chile (Rojas & Balboa, 2017); Rudna mine in Poland (Lasocki et al, 2017) and Glencore's Nickel Rim deep and Onaping depth projects (Butler & Simser, 2017).

This is explained by the continuous excavation and underground construction that goes under highly stressed ground and through increasingly complex geological settings, leading the mining industry to greater technical and economic challenges.

2.1. Seismic magnitudes

Different scales of magnitude will be mentioned and used in this research. These corresponds to the Local Magnitude (M_l), Moment Magnitude (M_w) and Nuttli Magnitude (M_n)

$$M_l = \log A(\Delta) - logA_o(\Delta), \tag{1}$$

$$M_w = \frac{2}{3} logM_o - 6.0. \tag{2}$$

The Local Magnitude was defined by Richter (1935) and it's based in the maximum amplitude, *A,* measured from a certain distance *Δ. Ao* is a regionally dependent factor. In

Richter's words *"The magnitude of any shock is taken as the logarithm of the maximum trace amplitude, expressed in microns, with which the standard short – period torsion seismometer would register that shock at an epicentral distance of 100 kilometers."*

The Moment Magnitude (Hanks & Kanamori, 1979) it is calculated from the seismic moment, *Mo*.

The seismic moment is a scalar measurement with units of *Nm* (Newton - meter). It measures the co – seismic deformation of the source. Its value is calculated as the integral of the far field displacement of the earthquake (Aki & Richards, 1980), which can be obtained directly from the seismograms. The seismic moment is also related to the size of the earthquake by the equation:

$$Mo = \mu AD \tag{3}$$

where μ is the shear modulus of the rocks involved in the earthquake (in *Pa*), *A* is the area of rupture along the geologic fault where the earthquake occurred (in m^2) and *D* is the average slip on *A* (in *m*).

The Moment magnitude is a parameter that is commonly used to estimate the source strength.

The Nuttli Magnitude (Nuttli, 1973) considered the amplitude of short – period waves. This magnitude is used in some mining sector at Canada.

2.2. Magnitude of completeness

An important value to define when working with seismic catalogs, whether in tectonic or induced seismicity, is the magnitude of completeness (*Mc*). This is defined as the minimum magnitude at which 100% of the events are detected within a volume and a defined period. The recorded seismicity with a magnitude smaller than *Mc* is not correctly detected by the seismic monitoring system, due to the lack of seismic stations, the operation of the personnel in charge or, in the case of aftershock sequences, because their magnitudes are very small to be detected after events of greater magnitude (Woessner & Wiemer, 2005).

There are several methodologies that allow estimating the value of *Mc*, which are described in detail by Woessner & Wiemer (2005) and Wiemer & Wyss (2000). Among the methods to be used are the method of Maximum Curvature ($M_{c,MaxC}$) and Goodness of Fit ($M_{c,GoF}$).

2.2.1. Maximum Curvature (MaxC)

It is one of the simplest, fastest non-parametric method to estimate *Mc*. This value is obtained as the bin of the non-cumulated histogram of the frequency-magnitude distribution whose frequency is maximum.

This method underestimates the value of *Mc* (Mignan & Woessner, 2012), especially in those gradually - curved distribution, the result from spatial and temporal heterogeneities. Woessner & Wiemer (2005) recommend using the value obtained from *Mc + 0.2*. The MaxC technique has also the advantage to require fewer events than other techniques to reach a stable result.

2.2.2. Goodness of Fit (GoF)

The goodness of fit method compares the frequency - magnitude distribution with a theoretical distribution, which is calculated using the *a* and *b* values of the Gutenberg – Richter's law (Gutenberg & Richter, 1944) and which are estimated by the maximum likelihood method.

For the selection of *Mc*, the bin of magnitude of the frequency - magnitude distribution in which the difference between the experimental and theoretical distributions is less than 5% - 10% is used.

Woessner & Wiemer (2005) emphasize that this methodology has a low bias, but more computational work is needed to carry it out. It is also a less robust method for small samples (<200).

Previously, Wiemer & Wyss (2000) use the Goodness of Fit method to estimate *Mc* in different tectonic seismicity catalogs. They use a metric *R* that allows them to evaluate the percentage of adjustment that the experimental and theoretical distribution possesses,

$$R(a, b, M_i) = 100 - \left(\frac{\sum_{M_i}^{M_{max}} |B_i - S_i|}{\sum_i B_i} 100 \right) \tag{4}$$

where B_i is the value of the experimental cumulative frequency for a value of M_i and S_i is the value of the cumulative frequency predicted for M_i by the theoretical distribution, using the estimated *a* and *b* values.

Wiemer and Wyss (2000) propose using as the *Mc* value the magnitude that explains 90% of the variability of the data, that is, a value of *R = 90%*.

2.3. Seismic laws

2.3.1. Gutenberg – Richter's law (GR)

The Gutenberg – Richter's law begins with the definition of the probability density proposed by Aki (1965):

$$f(M,\beta) = \beta e^{-\beta(M-M_c)}. \tag{5}$$

It is defined the number of seismic events between magnitude *M* and *M + dM* per time unit, *t*, as:

$$N = \frac{f(M) - f(M+dM)}{t} = \alpha e^{-\beta(M-M_c)}\left(1 - e^{-\beta dM}\right) \tag{6}$$

where α is the average number of events per time unit, β/t. β is defined by construction as $1/(\bar{M} - M_c)$; $\bar{M}$ is the average magnitude and M_c correspond to the magnitude of completeness. Eq. (6) can be approximate in first order Taylor's series as:

$$N \approx \alpha\beta e^{-\beta(M-M_c)} dM. \tag{7}$$

Applying logarithm in both sides, the Gutenberg – Richter's law is obtained:

$$logN = a - bM \tag{8}$$

where $a = log(\alpha\beta e^{\beta Mc} dM)$ and $b = \beta log(e)$. In particular, the *b - value* depends of the tectonic regimes and the stress regime (Scholz, 1968; Mikumo & Miyatake, 1979; Mori & Abercrombie, 1997; Enescu and Ito, 2003; Schorlemmer et al, 2005).

Scholz (1968) showed on a laboratory scale the relationship between the *b – value* and the fracture ratio σ/σ_c, for different types of rock, with σ_c as the uniaxial compression stress. Their results show that, regardless of the type of rock, if it is subjected to a higher level of stress, it has a lower *b – value*. This is the expected result when using the *b - value* as a seismic risk parameter.

Given the definition of the parameters *a* and *b*, the only parameter to be estimated is β, so the log-likelihood function to be maximized is:

$$ln\{\textstyle\prod_i f(M_i,\beta)\} = Nln\beta - \beta \sum_i (M_i - M_c). \tag{9}$$

The estimation error of the *b-value* is given by the formulation of Shi & Bolt (1982):

$$\sigma(\hat{b}) = 2.3b^2\sigma(\bar{M}) \tag{10}$$

where

$$\sigma^2(\bar{M}) = \sum_{i=1}^{n} \frac{(M_i - \bar{M})^2}{n(n-1)}. \tag{11}$$

The Gutenberg-Richter's *b-value* is calculated as:

$$b = \frac{\log(e)}{\bar{M} - M_c + {\Delta M_{bin}}/{2}} \tag{12}$$

where $\bar{M}$ is the mean magnitude of events that M ≥ M_c. ΔM_{bin} is the binning width of the catalogue. In this thesis, is considered that each bin has a width of 0.1.

Schorlemmer et al. (2005) showed how the Gutenberg – Richter's *b – value* varies depending on the mechanism of the seismicity, within a range of the rake. It is true that:

$$b_{nr} > b_{ss} > b_{th}$$

with b_{nr}, b_{ss} *y* b_{th} as the values of *b* for events with normal, strike slip and inverse mechanism, respectively. This is associated with the average stress needed to generate a fault, this is:

$$\sigma_{nr} < \sigma_{ss} < \sigma_{th}$$

generating an inverse relationship between the *b – value* and its stress level.

Some common errors in the calculation of the *b – value* are:

- Adjustment of the Gutenberg – Richter´s law with linear Least Squares (LSQ) that with the Maximum Likelihood Estimation (MLE) method (Aki, 1965). The results obtained with the MLE has lower dispersion.
- When using a very small data set, a greater variability in the *b – value* is obtained. Felzer (2006) recommends using more than 2000 seismic events to have an estimation error of 0.05 with a confidence interval of 98%.
- The use of earthquakes with magnitude smaller than the magnitude of completeness (*Mc*) of the catalog.

2.3.2. Modified Omori's law (MOL) parameters.

Immediately following a major seismic event, a rockburst or a blast in seismically active mines, there is an increase in the seismic frequency, known as aftershocks, which gradually decays to the normal levels of seismicity, knowns as seismic sequence (chapter 2).

Omori (1894) shows that the frequency of aftershocks per day at Nobi's earthquake in 1891 ($M = 8.0$) decreased according to the equation:

$$n(t) = \frac{K}{(c + t)} \tag{13}$$

where $n(t)$ is the rate of aftershocks per unit time interval at time t and K and c are constants.

The *K – value* corresponds to the seismic activity of the sequence, that is, the number of aftershocks after the main event are present in it (Vallejos & McKinnon 2010a). Also, Utsu et al. (1995) and Utsu (2002) showed that the *K – value* varies strongly with *Mc*, so the number of seismic events in the sequences is a relevant factor.

On the other hand, the physical meaning of the *c – value* can be attributed to the complex rupture process that involves seismicity (Yamakawa 1968) as the displacement in time related to the aftershocks in the first part of the sequence (Enescu et al., 2009), which have a lower signal amplitude, so they are not completely detected (Hamaguchi & Hasegawa 1968, Kagan & Houston 2005). In addition, *c – value* behaves mathematically as the constant that makes equation (13) not diverge at $t = 0$ (Narteau et al., 2002).

This refers to research related to tectonic seismicity, however, this behavior does not seem to be different for Canadian mining induced seismicity, as detailed in section 5.2.

Utsu (1961) found that the equation (13) adjust better considering a value of the exponent that could vary from 1, and proposed the so call Modified Omori's Law (MOL):

$$n(t) = \frac{K}{(c+t)^p}. \tag{14}$$

The *p – value* controls the decay rate and its value varies for each seismic sequence.

There are several investigations on tectonic seismicity related to the factors that influence in the *p – value* variations. Beginning with Mogi (1962), who studied 31 seismic sequences in Japan and showed that in areas where volcanism predominates (Sea of Japan) the *p – value* is high (higher rate of decay) and on the Pacific coast, where plate tectonics predominates, the *p – value* is lower (lower decay rate). That is, a greater decay is obtained in areas where the temperature of the crust is higher, where the stresses relax more quickly (Mogi, 1967).

This was corroborated by Kisslinger & Jones (1991), but with seismic sequences obtained in California. In their results, the highest *p – values* were obtained in the western zone of the volcanic front, while the lowest values were obtained in the subductant plate.

MOL's parameters were estimated by MLE methodology, described as follows. Given the occurrence times t_i (i=1,…, N) of the individual N events in a time interval [S, T] the log-likelihood function of equation (14) can be expressed by:

$$lnL(K,p,c,S,T) = NlnK - p\sum_{i=1}^{N}\ln(t_i + c) - KA(p,c,S,T) \tag{15}$$

where:

$$A(p,c,S,T) = \begin{cases} \ln(T+c) - \ln(S+c) & p = 1 \\ [(T+c)^{1-p} - (S+c)^{1-p}]/(1-p) & p \neq 1 \end{cases}. \tag{16}$$

The maximum likelihood estimates of the parameters K, p and c, are those values that maximize equation (15). The MOL's parameters have been estimated into the complete duration of the sequence, i.e. [S, T] = [t_0, t_N], where t_0 and t_N are the occurrence times of the main and last events in the clustered sequence, respectively.

The standard errors of the maximum likelihood estimation of the parameters K, p and c, are the square roots of the diagonal elements of the inverse of the observed Fisher information matrix (Ogata, 1983; equation (18))

$$J(K,c,p,S,T) = \int_S^T \begin{bmatrix} K^{-1}(t+c)^{-p} & -p(t+c)^{-p-1} & -(t+c)^{-p}\ln(t+c) \\ * & Kp^2(t+c)^{-p-2} & Kp(t+c)^{-p-1}\ln(t+c) \\ * & * & K(t+c)^{-p}\{\ln(t+c)\}^2 \end{bmatrix} dt. \tag{17}$$

The resolution of each integral is in Appendix A.

When the MOL curvature is traced in time, a characteristic point emerges at the maximum curvature, given by:

$$T_{MC} = \left[Kp\sqrt{\frac{2p+1}{p+2}}\right]^{\frac{1}{1+p}} - c. \tag{18}$$

T_{MC} has a physical attribute of a time sequence that obeys MOL decay, suitable for use in re-entry protocols (chapter 0), defining the transition between the highest to lowest event rate change (Vallejos & McKinnon, 2010).

2.3.3. Båth's law

Empirical Båth's law (Richter, 1958; Båth, 1965) states that the average difference in magnitude between a main shock and its largest aftershock in shallow earthquakes is constant and equal to 1.2 regardless of the main shock magnitude, i.e.,

$$\Delta M = M_{w,m} - M_{LA} \approx 1.2 \tag{19}$$

where $M_{w,m}$ and M_{LA} are the magnitudes of the main shock and the largest aftershock, respectively.

From the above it can deduce the following:

- There is a finite difference between the magnitudes $M_{w,m}$ and M_{LA} and this difference is independent of the magnitude.
- On average, the energy released by the main event is 53 times the energy released by the largest aftershock.

Shcherbakov and Turcotte (2004) proposes a modified Båth's law as follow:

$$\Delta M^* = M_{w,m} - M^* \tag{20}$$

where M^* is the inferred largest aftershock estimated by Gutenberg-Richter's law, considering $N = 1$ in equation (8):

$$M^* = \frac{a}{b} \tag{21}$$

which is the value of the aftershock magnitude that was used in this study to evaluate the Reasenberg – Jones model, explained in section 2.3.4.

Several authors have applied and interpreted Båth's law to tectonic seismicity (Hamaguchi & Hasegawa, 1970; Tsapanos, 1990; Narteau et al., 2002; Console et al., 2003; Kagan & Houston, 2005; Enescu et al., 2009), but few focus on induced seismicity (Vallejos & Mckinnon, 2009b; Vallejos & Estay, 2017).

Vallejos & McKinnon (2009b) explain that the application of Båth's law to induced seismicity is limited, since most of the largest aftershock tend to occur near the main event and, for some seismic sequences, the largest aftershock would not be found associated with the start of the sequence.

Below are the main results obtained by some authors who have researched and applied the Båth's law.

Vere - Jones (1969) reviews a theoretical version of Båth's Law. It assumes that the magnitudes of the aftershocks are independent and that they are distributed exponentially. It is proposed that this distribution has a negative exponent equal to *2.3b*, where *b* is the Gutenberg – Richter's parameter.

The results obtained differ from that proposed by Båth, since the theoretical distribution does not center on 1.2 and, in addition, there is a positive correlation between the magnitude difference proposed by Båth and the magnitude of the main event. The explanation, besides this difference in the results, is attributed to a bias due to the use of different cut magnitudes (*Mc*) used in the Utsu's (1961) research catalog which was used in Vere – Jones's research.

A similar work was developed by Console (2003), using the Gutenberg – Richter's distribution, reaching similar conclusions to those of Vere – Jones. Console selects two cutoff magnitudes, *Mo** and *Mc*, related to the magnitude of the main event and the magnitude of completeness respectively. When the difference between both magnitudes is equal to 2 and the number of events in the sequence is close to 10, Båth's law is fulfilled.

Tsapanos (1990) analyzes the distribution of the difference $\Delta M = M_{w,m} - M_{LA}$ for seismicity that occurred in the Pacific coast and in forearc zones. In this distribution there are 2 peaks, one in $\Delta M = 1.2$, coinciding with Båth's law, and another peak in $\Delta M = 1.8$. These differences are explained by pointing out that ΔM is related with the variation of the stress field, in accordance with what other authors have investigated, including:

- Gibowitz (1973) showed that the variation that can exist with respect to the original result of Båth, is associated with the stress drop produced by the main event.
- In laboratory tests, Mogi (1962) and Scholz (1968) showed that the Gutenberg – Richter's *b – value* depends on the stress conditions and the homogeneity of the rock where the fracture occurs. Okada (1979), on the other hand, showed that the variation with respect to the Båth's law, would be related with the *b – value*.
- Purcaru (1974) observed that the value of ΔM is a linear function of the *b – value*.

Finally, in subduction zones there is a high concentration of stress, whose accumulated energy is released by the main event and its aftershocks, obtaining a lower value of ΔM. In the opposite case, in areas of forearc, there are lower levels of concentration of stress, so the accumulated energy is released mostly by the main event, obtaining values greater than ΔM.

Lombardi (2002) delved further into what was proposed by Vere – Jones (1969), performing a mathematical analysis of Båth's law, based only on elements of probability. She

defined a cutoff magnitude for the main events, *Mc**, with which she obtained that the magnitudes of the main event and that of their largest aftershock depends on the difference between *Mc**, the magnitude of completeness of the sequence (*Mc*) and the number of events in each sequence (*N*). In addition, she obtained that the expected value of the difference $M_{w,m}$ - M_{LA} increases with increasing difference *Mc** - *Mc* for any value of *N*.

In probabilistic and statistical terms, Lombardi reached the following conclusions:

- $M_{w,m}$ converges to an exponential distribution.
- $M_{w,m}$ and M_{LA} are random variables with different distributions.
- The choice of *Mc** and *Mc* is crucial for the distributions of $M_{w,m}$, M_{LA} and $M_{w,m}$ - M_{LA}. In addition, these distributions depend on *N* and on the Gutenberg – Richter's *b – value*.
- Although the model predicts the existence of a positive correlation between $M_{w,m}$ and the difference $M_{w,m}$ - M_{LA}, for each value of $M_{w,m}$ - M_{LA} and *N*, Lombardi showed that the coefficient of these correlations can be close to 0 or, even, negative.

Finally, Tahir et al. (2011 – 2012) proposes a study in tectonic seismicity, including time, distance and size of the largest aftershock, finding different relationships for the cases of strike slip, inverse and normal faults.

In the research it is concluded that:

1. More aftershocks are observed when the seismicity is related to an inverse failure process than to a strike slip fault.
2. The value of ΔM associated with inverse faults is, on average, less than the value of ΔM in case of strike slip faults.
3. The distance between the main event and the largest aftershock is less in the case of inverse faults than in the case of strike slip failures.
4. The distribution of time between the main event and the largest aftershock is adjusted to a power law, but with a faster decay rate than for aftershocks in general.

2.3.4. Reasenberg – Jones probability model

Reasenberg – Jones model (1989; 1994) expresses the rate λ of aftershocks with magnitude *M* or larger, at time *t* following a main shock of magnitude $M_{w,m}$ as follows:

$$\lambda(t, M) = \frac{10^{a' + b(M_{w,m} - M)}}{(t + c)^p} \tag{22}$$

where *p* and *c* are the modified Omori's law parameters, *b* is the Gutenberg-Richter's coefficient. The authors refer the *a' – value* as the "productivity" of the sequence and can be expressed as:

$$a' = log(K) - b(M_{w,m} - M) \tag{23}$$

where K is also a MOL's parameter.

The probability, P, of one or more earthquakes occurring between magnitudes M_1 and M_2 in the time range $[t, t+\Delta t]$ is:

$$P(M_1 \leq M < M_2; S \leq t < T) = 1 - \exp\left(\int_t^{t+\Delta t} \lambda(t, M)dt\right)_{M_1}^{M_2}. \tag{24}$$

A common error in calculating probability is that it integrates with respect to time and magnitude. The error arose from our incorrectly treating $\lambda(t,M)$ as a density function, when in fact it is a density with respect to t and a rate with respect to M.

Solving equation (24) gives:

$$\begin{aligned} P &= 1 - exp\left\{-\frac{(t+\Delta t+c)^{1-p} - (t+c)^{1-p}}{(1-p)}\left(10^{a'+b(M_m-M_1)} - 10^{a'+b(M_m-M_2)}\right)\right\} \quad for\ p \neq 1 \\ P &= 1 - exp\left\{-\ln\left(\frac{t+\Delta t+c}{t+c}\right)\left(10^{a'+b(M_m-M_1)} - 10^{a'+b(M_m-M_2)}\right)\right\} \quad for\ p = 1 \end{aligned} \tag{25}$$

where, in this thesis, M_2 is considered as the main shock magnitude, M_1 is the largest aftershock magnitude, and Δt was considered as 1 hour.

2.4. Space and Space – Time clustering

Clustering is a non – supervised data mining classification method for discovering groups. Clustering problem is about partitioning a given data set into groups (clusters) such that the data points in a cluster are more like each other than points in different clusters (Guha et al, 1998) (Figure 3).

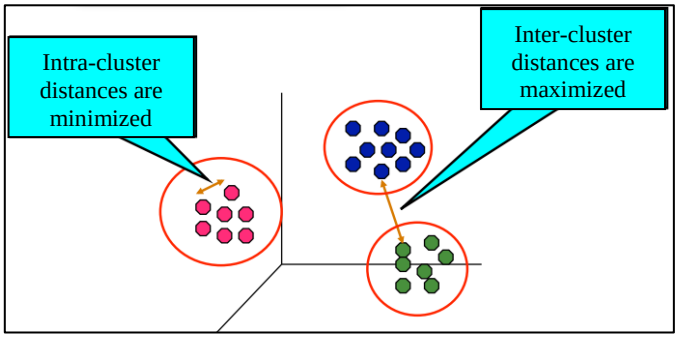

Figure 3. Scheme that shows the goal of clustering.

There exist different categories of clustering algorithms (Partitional, Hierarchical, Density based, Grid based). This thesis is focused in the hierarchical clustering. Halkidi et al. (2001) describes the methodology of the hierarchical clustering as successively by either merging smaller clusters into larger ones (agglomerative), or by splitting larger ones (divisive). This result of the algorithm is a tree of clusters, called dendrogram (Figure 4), which shows how the clusters are related. By cutting the dendrogram at a desired level, a clustering of the data items into disjoint groups is obtained.

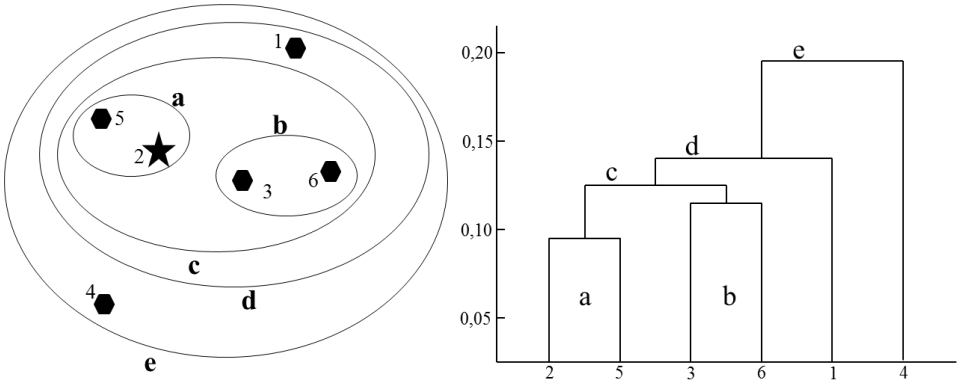

Figure 4. Example of agglomerative hierarchical clustering (left) and its dendrogram (right).

Hierarchical clustering method is one of the oldest methods of cluster analysis (McQuitty, 1957; Sneath, 1957) and it has been used to evaluate clustering in numerous fields (Ling, 1973; Hartigan, 1975; Day and Edelsbrunner, 1984; Frohlich & Davis, 1990; Davis & Frohlich, 1991; Estay, 2014; Cornejo et al, 2014; Rebuli & Kohler, 2014).

On the other hand, Frohlich & Davis (1990) and Davis & Frohlich (1991) developed a distance metric involving space and time (d_{ST}) had been developed and applied:

$$d_{ST} = \sqrt{d^2 + C^2T^2} \leq D \tag{26}$$

where d_{ST} is the space-time distance, d, the Euclidian spatial separation of events (in meters), T, the time separation (in hours) between events, C, the parameter to be estimated, which relates space and time (in meters/hour) and D is the minimum distance to form a cluster.

Davis & Frohlich (1991) estimate the parameters C and D by a scoring system in which, using a synthetic catalogue, calculate the difference between the fraction of aftershock linked to parent event and the fraction of main shocks correctly identified. A value of C is chosen such that two simultaneous events separated by a distance d are a likely to be related to each other as two events with identical location occurring at time t apart. The values proposed, for tectonic events, were $C = 1$ *km/day* and $D = 80$ *ST-km*.

Given the above, it is logical to apply clustering tools to induced seismicity data, where there is a spatial and temporal dependence between them.

In this thesis is expected to use these tools to analyze the spatial and temporal variation of the cluster looking for behaviors that describe the seismicity before and after a main event or a blast.

2.5. The Akaike Information Criterion (AIC)

The Akaike Information Criterion (AIC; Akaike, 1973, 1974) is a method for comparing non – nested models. As Wagenmakers & Farrell (2004) explain, the objective of the AIC model is to estimate the information loss when the probability distribution associated with the true model is approximated by a probability distribution associated with the model that is to be evaluated.

The AIC is defined as:

$$AIC_i = -2lnL_i + 2V_i \tag{27}$$

where L_i = Maximum Likelihood Estimation (MLE) (Aki, 1965; Newman, 2005) for the candidate model *i*, which is determined by adjusting the V_i free parameters.

The model with smaller AIC values is selected.

Eq. (27) is valid with enough amounts of data. When the number of data (n) is less than 40 times V (Burnham & Anderson, 2002), a correction of the AIC is applied:

$$AIC_c = -2logL + 2V + \frac{2V(V+1)}{n-V-1}. \tag{28}$$

The AIC was used to determine the values of *C* and *D* (equation (26)) in the space – time clustering (more details in section 7.2)

3. Sources of aftershock sequences

Twenty – one aftershock sequences have been collected from several mine-wide large magnitude events at different mines in Ontario, Canada (Table 3).

Table 3. List of analyzed aftershock sequences (Seq) following large magnitude events collected from Ontario mines, Canada. M_n is the main shock magnitudes of the sequence in Nuttli magnitude (Nuttli, 1973), Date is the date of the main shock, t_N is the total duration of the sequence and N the number of seismic events in the sequence.

Seq	Site	Date (mm/dd/yyyy)	M_n	t_N (hours)	N
1	A	10/13/2006	1.1	27.3	48
2	Copper Cliff North	09/30/2004	1.9	25.6	51
3		06/10/2005	2.1	10.3	172
4		11/30/2004	2.4	29.9	855
5		09/24/2008	2.4	69.4	164
6		06/11/2006	2.8	72.1	1880
7		09/11/2008	3.8	165.6	1411
8	Craig	06/22/2007	2.2	37.5	507
9	Creighton	10/17/2007	1.0	18.4	86
10		04/17/2008	1.5	7.1	23
11		02/07/2008	2.4	45.9	197
12		03/14/2009	2.6	197.7	2933
13		12/06/2008	2.9	25.3	161
14		06/15/2007	3.0	27.6	591
15		10/07/2007	3.1	53.6	801
16		11/29/2006	4.1	165.5	3742
17	Fraser	10/16/2008	2.4	19.0	86
18	Garson	12/05/2008	3.3	14.4	117
19	Kidd Creek	03/02/2006	1.6	23.5	223
20		01/06/2009	3.8	71.6	116
21	Macassa	07/12/2008	3.1	469.7	583

The total duration of the sequence (t_N) was estimated by ratios method, described by Frohlich & Davis (1985) and following the considerations of Vallejos & McKinnon (2010). This method evaluates the ratio:

$$r(N_b, N_a) = {T_{N_a}}\Big/{T_{N_b}} \tag{29}$$

where T_{Na} and T_{Nb} are the time of occurrence of the $N_a{}^{th}$ and $N_b{}^{th}$ event following and preceding the principal event, respectively. Subsequent events are identified as aftershocks if the above ratio is smaller than a critical value generated by a random process with a certain probability. For our

analysis, we set $N_a = 1$, $N_b = 5$ with a probability of 1%, giving a critical value of $r_c(5,1) = 0.002$. The start of the sequence is defined if the ratio $r(5,1)$ is less than the critical value for a group of at least three consecutive events.

Each mine has a monitoring system provided by the company Engineering Seismology Group (ESG), ensuring that the location of hypocenters and the calculation of magnitudes are consistent. In this thesis the hypocenter relocation of the seismic events is not considered. The wide variety of mining and geology is selected to evaluate the range of aftershock statistics that can be found in mining operations in Ontario.

Each mine, except Kidd Creek and Macassa, are located around the Sudbury Igneous Complex (SIC) (Figure 5), which corresponds to 2.5 to 3.0 km thick with ~60 × 27 km elliptical igneous rock body (Therriault, et al., 2002). The geology of the Sudbury Igneous Complex is described in Figure 6.

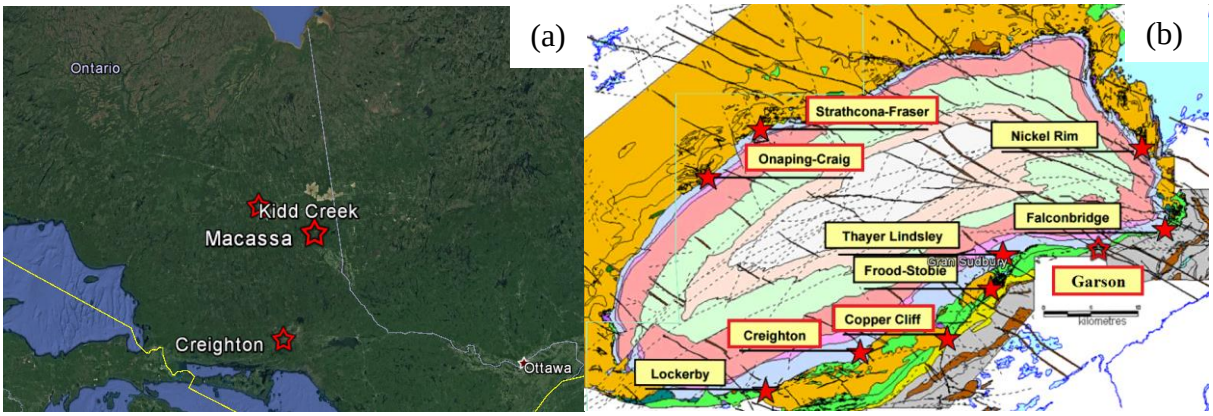

Figure 5. (a) Location of Kidd Creek and Macassa mines. Creighton Mine indicates the location of the Sudbury Igneous Complex. (b) Location of the mines around the Sudbury Igneous Complex. The names of the mines framed with a red rectangle are those used in this study (modified from Villaescusa et al, 2007).

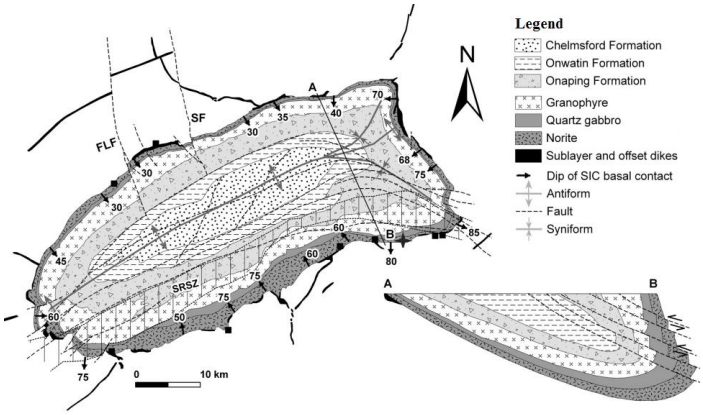

Figure 6. Geology of Sudbury Igneous Complex (modified from Mukwakwami et al, 2011). FLF: Fecunis Lake Fault, SF: Sandcherry Fault, SRSZ: South Range Shear Zone.

1. *Copper Cliff North, Sudbury.* It's located at N46° 26.930', W81° 05.725'. The study area consists of the upper part of the 100/900 orebodies, between the 2700 and 3400 levels. The microseismic monitoring system covering this zone is composed of 13 uniaxial and 2 triaxial accelerometers. A variety of mining methods have been used over the years at North Mine but the main methods used presently are slot/slash and vertical retreat mining in the main mining block of the mine. The ore deposits of the North Mine environment predominantly occur within the intrusive quartz diorite dyke (Figure 7). The quartz diorite dyke striking north – south, is approximately 50 meters wide and generally dips vertically or steeply west. The nickel – copper sulphides are generally located in the central portion of the quartz diorite dyke, and form elongated steeply plunging pipe-like orebodies. The country rocks west of the dyke are predominantly granite and granodiorite rocks of the Creighton Pluton. The country rock, east of the dyke, are metavolcanic and metasedimentary rocks of the Elsie Mountain Formation. Sudbury Breccia predominantly occurs east of the dyke and is widespread at breaks in the dyke. Narrow quartz diabase and olivine diabase dykes crosscut the quartz diorite dyke. The North Mine is associated with four major faults: number 2 mine fault, number 1 cross fault, 900 Orebody Cross fault and Creighton fault at the south end of the North Mine. The faulting was the last geological event affecting the North Mine environment: it displaced the quartz diorite dyke and its associated ore deposits, the quartz diabase dykes, and the olivine diabase dykes.

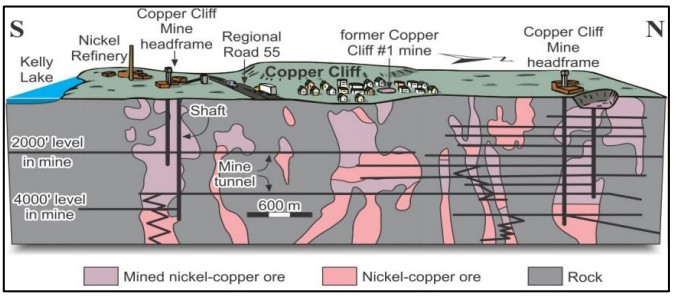

Figure 7. A cross-section of the underground workings of the Copper Cliff Mine, looking west (from Natural Resources Canada and Ontario Geological Survey, 2015)

2. *Craig Mine, Sudbury.* Craig Mine is a nickel – copper deposit located on the Northwest rim of the Sudbury Basin (N46° 38.1', W81° 22.2'). These zones of Craig Mine have a fault region obliquely traversing the orebody generating high seismic activity and occasional large magnitude events. These zones are currently being extracted via blast hole open stopping. The seismic array has 55 uniaxial sensors and covers a volume of approximately 1000 x 1300 x 900 meters.

3. *Creighton Mine, Creighton***.** Creighton Mine is located within the Creighton embayment on the outer rim of the South Range of the Sudbury Igneous Complex (N46° 27.7', W81° 11.4'). At depth, the Creighton main ore zone strikes roughly east – west and dips steeply to the north. Creighton Mine comprises 15 orebodies of which most of the higher-grade mineralization has been depleted. Mineralization is contained within a northwest plunging embayment of norite in the footwall. Creighton Mine is characterized by several late-stage faults, locally termed shears.

The structures consist of foliated material. Depending on structure, shear zones vary in thickness from a few centimeters to tens of meters (Malek et al, 2009). The study region corresponds to the Creighton Deep, between the 6600 and 7800 levels (between 1828 and 2377 meters below surface) (Figure 8). The underground microseismic monitoring system covering this area consists of 24 uniaxial and seven triaxial accelerometers.

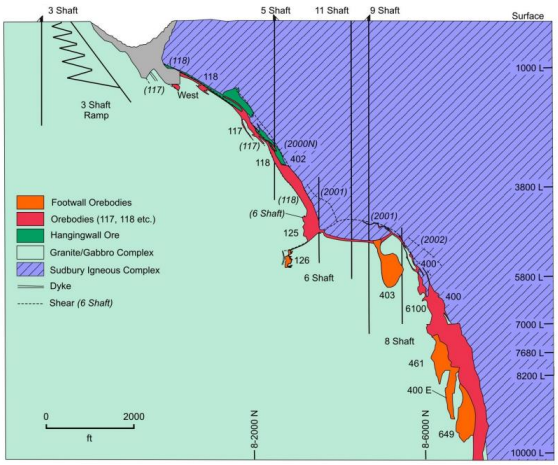

Figure 8. Cross section of the Creighton Mine (from Malek et al, 2009).

4. *Fraser, Sudbury*. The Fraser mine is in the north range of the SIC (N46°40.874', W81°19.559') and is part of the McCreedy East deposit (Figure 9). The McCreedy East deposit is in the Onaping Levack embayment which is a shallow, 8 – km – long embayment along the north side of SIC and hosts more than 18 deposits, including Strathcona, Fraser, Coleman, McCreedy West, and Craig. These deposits are in a granite breccia which is a 1 – km – thick contact metamorphic aureole with brecciated footwall rocks (Dara et al, 2011).

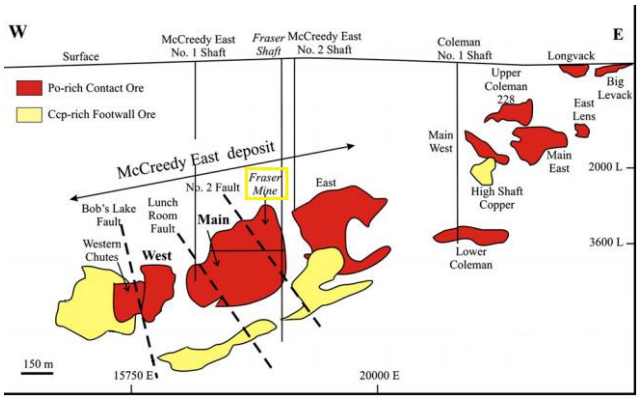

Figure 9. Longitudinal (W–E) section of the McCreedy East and Coleman deposits. Fraser Mine is framed in a yellow rectangle. Po-rich: pyrrhotite rich, Ccp-rich: chalcopyrite rich (modified from Dara et al., 2011)

5. *Garson, Sudbury*. Garson Mine is located at 15 kilometers northeast from Sudbury (N46° 34.933', W80° 52.183'), at the southern east part of the SIC. The Garson deposit is a Ni – Cu – platinum group elements deposits that formed along the basal contact between the SIC and the Paleoproterozoic Elsie Mountain Formation (Mukwakwami, et al., 2011).

6. *Kidd Creek, Timmins*. Kidd Creek Mine is located 24 kilometers north from Timmins, Ontario (N48° 41', W81° 22.3') The study region corresponds to the complete mine D, covering a volume of approximately 300 x 9200 x 9500 meters, between the 6800 and 8800 levels (between 2073 and 2682 meters below surface) (Figure 10a). In this zone, the underground microseismic monitoring system consists of 15 uniaxial and 4 triaxial accelerometers. Blasthole mining with delayed paste backfill is used to extract the ore underground. A general description of the mine's geology can be found in Board et al. (2001). Kidd Mine's main mineralized lenses are called the main (copper stringer and massive sulphides) and south lenses. These orebodies are located near the top of a locally thickened rhyolite, which is underlayed to the east by ultramafics and overlayed to the west by mafic flows and associated intrusions. The stratigraphy trends north – south, is overturned, and dips steeply to the east. All the lithologies in the Kidd Mine (Figure 10b), including the ore, have been subjected to complex folding and faulting. The major faults that potentially affect mine-wide stability can be defined in two systems: The Gouge Fault and the south-dipping echelon faults. The south-dipping faults have been associated with the larger seismic events at Kidd, while the Gouge Fault and its splays primarily impact hanging wall dilution.

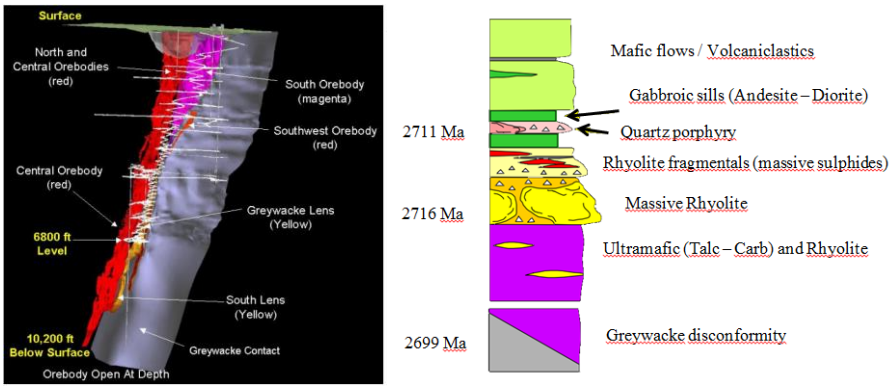

Figure 10. (a) Kidd Creek Mine ore bodies looking East from surface to 3110 meters (10200 ft). (b) Stratigraphy and lithology in Kidd Creek Mine (Gibson, et al. 2003)

7. *Macassa, Kirkland Lake.* Macassa is located southwest of Kirkland Lake, at the eastern region of Ontario (N48° 7.7', W80° 5.4') The zone is composed of a set of primary, longitudinal, continuous retreat sublevel longhole stopes with delayed paste backfill at a depth below surface of 1500 m. The geotechnical domains include very brittle, massive, high – strength tuff rocks in the hanging wall and massive – to – moderately jointed high strength orebody in a series of sub-parallel faults. These faults strike northeast and dip steeply (~70°) to the south. The footwall consists of a medium-strength basic syenite, which is generally quite blocky. The average stope dimensions are approximately 3 m in thickness and 30 m in width. The dominant geological structure of the zone is a single major fault intersecting the stopes, which can be parallel to the hanging wall or footwall contact or be the actual contact itself. Inclusions are infrequent and discontinuous. The underground micro seismic monitoring system surrounding the zone consists of a dense array of 66 uniaxial accelerometers and covers a volume of approximately 150 x 100 x 100 meters.

4. Aftershock sequences magnitudes and filtering

In the next subsections it is explain the conversion from Nuttli to Moment and Local magnitude (subsection 4.1) and the filters that were applied to the seismic sequence: location error, magnitude of completeness (subsection 4.2) and space hierarchical clustering (subsection 4.3).

The first two filters are necessary to remove the poorly located seismic events from the analysis and to provide some degree of uniformity to the data. The clustering filtering allows to include in the aftershock sequence only the seismic events that have some degree of space similarity excluding the rest of seismicity as noise.

4.1. Estimate of Moment (M_w) and Local (M_l) magnitude from Nuttli magnitude (M_n)

The main shock magnitude of the sequences was given in the Nuttli scale (M_n, Nuttli, 1973) which is used to express the magnitude of large seismic events for mines in the Canadian Shield.

To ensure the correct estimation of the seismic parameters, the Nuttli magnitude will be converted into Moment magnitude ($M_{w,m}$) through the following relation:

$$M_{w,m} = 1.03M_n - 0.61. \quad (30)$$

Sonley and Atkinson (2005) found these empirical relationships between M_n and $M_{w,m}$, using small earthquakes in Brunswick Mine (Canada) with $1.0 \leq M_n \leq 6.0$ (Table 4).

Moreover, Hudyma and Potvin (2004) summarize several researches in which M_w and M_L are estimated using micro – seismic parameters with $M_L \geq 1,0$, founding relationship between both magnitudes. One of the proposed empirical relationships is:

$$M_w = 0.67M_L + 0.67. \quad (31)$$

Therefore, replacing equation (30) into (31), we obtained an equation to estimate the Local magnitude for the Ontario sequences from its Nuttli magnitude:

$$M_L = 1.54M_n - 1.91. \quad (32)$$

This equation is valid only for those sequences which mainshock magnitude was $M_n \geq 1.9$.

Table 4. Conversion of Nuttli (M_n) magnitude to Moment ($M_{w,m}$) and Local (M_L) magnitude.

Seq	Site	M_n	$M_{w,m}$	M_L
1	A	1.1	0.5	--
2	Copper Cliff North	1.9	1.3	1.0
3		2.1	1.6	1.3
4		2.4	1.9	1.8
5		2.4	1.9	1.8
6		2.8	2.3	2.4
7		3.8	3.3	3.9
8	Craig	2.2	1.7	1.5
9	Creighton	1.0	0.4	--
10		1.5	0.9	--
11		2.4	1.9	1.8
12		2.6	2.1	2.1
13		2.9	2.4	2.6
14		3.0	2.5	2.7
15		3.1	2.6	2.9
16		4.1	3.6	4.4
17	Fraser	2.4	1.9	1.8
18	Garson	3.3	2.8	3.2
19	Kidd Creek	1.6	1.0	--
20		3.8	3.3	3.9
21	Macassa	3.1	2.6	2.9

4.2. Location error and magnitude of completeness filtering

Each aftershock sequence was filtered by limiting the source location error (Δr), and by magnitude of completeness (Mc). The objective of these two constraints is to remove the poorly located seismic events from the analysis and to provide some degree of uniformity to the data. For the analysis, only seismic events with an associated hypocentral location residual error less than or equal to 50 meters were considered. This distance matches with the minimum spherical radius used to restrict access from the potential source after a large magnitude event (Vallejos & McKinnon, 2008). The Mc value for each sequence was estimated by the Maximum Curvature ($M_{c,MaxC}$) and Goodness of Fit ($M_{c,GoF}$) methods (section 2.2) (Figure 11).

It is known that the MaxC approach often underestimates the value of Mc compared to the GoF approach (Wiemer & Wyss, 2000; Woessner & Wiemer, 2005; Mignan et al., 2011). Considering this, it was decided to select the Mc value for each sequence with the GoF method.

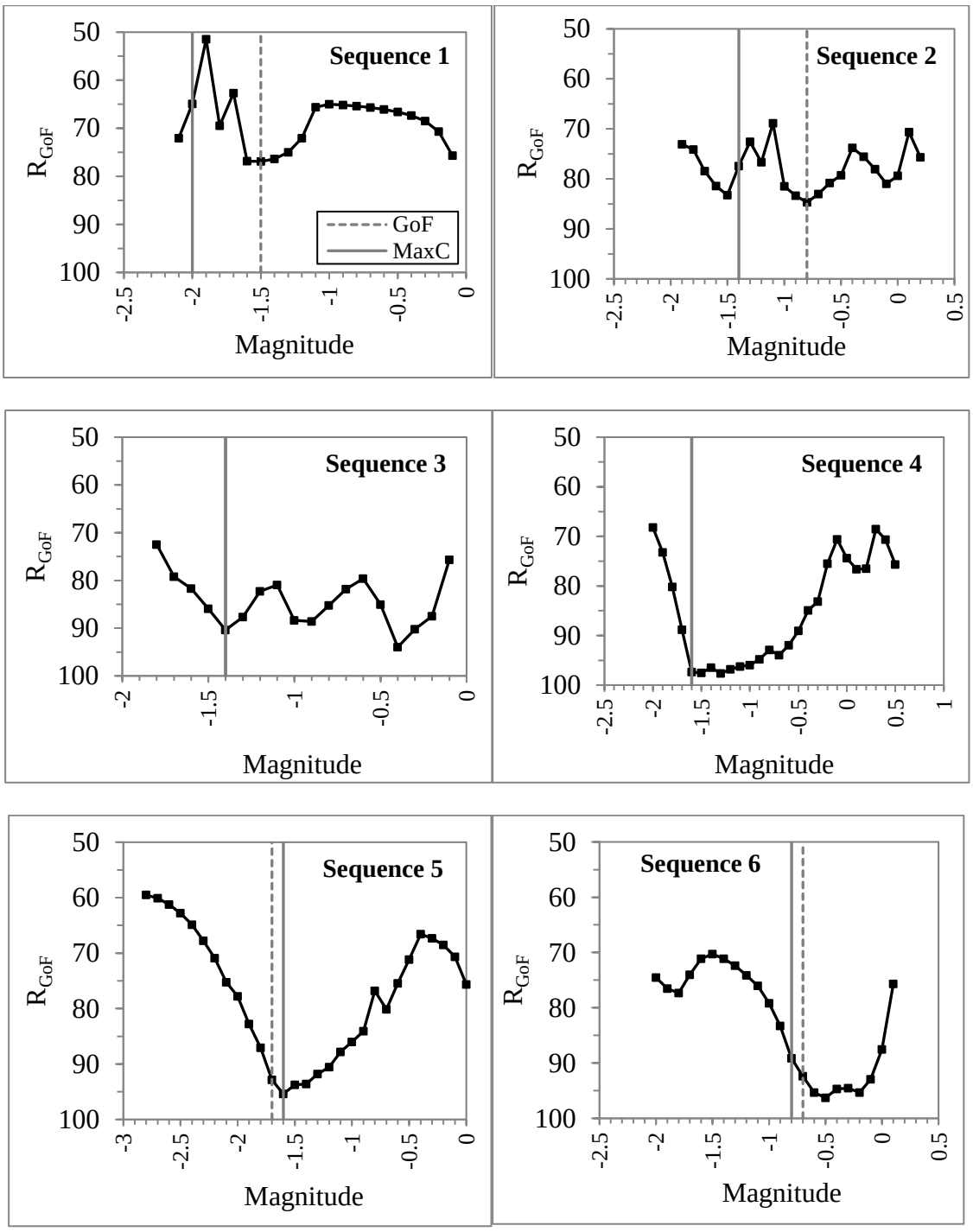

Figure 11. Goodness of Fit, R_{GoF}, for each sequence. Vertical lines show the *Mc* value selected with *MaxC* method (continuous line) and Goodness of Fit method (dashed line). In the case when just one line appears, means that the value of *Mc* using the *MaxC* and the R_{GoF} methodologies are the same.

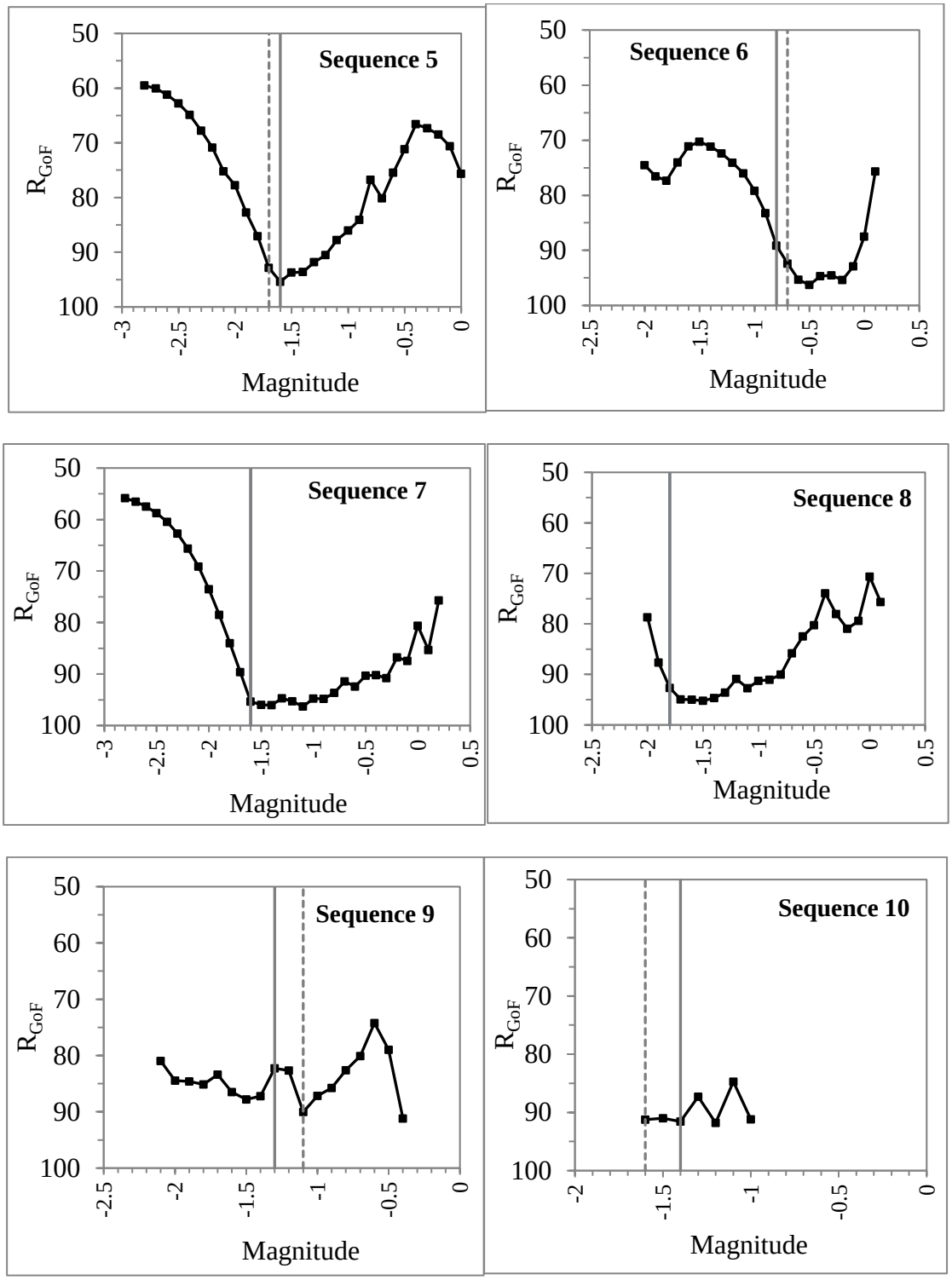

Figure 11. (Continued)

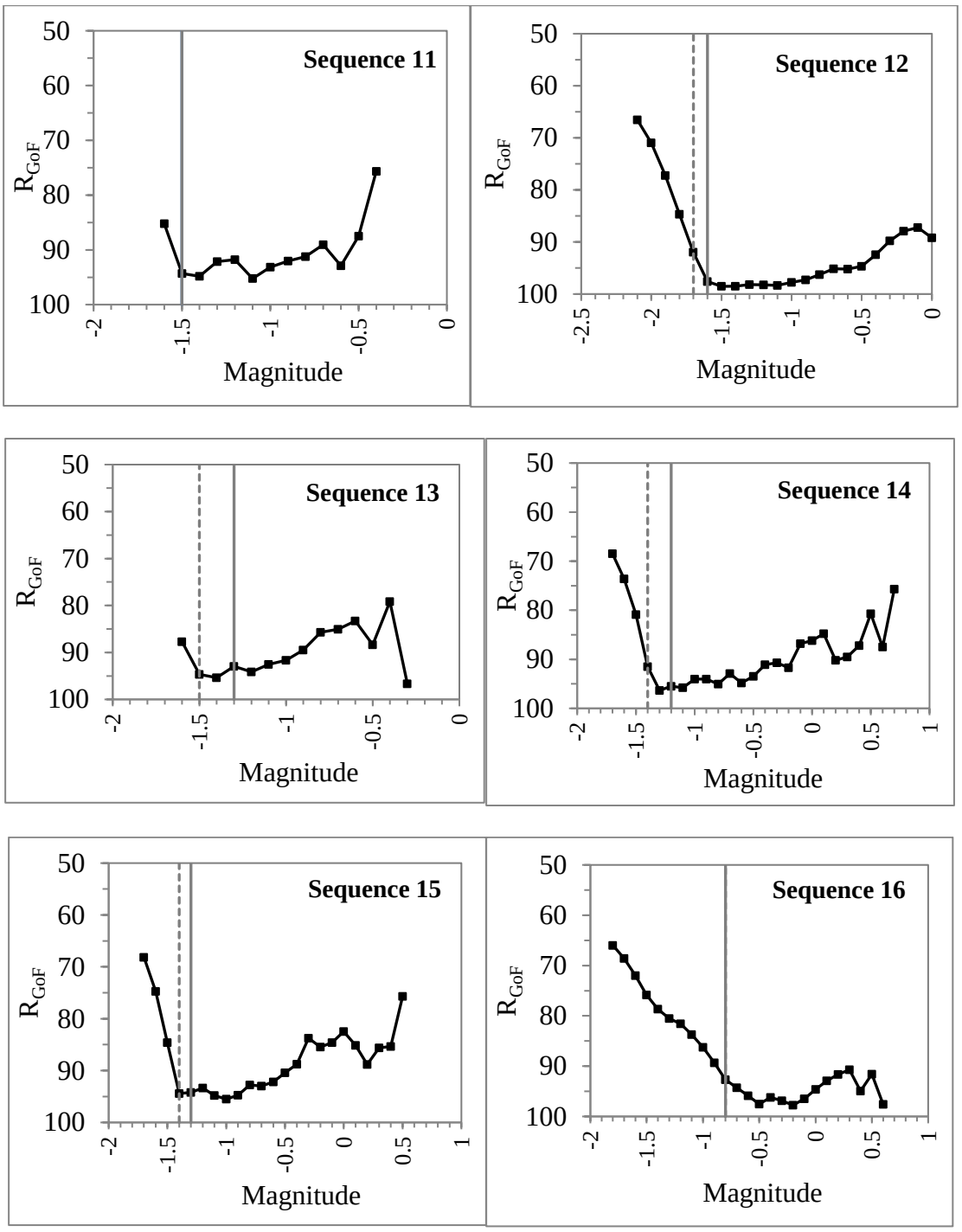

Figure 11. (Continued)

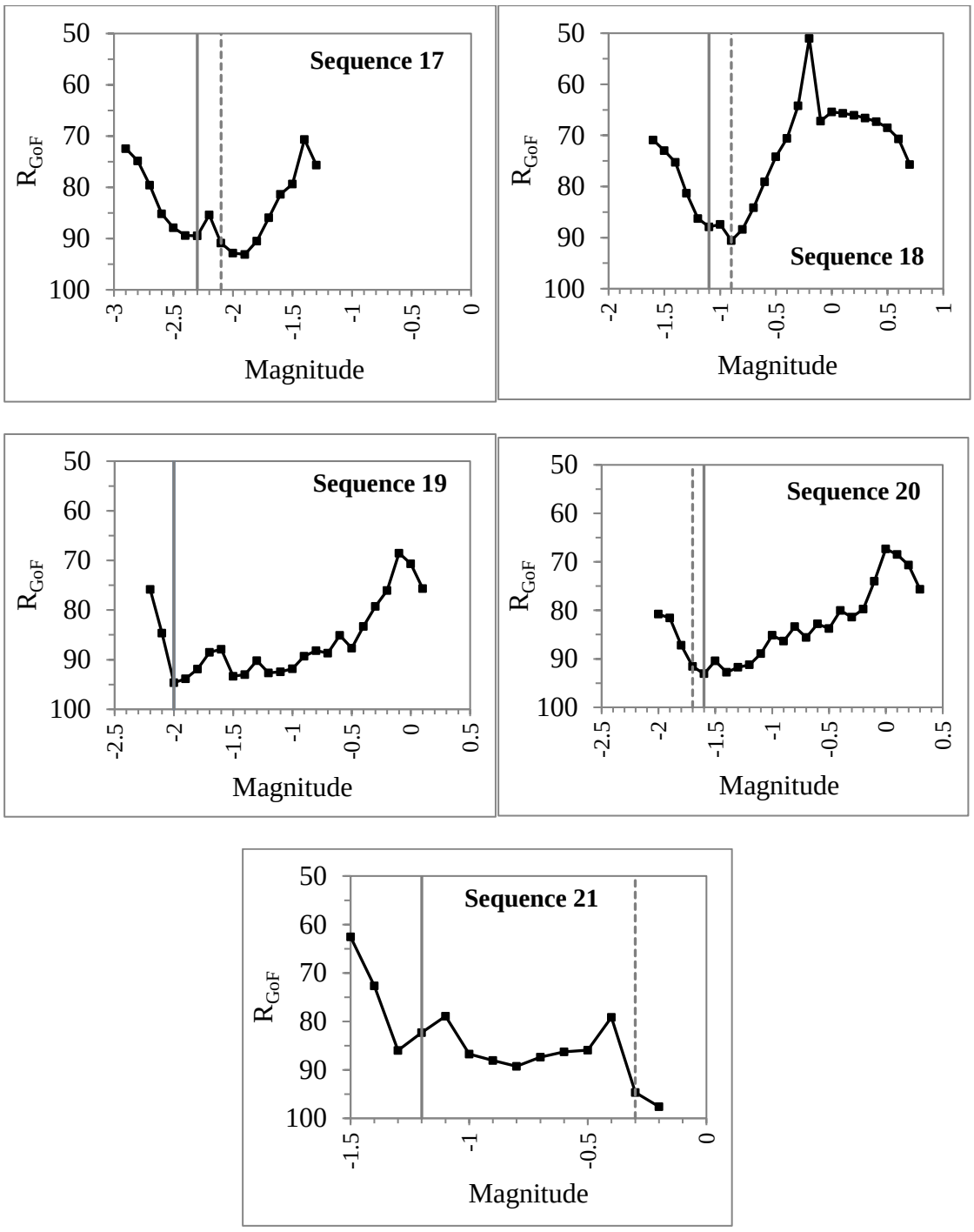

Figure 11. (Continued)

To select a unique *Mc** value for the analysis of the sequences the following methodology was applied:

1) A tentative *Mc** value was selected.
2) Aftershock sequences that satisfies $Mc \leq Mc^*$ are considered for the analysis.
3) Next, the procedure presented in the

4) Figure **12** is applied. This includes the estimation of Gutenberg – Richter's seismic parameters and the Modified Omori´s Law. Only sequences with more than 10 events are considered for the analysis. The correlations between the seismic parameters and the magnitude of the main shock are estimated.
5) Point two and three are repeated N times, where N is the number of sequences to be analyzed.
6) Return to point (1). It is selected the Mc* value that maximizes the correlations between the seismic parameters and the magnitude of the main shock and contains the higher number of sequences for the analysis.

After the previously procedure is finished for various tentative $M_{w,c}$*, the results are compared as shown in Table 5.

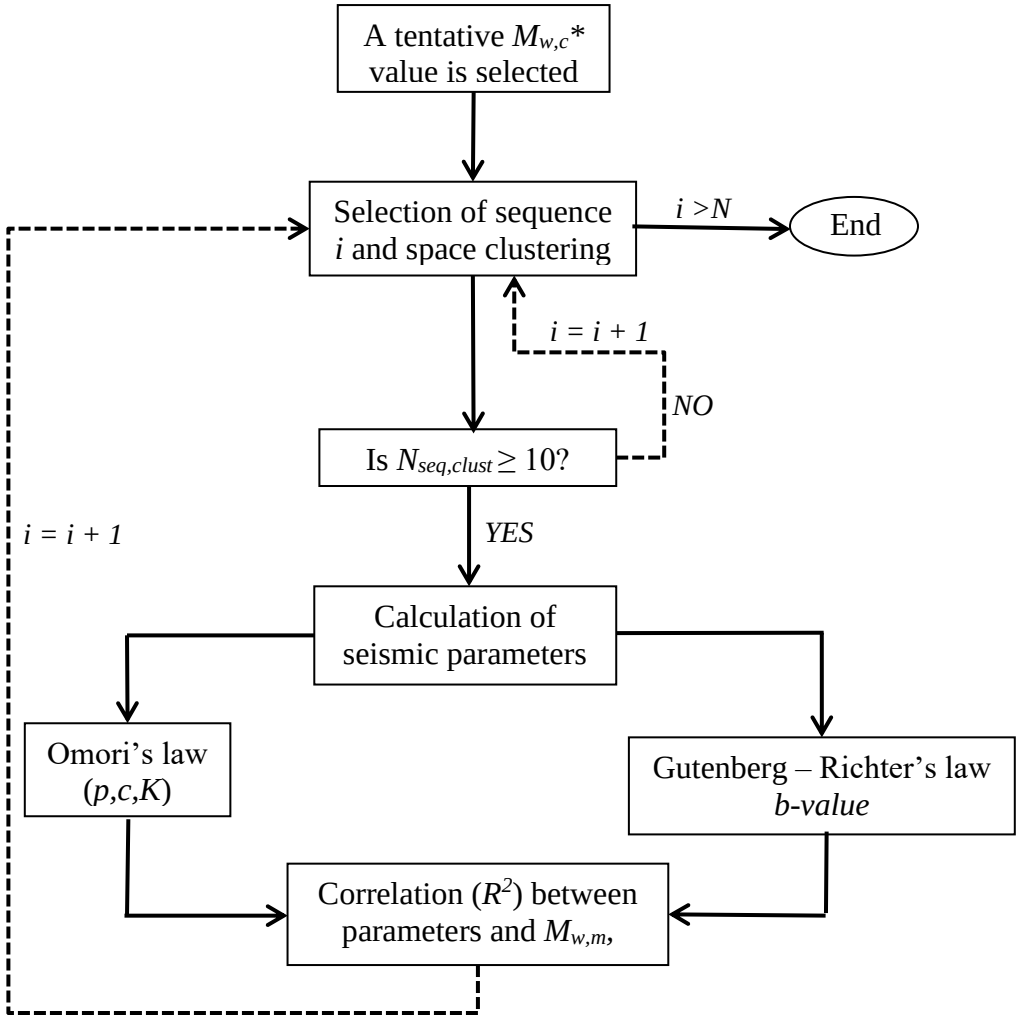

Figure 12. Methodology diagram to estimate *Mc**.

Table 5. Results of optimal R^2 for each combination of seismic parameters obtained by applying methodology presented in Figure 13. For example, the higher value of R^2 for the combination *Mn* and *b*, with a value of *Mc* = -1.3* was 0.01. N_{seq} corresponds to the number of sequences which comply with the conditions $M_{c,seq\,i} \leq Mc^*$ and had more than 10 events in the sequence after the filtering process.

		Mn				log(c)			p		
Mc*	**Nseq**	**log(c)**	**p**	**logK**	**b**	**p**	**logK**	**b**	**logK**	**b**	**logK,b**
-1,8	3	0,06	0,32	0,53	0,53	0,87	0,71	0,70	0,96	0,95	1,00
-1,7	5	0,40	0,33	0,01	0,26	0,31	0,14	0,86	0,26	0,33	0,02
-1,6	8	0,77	0,73	0,27	0,00	0,62	0,50	0,09	0,13	0,01	0,02
-1,5	10	0,52	0,40	0,30	0,00	0,59	0,30	0,08	0,05	0,12	0,02
-1,4	9	0,85	0,28	0,20	0,01	0,34	0,11	0,00	0,05	0,02	0,08
-1,3	**11**	**0,60**	**0,12**	**0,48**	**0,01**	**0,09**	**0,45**	**0,11**	**0,02**	**0,06**	**0,00**
-1,2	11	0,47	0,04	0,38	0,00	0,06	0,28	0,06	0,01	0,29	0,03
-1,1	10	0,00	0,00	0,25	0,00	0,02	0,00	0,60	0,01	0,01	0,09

Based on the above procedure a value of *Mc* = -1.30* was determined. Figure 13 presents the $M_{c,Gof}$ value for each sequence and the 12 sequences selected for further analysis (gray circles). The black (6 sequences) and white circles (3 sequences) are those sequences with $Mc \geq Mc^*$ and with less than 10 events after the pre – processing, respectively. Table 6 shows the detail of the number of events in each seismic sequence after filtering by the magnitude of completeness.

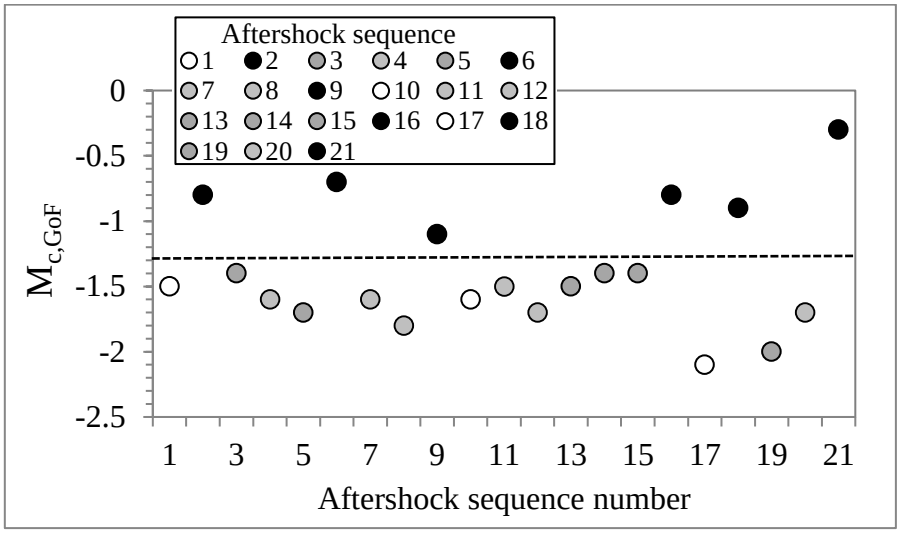

Figure 13. Magnitude of completeness, *Mc*, for each sequence. In white are those sequences with less than 10 seismic events after filtering by *Mc*. In black are those sequences with *Mc* ≥*-1.30*. The dashed line indicates the value of *Mc* = -1.3* for MaxC and GoF methods.

Table 6. Number of events in each seismic sequence after the magnitude of completeness filtering. In bold are those sequences with $Mc \geq Mc^*$ or with less than 10 events.

Seq	Site	M_n	$M_{c,GoF}$	N_{filt}
1	A	1.1	-1,5	**2**
2	Copper Cliff North	1.9	**-0,8**	17
3		2.1	-1,4	61
4		2.4	-1,6	279
5		2.4	-1,7	25
6		2.8	**-0,7**	0
7		3.8	-1,6	249
8	Craig	2.2	-1,8	78
9	Creighton	1.0	**-1,1**	23
10		1.5	-1,6	**9**
11		2.4	-1,5	69
12		2.6	-1,7	711
13		2.9	-1,5	80
14		3.0	-1,4	445
15		3.1	-1,4	498
16		4.1	**-0,8**	2974
17	Fraser	2.4	-2,1	**1**
18	Garson	3.3	**-0,9**	0
19	Kidd Creek	1.6	-2	22
20		3.8	-1,7	33
21	Macassa	3.1	**-0,3**	0

4.3. Space hierarchical Clustering

Once the filtering by magnitude of completeness is done, the hierarchical spatial clustering of the seismic sequences is applied. The different clusters were formed considering a maximum distance of 50 meters. Of all the clusters formed, only the one that contained the main event was considered for further analysis. This ensures that only the main group of seismicity associated in space to the large magnitude event is included into the sequence. The Table 7 summarizes the number of events in the selected cluster of each sequence.

Finally, there will be 11 sequences that will be considered for the next analysis, since the Kidd Creek's cluster has less than 10 events, a value that was considered as a minimum to be able to perform the subsequent calculations.

Appendix B shows the figures with the spatial distributions of the clusters formed in each selected seismic sequence.

Table 7. Number of events in the sequences after filtering and hierarchical clustering (N_{clust}). Value in bold correspond to $N_{clust} < 10$.

Seq	Site	M_n	$M_{c,GoF}$	N_{clust}
3	Copper Cliff North	2.1	-1,4	53
4		2.4	-1,6	192
5		2.4	-1,7	17
7		3.8	-1,6	213
8	Craig	2.2	-1,8	77
11	Creighton	2.4	-1,5	41
12		2.6	-1,7	627
13		2.9	-1,5	54
14		3.0	-1,4	402
15		3.1	-1,4	408
19	Kidd Creek	1.6	-2	21
20		3.8	-1,7	**8**

5. Seismic parameters of mining – induced aftershock sequences

In the following section, the statistical properties of the seismic parameters of mining induced aftershock sequences are presented. The scaling relations (Modified Omori's law, Gutenberg-Richter and Båth's law) and a stochastic model (Reasenberg & Jones) are applied to the mining-induced aftershock sequences from Ontario, Canada.

Some of these results are published in Vallejos & Estay (2018).

5.1. Gutenberg – Richter's law

Figure presents the frequency distribution of each sequence and its Gutenberg – Richter's adjustment. Figure 15 shows the *b-values* from Gutenberg-Richter's law for each filtered and clustered sequence as a function of the main shock magnitude. The regression line for all the data is included in this figure. In general, there is no clear dependency of the *b-value* on the main shock magnitude.

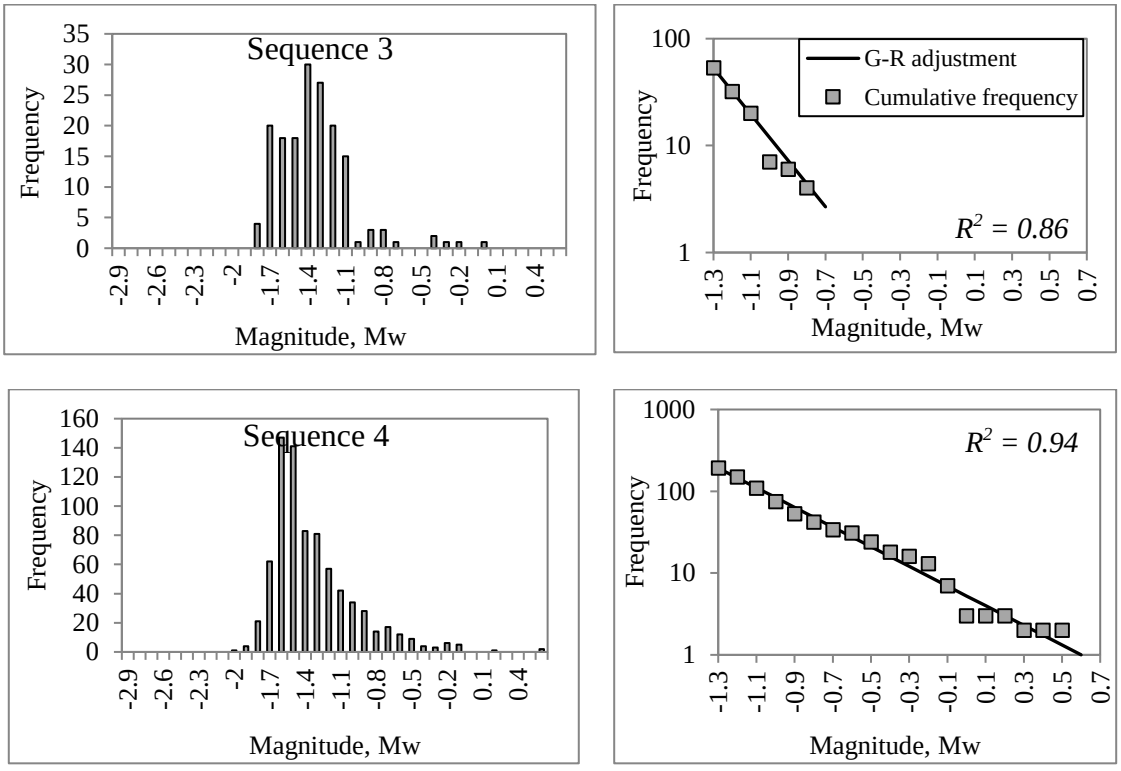

Figure 14. Frequency – magnitude distribution of each aftershock sequence in analysis before filtering and its respective Gutenberg – Richter adjustment after filtering.

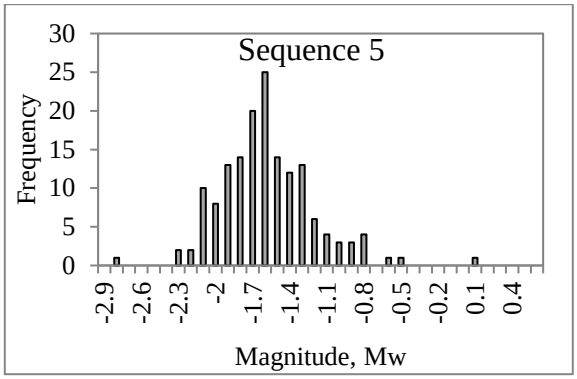

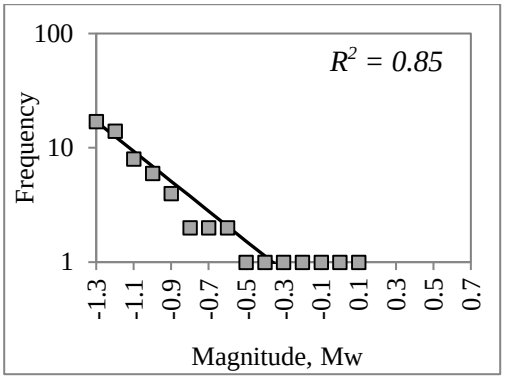

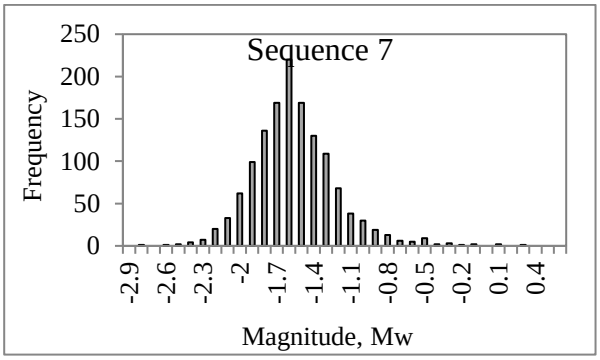

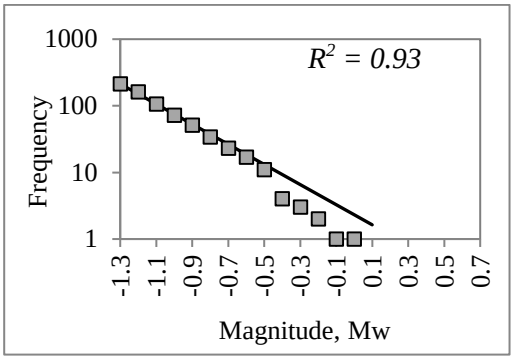

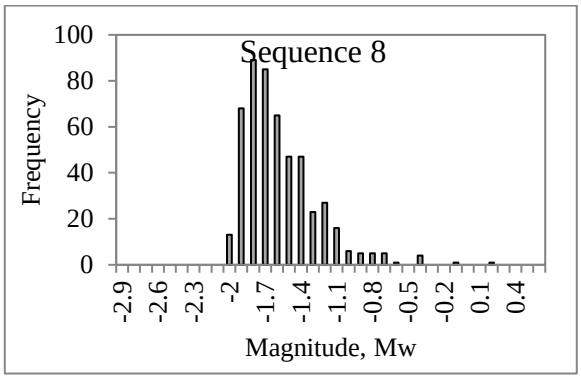

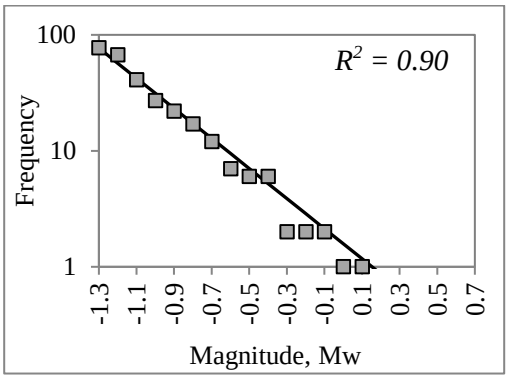

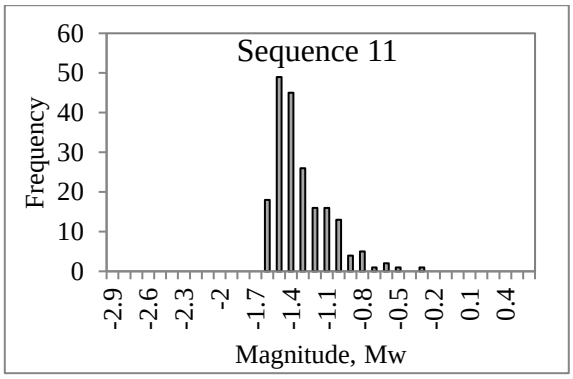

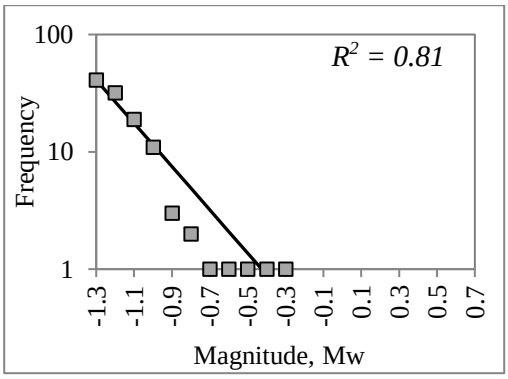

Figure 14. (continued)

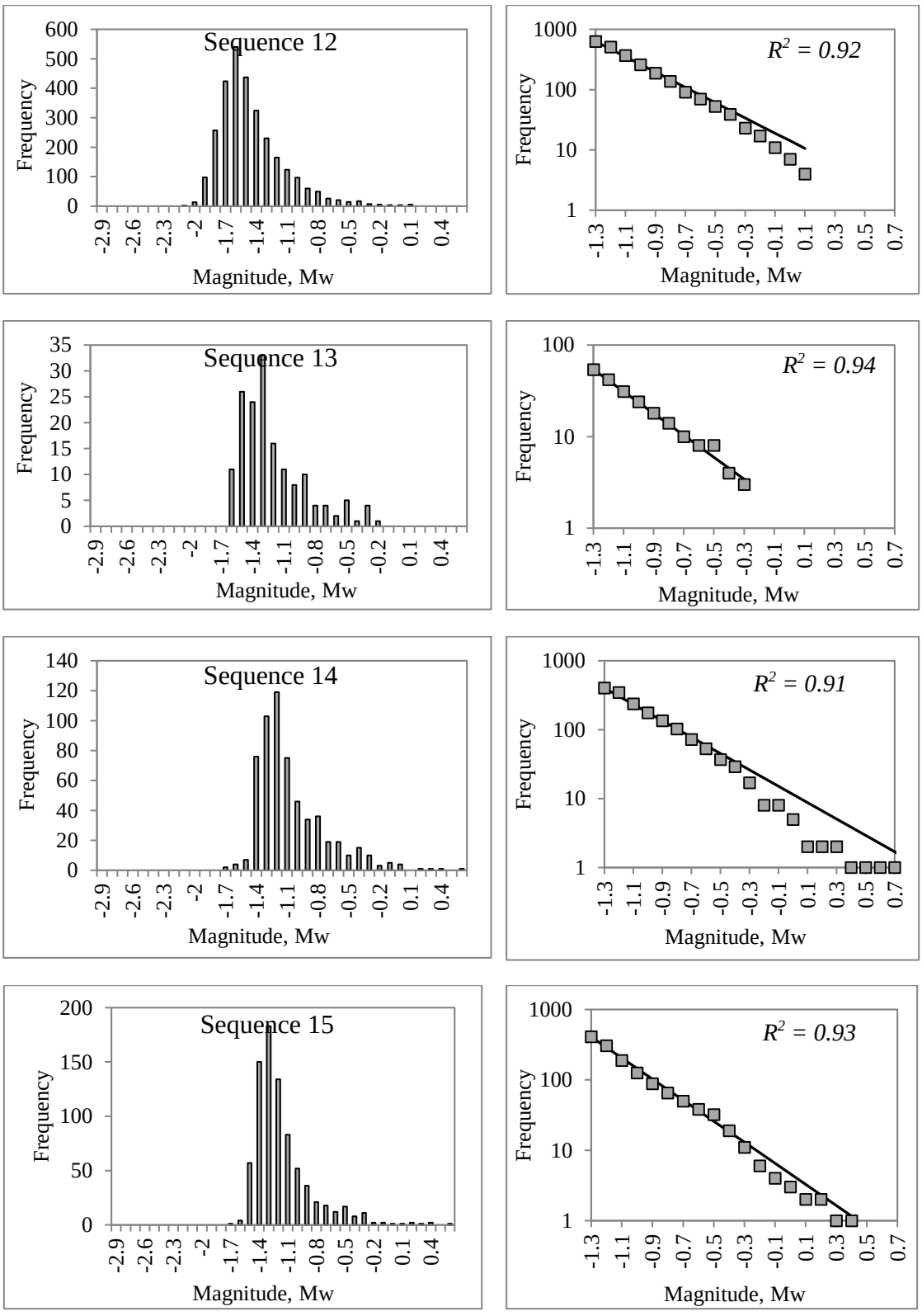

Figure 14. (continued)

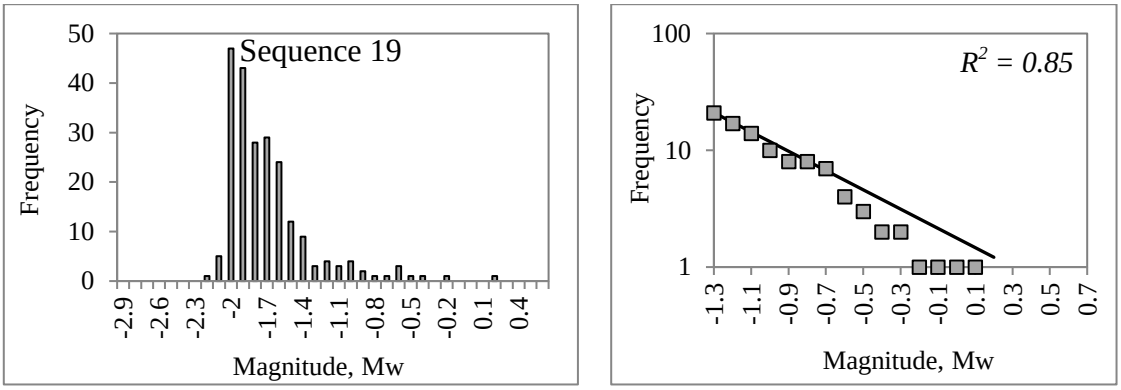

Figure 14. (continued)

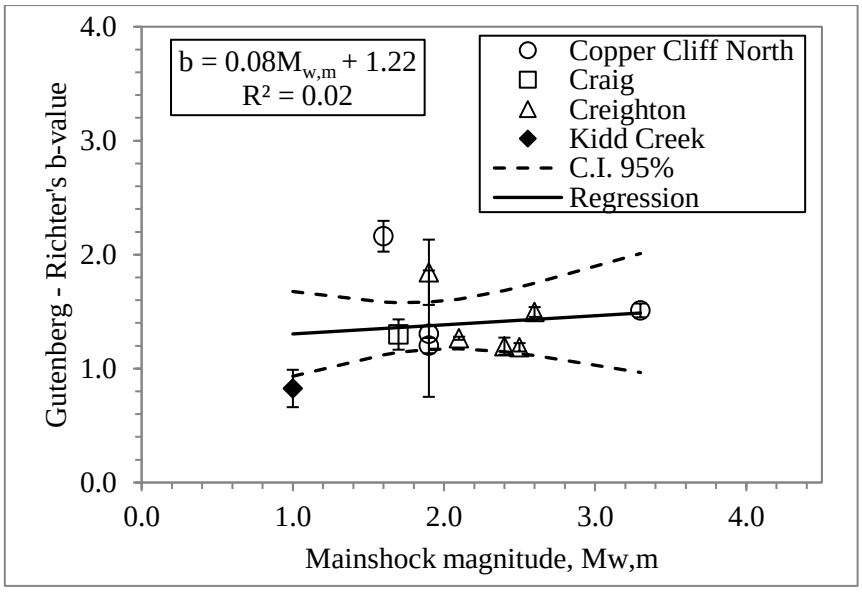

Figure 15. Dependence of *b-value* on the main shock magnitude, $M_{w,m}$ for each filtered and clustered sequence. Errors bars correspond to the standard error proposed by Shi & Bolt (1982).

The *b-value* has a mean of 1.39 ± 0.4. This mean value is higher the ranges published, for example, by Wiemer, et al. (2002) and Nuannin, et al. (2002), for induced seismicity in South Africa and Sweden, respectively, but lower that those obtained for El Teniente Mine (Estay, 2014). Variations of *b-values* in induced seismicity can be explained by the high and low stress conditions (Schorlemmer, et al. 2005) (for low values of b, higher stress in the mine), thermal gradients (Scholz, 1968) and the effects of pore pressure in rock (Warren and Latham, 1970). Schorlemmer et al (2005) indicates that normal faulting events show the highest *b-values*, strike slip events show intermediate values and thrust events the lowest.

However, when considering only the results for the Creighton mine, a value of $R^2 = 0.32$ indicating a possible positive correlation between the *b - value* and the magnitude of the main event.

5.2. Modified Omori's law

The modified Omori's law *p-value* varies from sequence to sequence within range of 0.70 to 1.09, and an average of 0.83 ± 0.13, in accordance with the results obtained by Utsu et al. (1995), Wang (1994) and Nyffeneger & Frohlich (2000). Null correlation between *p* and the magnitude $M_{w,m}$ of the main event is found (Figure 16a).

It is expected that for mining – induced aftershock sequences, the mechanism involved (e.g., pillar burst, fault slip, strain burst) may play a role in the aftershock productivity and p – value. This has been accounted – for separately in the statistics for intra – plate and inter – plate earthquakes (Guo & Ogata, 1995; Yamanaka & Shimazaki, 1990). The dispersion showed in Figure 16a reflects the nature of induced seismicity, suggesting that the mechanism of seismicity may play a role in determining the speed of decay as occur in tectonic earthquakes.

As was done in section 5.1 for the *b – value*, considering only the values obtained for the Creighton mine, a relatively high correlation between *p* and $M_{w,m}$ is obtained ($R^2 = 0.66$).

Figure 16 also presents the correlations between the parameters *K* and *c* of the Modified Omori's law (MOL) with the magnitude of the main event. Both parameters present significant positive correlations, with value of the coefficient of adjustment R^2 equals to 0.49 and 0.59 respectively.

As expected, *K-value* increases as the main shock magnitude increases too. This is because *K-value* is an activity parameter related to the number of events within the sequence.

On the other hand, in tectonic analysis, the physical meaning of the *c-value* is attributable to the complex feature of the rupture process (Yamakawa, 1968) as a time shift that relates to the rate of aftershocks in the early part of the sequence (Enescu, et al., 2009) that have smaller signal amplitudes and are not completely detected (Hamaguchi & Hasegawa, 1970; Kagan & Houston, 2005). Also, *c-value* behaves as the constant which does not allow the equation (12) to be undefined at $t = 0$ (Narteau, et al., 2002). This behavior seems to be replicated by the *c-values* in induced seismicity (Figure 16c), which at higher magnitudes, present higher *c-values*, so there would be aftershocks in an early stage of the sequence that the monitoring system is unable to detect.

The values of the MOL's parameters for each sequence are shown in Table 8.

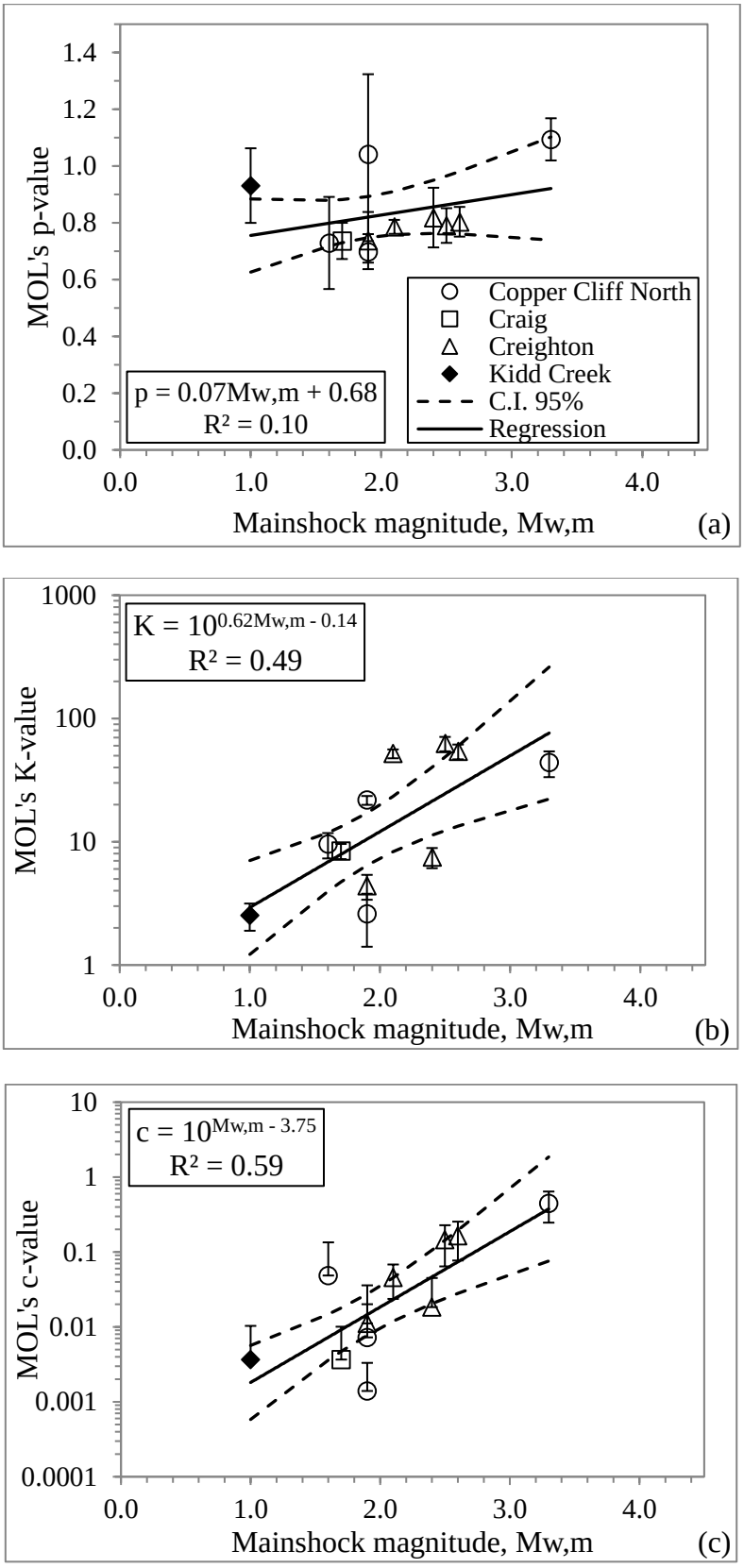

Figure 16. Dependence of the MOL parameters (a) *p-value* (b) *K-value* and (c) *c-value* with the main shock magnitude. *p*, *c* and K error bars correspond to the uncertainty estimation from the MLE method.

Table 8. MOL's parameters for each aftershock sequence.

Sequence	Site	$M_{w,m}$	*K (events/hr)*	*c (hrs)*	*p*
3	Copper Cliff North	1.6	9.54	0.05	0.73
4	Copper Cliff North	1.9	21.72	0.00	0.70
5	Copper Cliff North	1.9	2.60	0.01	1.04
7	Copper Cliff North	3.3	43.76	0.44	1.09
8	Craig	1.7	8.41	0.00	0.74
11	Creighton	1.9	4.39	0.01	0.74
12	Creighton	2.1	51.82	0.05	0.79
13	Creighton	2.4	7.50	0.02	0.82
14	Creighton	2.5	62.51	0.15	0.79
15	Creighton	2,6	54.03	0.17	0.80
19	Kidd Creek	1.0	2.53	0.00	0.93

5.3. Båth's law

The Table 9 shows the values of the difference ΔM and ΔM^* considering the 11 selected sequences for the analysis.

A mean of $\Delta M = 2.1 \pm 0.6$ is obtained, which is clearly larger than proposed by Båth for tectonics seismicity. Table 9 also presents the results of applying equation (20) to the induced seismicity sequences. An average of $\Delta M^* = 1.5 \pm 0.6$ is obtained. This value is very close to the value proposed by Båth, which, also, is a better result that the one obtained with ΔM.

Table 9. Results of ΔM and its modified form, ΔM^*.

# sequence	Site	$M_{w,m}$	M_{LA}	*a*	*b*	*M**	ΔM	ΔM^*
3	Copper Cliff North	1.6	-0.8	-0.50	2.16	-0.2	2.4	1.8
4	Copper Cliff North	1.9	0.6	1.10	1.20	0.9	1.3	1.0
5	Copper Cliff North	1.9	0.1	-0.06	1.31	0.0	1.8	1.9
7	Copper Cliff North	3.3	0.1	0.83	1.51	0.6	3.2	2.7
8	Craig	1.7	-0.1	0.61	1.30	0.5	1.8	1.2
12	Creighton	1.9	-0.8	-0.25	1.85	-0.1	2.7	2.0
13	Creighton	2.1	0.1	1.55	1.27	1.2	2.0	0.9
14	Creighton	2.4	-0.3	0.56	1.20	0.5	2.7	1.9
15	Creighton	2.5	0.3	1.44	1.19	1.2	2.2	1.3
16	Creighton	2.6	0.4	1.13	1.50	0.8	2.2	1.8
20	Kidd Creek	1.0	-0.2	0.49	0.83	0.6	1.2	0.4

5.4. Reasenberg – Jones model

In order to estimate *p, c, a'* and *b* values for Reasenberg – Jones model, the empirical tendencies obtained in sections 5.1 and 5.2 were used.

Because the correlation obtained for the parameter *p* with $M_{w,m}$ is close to 0, a mean value of $p = 0.83$ was used.

The value of the parameter *c* was estimated using equation (33):

$$c = 10^{-3.75+M_{w,m}} \tag{33}$$

Considering a *Mc – value* of -1.3, equation (16) can be expressed as

$$c = 10^{-2.50+(\bar{M}_{w,m}-M_c)}. \tag{34}$$

Furthermore, *a'* and *b* values were directly obtained from the equation presented in Figure 16b, where *K – value* is written as:

$$K = 10^{-0.14+0.62M_{w,m}}. \tag{35}$$

Considering a *Mc – value* equal to -1.3, equation (35) can be written in function of the difference $M_{w,m} - M_c$ as:

$$K = 10^{-0.95+0.62(M_{w,m}-M_c)}. \tag{36}$$

This relation is associate to $10^{a'+b(M_{w,m}-M)}$ of equation (22), so $a' = -0.95$ and $b = 0.62$.

5.5. Comparison between mining – induced and tectonic seismic parameters of aftershock sequences

The paper that presents the results of this subsection is under preparation to be submitted to the *Tectonophysics journal* (Estay & Vallejos, xxxx).

Several authors have calculated *a', b – value* and Omori's seismic tectonic parameters worldwide (Wang, 1994; Wiemer & Katsumata, 1999; Nyffeneger & Frohlich, 2000), and particularly in Japan (Utsu, 1969; Utsu, 1970; Guo & Ogata, 1995; Enescu & Ito, 2003; Nanjo et al, 2007; Enescu et al, 2009), California (Gutenberg & Richter, 1944; Reasenberg & Jones, 1989; Kisslinger & Jones, 1991; Mori & Abercrombie, 1997; Gasperini & Lolli, 2006; Lolli & Gasperini, 2006), Italy (Gasperini & Lolli, 2006; Lolli & Gasperini, 2006) and New Zealand (Eberhart – Phillips, 1998; Gasperini & Lolli, 2006). A summary of the values of tectonic seismic parameters exposed in some of the previous research are presented in Table 10. For comparison the first line of Table 10 presents the average results obtained for mining – induced aftershock sequences.

Table 10 has the following implications:

- The average of the *b – value* of mining induced seismicity is higher than each *b – value* of the tectonic seismicity.
- The average of the *a', p* and *c* values of the mining induced seismicity are lower than the average of the tectonic seismic parameters.
- The average value of *p* for tectonic aftershock sequences is almost 1.0 with a variation ranging from 0.12 to almost 2.1, close to that described by Utsu et al. (1995).
- The value of *a'*, on average, is much lower for the mining induced aftershock sequences. However, considering equation (36) the value of *a'* is within the order of those obtained from the tectonic seismicity.
- c – value is similar between tectonic seismicity and the average obtained for mining induced seismicity. However, in several tectonic investigations, the value of *c* is simply considered equal to cero.

The Table 11 presents a summary of the correlations between seismic parameters of aftershock sequences for mining induced and tectonic seismicity.

For the seismic parameters of Ontario mining induced aftershock sequences, it is observed that:

- A high positive correlation exist between parameters *c* and *K* with $M_{w,m}$. Also, parameter *a'* has a good negative correlation with *b – value*.
- In a lower degree, *p* and *b values* are correlated with $M_{w,m}$, and parameter *c* are correlated with *a'* and *p*.

- No correlation was found between *p* and the *b – value*.
- *a'* and *b* has the highest negative correlation (-0.88).

For tectonic aftershock sequences:

- *b – value* has a good negative correlation with *a'* in all cases (lower than -0.59).
- *a'* with *log(c)* and *p* for Italy and New Zealand presents regular positive correlation (0.31 – 0.57).
- Similar too mining induced aftershock sequences, no significant correlations were found between *p* and *b*, except for Japanese sequences which has a correlation of 0.54.

Table 10. Summary of some researches that estimates the Gutenberg-Richter's, Omori's and Reasenberg – Jones's parameters for tectonic aftershock sequences from different regions. The first line includes the results of this thesis for mining induced aftershock sequences. (1) Eberhart-Phillips (1998); (2) Reasenberg & Jones (1989); (3) Kisslinger & Jones (1991); (4) Enescu et al. (2009); (5) Ogata (1983); (6) Guo & Ogata (1995); (7) Mori & Abercrombie (1997); (8) Gasperini & Lolli (2006); (9) Lolli & Gasperini (2006). The values of *K* and *c* are in [events/day] and [days] respectively, except Ontario sequences which K and *c – values* are in events/hour and hour respectively.

a'		**b**		**p**		**K**		**c**		**Number of sequences**	**Years**	**Geographic region**
mean	std. dev	mean	std. dev	mean	std. dev	mean	std. dev	mean	std. dev			
-3.60	**1.29**	**1.39**	**0.36**	**0.83**	**0.13**	**24.44**	**23.62**	**0.08**	**0.13**	**11**	**2004 – 2009**	**Ontario, Canada**
-1.79	0.74	1.01	0.15	1.04	0.31	--	--	0.08	0.11	17	1987 – 1995	New Zealand[(1)]
-1.76	0.07	0.9	0.02	1.07	0.03	--	--	--	--	62	1933 – 1987	California[(2)]
--	--	1.06	0.26	1.11	0.25	--	--	--	--	37	1933 – 1981	California[(3)]
--	--	0.96	0.1	1.06	0.07	8.51	3.34	0.01	0.01	4	2000 – 2007	Japan[(4)]
--	--	--	--	1.27	0.35	351.38	482.54	0.30	0.47	3	1948 – 1964	Japan[(5)]
--	--	0.97	0.20	1.11	0.24	--	--	--	--	32	1972 – 1993	Japan[(6)]
--	--	1.14	0.01	--	--	--	--	--	--	--	1978 – 1994	Northern California[(7)]
--	--	1.24	0.01	--	--	--	--	--	--	--	1978 – 1994	Northern California w/o aftershock[(7)]
--	--	1.18	0.01	--	--	--	--	--	--	--	1983 – 1994	Southern California[(7)]
--	--	1.27	0.01	--	--	--	--	--	--	--	1983 – 1994	Southern California w/o aftershocks[(7)]
-1.81	0.62	0.9	0.18	1.09	0.25	13.07	16.69	0.05	0	64	--	California[(8)]
-1.79	0.74	1.01	0.15	0.99	0.34	45.03	29.26	0.08	0.11	17	--	New Zealand[(8)]
-1.83	0.67	0.99	0.17	0.99	0.34	33.21	54.52	0.61	1.53	30	--	Italy[(8)]
--	--	--	--	0.79	0.26	28.13	25.45	0.09	0.42	37	1933 – 2004	California[(9)]
--	--	--	--	0.86	0.25	24.82	20.68	0.15	0.22	9	1976 – 2003	Italy[(9)]
-1.80	***0.03***	***1.05***	***0.12***	***1.03***	***0.13***	***72.02***	***123.8***	***0.17***	***0.20***			

Table 11. Coefficients, intercepts and correlation, ρ, between seismic parameters of the Ontario's mining induced and tectonic aftershock sequences. The first parameter corresponds to the dependent variable and the second one to the independent variable.

Parameters	Dataset	Coefficient	Intercept	ρ
b, $M_{w,m}$	Ontario	0.08	1.22	0.14
p, $M_{w,m}$		0.07	0.68	0.32
log(K), $M_{w,m}$		0.62	-0.14	0.70
log(c), $M_{w,m}$		1.0	-3.75	0.77
a', b	Ontario	-3.15	0.78	-0.88
	Italy	-2.37	0.52	-0.59
	California	-2.50	0.45	-0.72
	New Zealand	-3.51	1.76	-0.71
a', p	Ontario	-1.26	-2.55	-0.13
	Italy	0.61	-2.43	0.31
	California	0.20	-2.03	0.08
	New Zealand	1.12	-2.96	0.47
a', c	Ontario	-4.26	-3.25	-0.44
	Italy	0.16	-1.93	0.37
	New Zealand	2.76	-2.01	0.41
a', log(c)	Ontario	-0.80	-4.92	-0.49
	Italy	0.50	-1.36	0.57
	New Zealand	0.47	-1.11	0.35
b, p	Ontario	-0.67	1.95	-0.25
	Italy	-0.10	1.09	-0.19
	California	-0.15	1.07	-0.21
	New Zealand	-0.06	1.07	-0.12
	Japan	0.44	0.48	0.54
p, c	Ontario	0.55	0.79	0.55
	Italy	0.10	0.93	0.43
	New Zealand	1.57	0.92	0.55
p, log(c)	Ontario	0.05	0.92	0.30
	Italy	0.16	1.14	0.36
	New Zealand	0.37	1.59	0.67

Figure 17 to Figure 20 presents a graphical comparisson between the results obtained for mining induced and tectonics aftershock sequences from California, Italy, New Zealand and Japan was made.

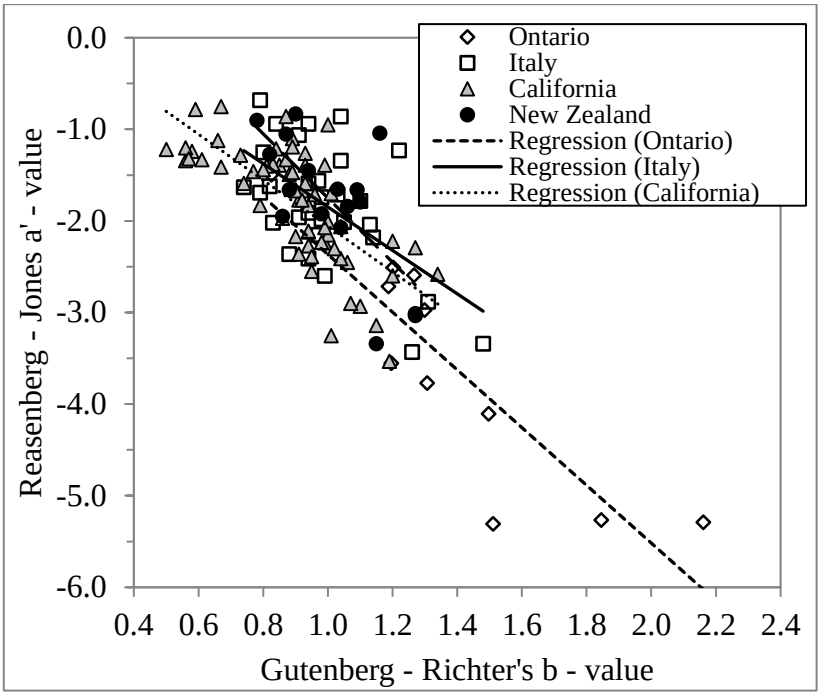

Figure 17. Comparison between the *a'* and *b* parameters estimated for mining induced (Ontario) and tectonic (Gasperini & Lolli, 2006) aftershock sequences.

Tendencies of tectonic and induced sequences are similar, with decreassing *a'* value while *b* value increases.

The Figure 18 compares *p* and *b-values*. There is no significant correlation between them in any sequence, according with the results of Gasperini & Lolli (2006). Also, the decreasing tendencies in all cases coincide with Kisslinger & Jones (1991).

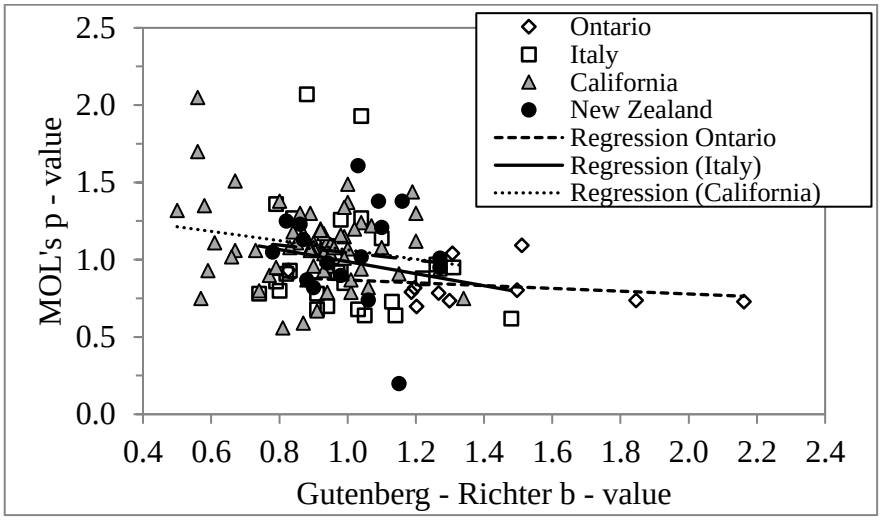

Figure 18. Comparison between the b values of Gutenberg – Richter's law and the *p – values* of the Modified Omori's law for Ontario mining induced and tectonic (Gasperini & Lolli, 2006) aftershock sequences.

Guo & Ogata (1995) have shown a better correlation between *b* and *p-values* using Japan's tectonic aftershock sequences (Figure 19). Also, unlike the results in Figure 18, Figure 19 exhibit a positive tendency between *p* and *b-values*, coinciding with the result obtained by Utsu (1961).

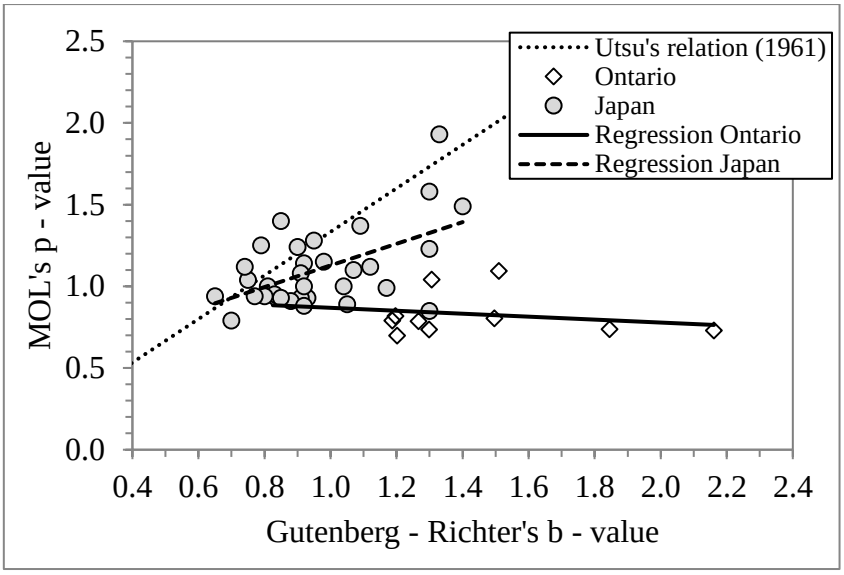

Figure 19. Comparison between *p* vs *b* parameters from Ontario's induced and Japan (Guo & Ogata, 1995) aftershock sequences. Utsu's relation is also included as a reference (Utsu, 1961).

The variability and differences in tendencies in the different seismogenic zones, are not explained by Gasperini & Lolli (2006) or Guo & Ogata (1995). Several studies that have researched about the diverse factors that affect the *p-value* (Mogi, 1962; Nur & Booker, 1972; Reasenberg & Jones, 1989; Kisslinger & Jones, 1991; Wiemer & Katsumata, 1999), not drawing any conclusions of the significant factors that control the *p – value* in tectonic seismicity.

Tahir (2011) found that *p – value* is related to the focal mechanism associated to seismicity using earthquake sequences from western Asia, with mainshock magnitude $M_s \geq 7.0$. He found that *p – values* are higher for thrust events than for strike slip events. In the other hand, using the world wide Global Centroid Moment Tensor (CMT) and the United States Geological Survey (USGS) seismic catalogues, the author found a higher *p – value* for normal mechanism than for thrust or strike slip ones.

The Figure 20 presents a comparison between the *p* and *log(c)* Modified Omori's law parameters for mining induced and tectonic aftershock sequences. The induced seismicity parameters presents a positive highly correlation, which also occurs for the data of Italy and New Zealand. This correlation was explained by Gasperini & Lolli (2006) because of the interplay between those parameters within the maximum likelihood estimation procedure.

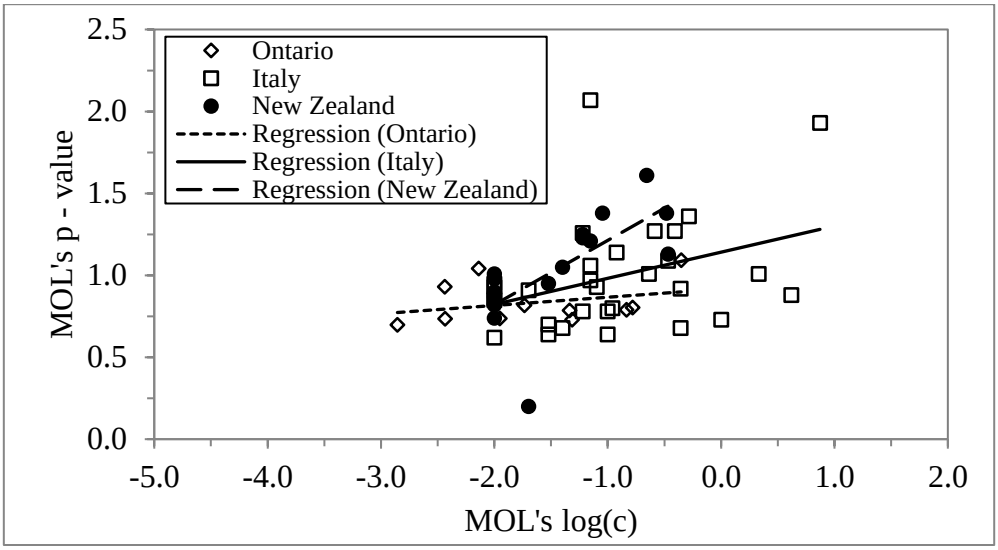

Figure 20. Comparison between *p* and *log(c)* parameters of the Modified Omori's law for Ontario Italy and New Zealand (Gasperini & Lolli, 2006) aftershock sequences.

Figure 21 compares the results obtained by Ouillon & Sornette (2005), and the mining induced aftershock sequences uses in this thesis. This figure indicates that mining induced aftershock sequences presents higher *p – values* than those exposed by Ouillon & Sornette (2005) for $M_L < 4.0$, which corresponds to a faster decay of the Omori's law. Some reasons of this difference are, among others:

1. The seismic catalogue used by Ouillon & Sornette is not complete. Given the years of the seismic data (1932 – 2003) it is difficult to reach a magnitude of completeness lower than 4.0. This effect could underestimate the *p – value* or incorporate higher errors in its estimation.
2. Effect of the focal mechanism. As discussed before, the *p – value* has a relation with the type of focal mechanism (normal, strike slip and thrust). Considering the magnitude of completeness not a problem, then, following the results of Tahir (2011), the lower values of *p* coincide with the strike slip mechanism. Thus, the higher values o *p* for the induced aftershock sequences may represent a normal mechanism.

This last point can be verified approximately using the seismic aftershock sequences of Gasperini & Lolli (2006).

Chiarabba et al (2005) and Stirling et al (2002) defined certain zones of seismotectonics for Italy and New Zealand, respectively (Figure 22). Using this and the data of Gasperini & Lolli the *p – value* can be estimate for each focal mechanism (Table 12), agreeing with the results of Tahir (2011).

However, the slope of 0.10 is within the range 0.10 – 0.15 proposed by Ouillon & Sornette (2005) based on the superposition of crustal aftershock sequences and inferences from multifractal model.

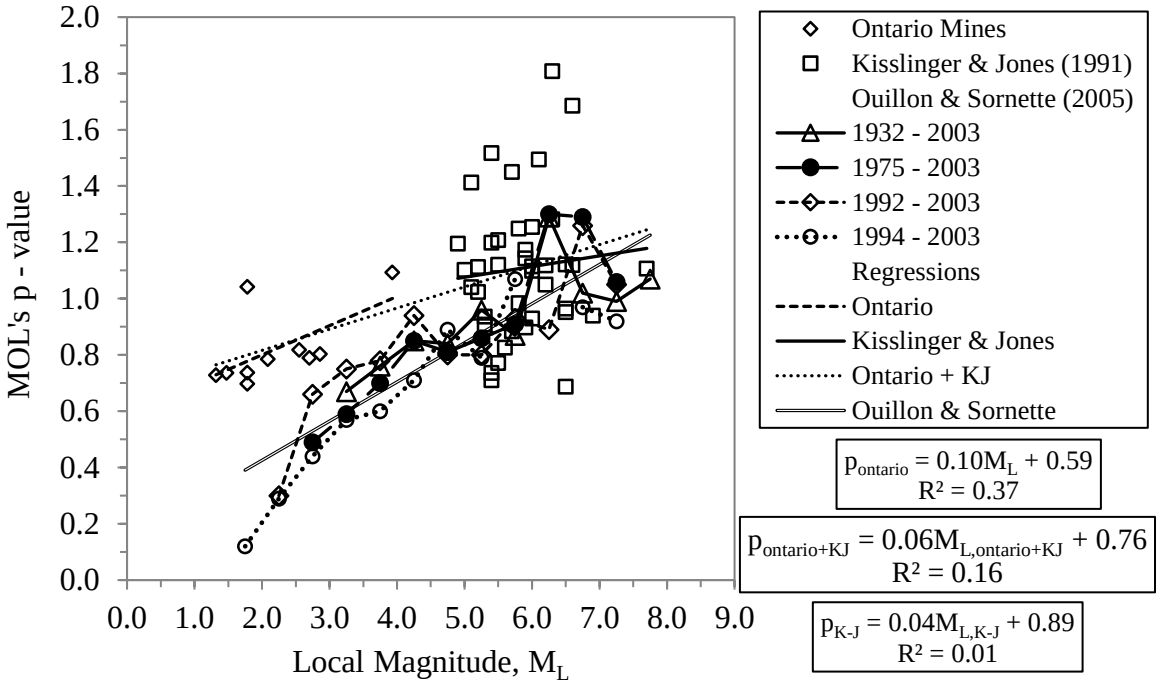

Figure 21. *p-values* as a function of the main shocks in local magnitude (M_L, Table 4) for the mining induced aftershock sequences (Ontario Mines), Ouillon & Sornette's California aftershock sequences from 1932 to 2003 and Kisslinger & Jones's California aftershock sequences from 1932 to 1988 (graph modified from Ouillon & Sornette, 2005).

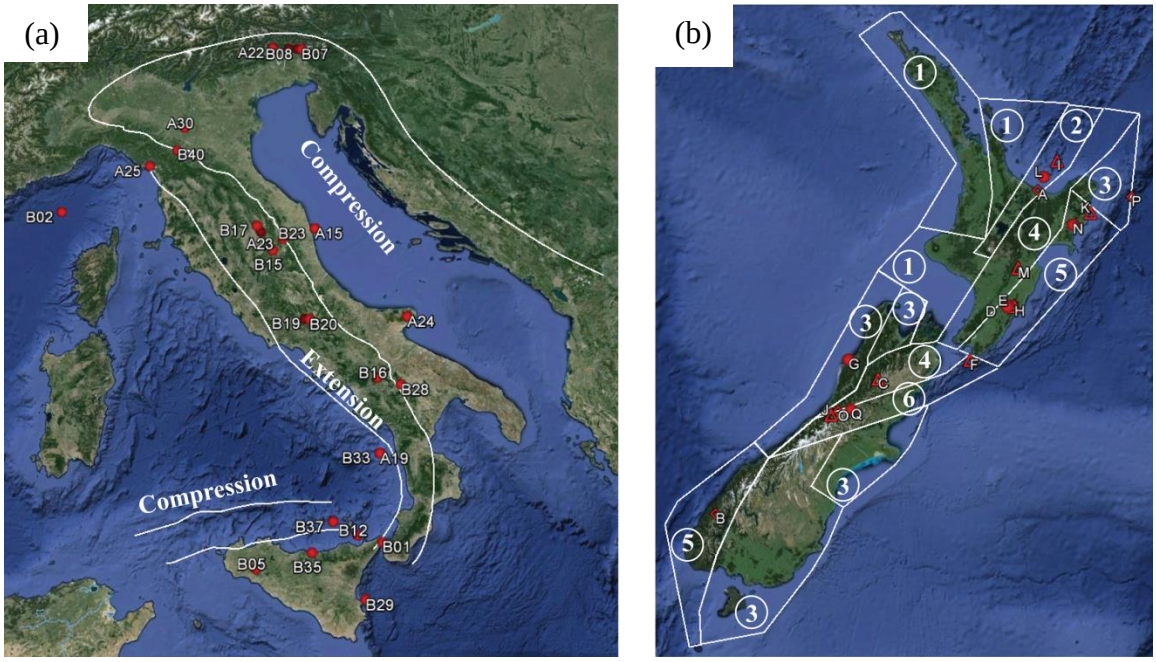

Figure 22. Faulting zones defined by: (a) Modified from Chiarabba et al (2005). Each name in the red dots corresponds to the originally sequence's name used by Gasperini and Lolli (2006); (b) Modified from Stirling et al (2002). Each number refers to a faulting style: 1. Normal, 2. Normal (Termal Volcanic Zone), 3. Reverse, 4. Strike-slip, 5. Reverse & Strike-slip, 6. Strike-slip & Reverse. Symbols and labels are the same used by Eberhart-Phillips (1998): $M_w \geq 5.5$ (triangles), $M_w \geq 6.0$ (circles), $M_w \geq 6.5$ (rhombus).

Table 12. *p – values* for Italy and New Zealand for each type of focal mechanism. In case of New Zealand, the mechanism Strike Slip + Normal/Thrust or Normal/Thrust + Strike Slip were considered as Strike Slip and Normal/Thrust respectively.

Focal Mechanism	Italy	New Zealand
Normal	1.05	1.27
Thrust	0.94	1.04
Strike Slip	--	0.93

6. Re-entry protocol development

In this section, a space – time – magnitude re – entry protocol is proposed (Vallejos & Estay, 2018). The space and time part that state the exclusion zone after a main shock, were defined by a radius of exclusion and the Time of Maximum Curvature, T_{MC}.

Also, the correlation between this values and the main shock magnitudes of each sequences are show. Based on these correlations seismic decay curves are estimated considering the MOL's parameters. These curves provide information on the decay patterns of an on – going sequence.

The Reasenberg – Jones probability of occurrence of the maximum expected magnitude is estimated using the results previously obtained with Gutenberg – Richter's law, Omori's Law and Båth's law.

6.1. Methodology

The Figure 23 presents a flowchart of the methodology applied in this thesis that combines filtering, clustering tools and estimation of seismic parameters of the three scaling relations: Omori´s Law, Gutenberg-Richter Law and Båth´s Law. The implications of these scaling relations for re-entry protocol development are presented as the outcome of the analysis.

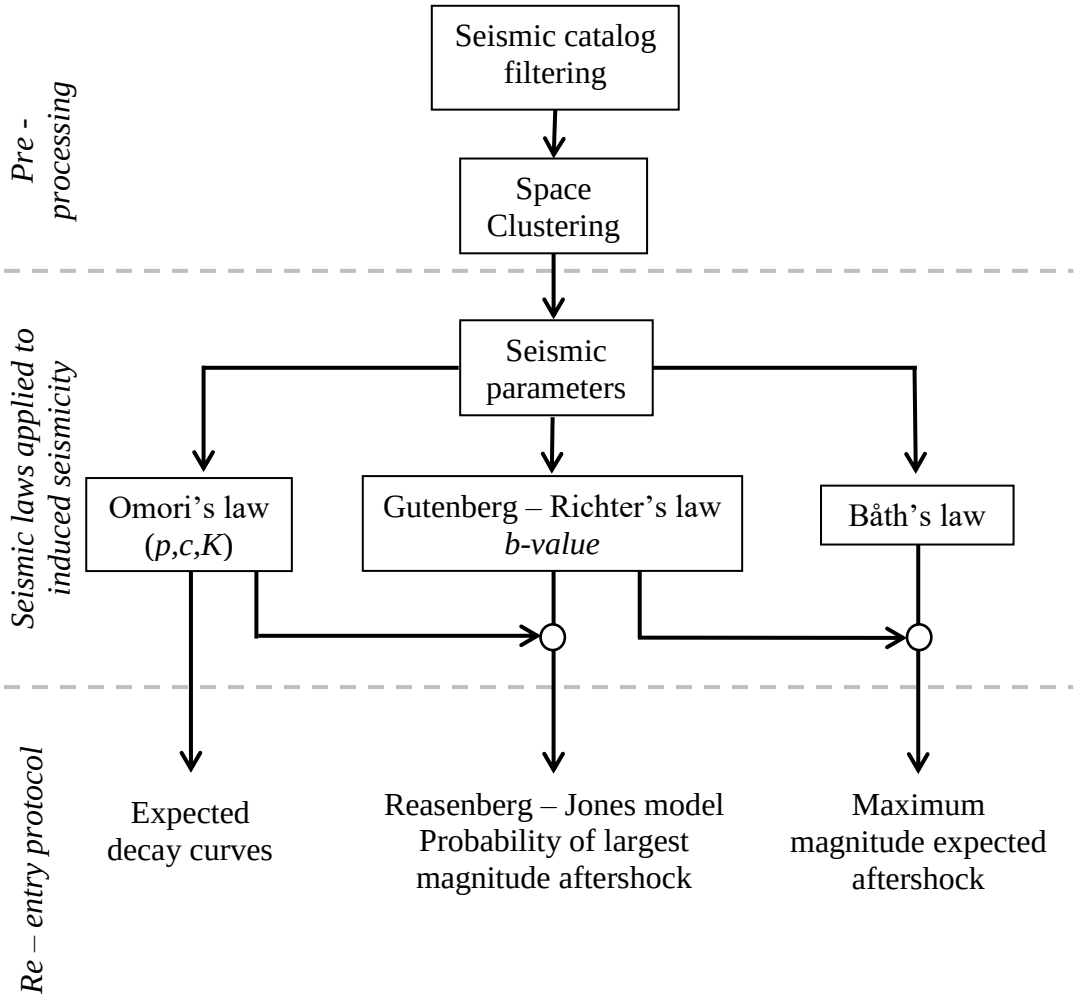

Figure 23. Methodology and results obtained in this section.

6.2.Exclusion zone

The exclusion zone is defined as the volume around the main event's hypocenter for which access is restricted by the re-entry protocol. To provide some guidance on the possible exclusion zone size after large magnitude events, the spatial extent of the events was analyzed. For simplicity this zone was represented by a sphere with radius R^*.

In some cases, the first event in the sequence was not necessarily associated with the cluster of seismicity. Considering this, the center of the sphere will be the centroid of the seismicity that occurs during the first hour after the main shock. This point ensured a better statistical representation of the size of the affected zone, allowing a greater representativeness of the zone where the rupture begins. Three spherical radii for the exclusion zone was estimated: best fit radius (*Rmin*), Seismic Moment radius (*R(Mo)*) and sequence radius (*Rseq*) (Figure 24).

The best fit spherical radius was estimated minimizing the quadratic difference between the distances of the events belonging to the clustered sequence and the centroid of the exclusion

zone. This allows including those events that could be generated and grouped in the edges of the rupture zone.

The Seismic Moment radius was estimated considering the minimum radius which includes the 90% of the total seismic moment of the sequence.

Finally, the sequence radius was estimated considering the 90% of the events clustered in each sequence.

Figure 24 presents the resulting for the three spherical radiuses estimated as a function of the main shock moment magnitude for all the sequences analyzed. Despite some natural dispersion in the data, a significant adjustment (Table 13) between the spherical radius and the magnitude of the main shock can be recognized.

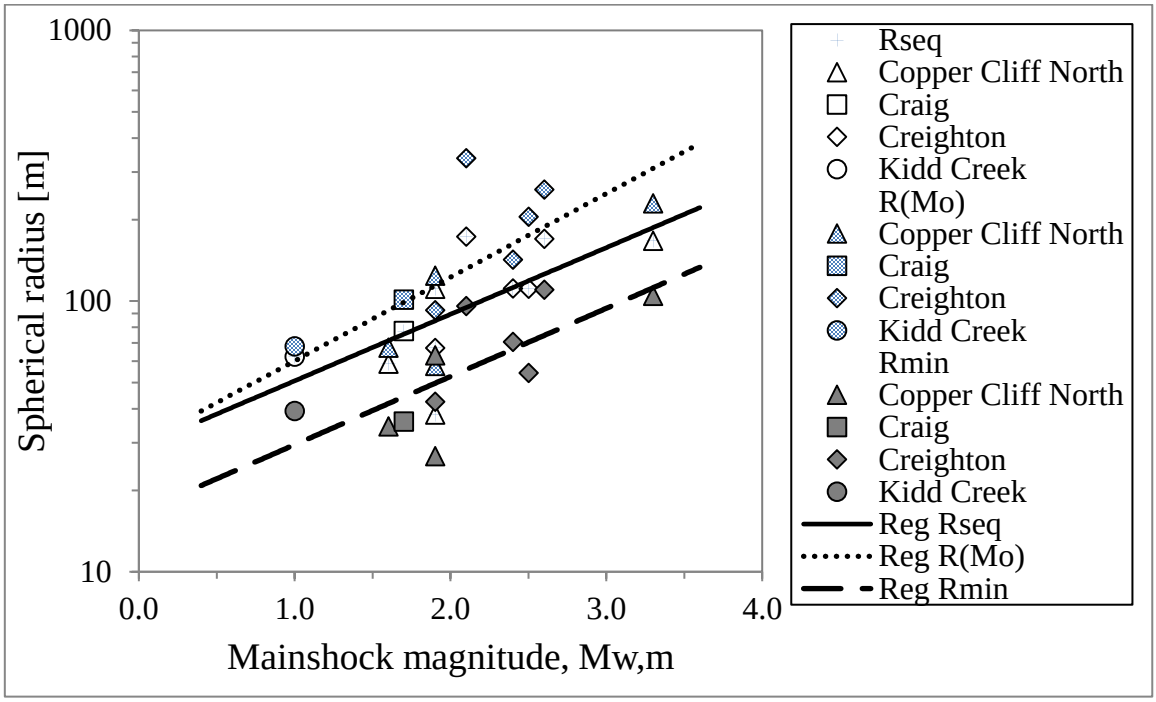

Figure 24. Spherical radiuses as a function of the main shock magnitude of the main event.

Table 13. Regression equations and coefficient of adjustment (R^2) for each option of the exclusion zone radius.

Methodology	Regression equation	R^2
Best spherical radius	$R_{min} = 10^{1.22+0.25M_{w,m}}$	0.52
Seismic Moment radius	$R(Mo) = 10^{1.47+0.31M_{w,m}}$	0.52
Sequence radius	$R_{seq} = 10^{1.46+0.25M_{w,m}}$	0.47

So, for example, in case of a seismic event with $M_{w,m} = 2.0$ results values of *Rmin = 53 m*, *Rseq = 89 m* and *R(Mo) = 123 m*.

Moreover, in Ontario mines, depending on the type of rupture, different exclusion radiuses are used (Vallejos, 2010):

$$Exclusion\ radius\ (ER) = \begin{cases} < 50\ m & Strain\ burst\ and\ entry\ mining\ methods \\ 50 < ER < 100 & Open\ stope\ mining \\ > 100 & Regional\ fault\ slip \end{cases}$$

Given the above, the values proposed for the exclusion zone radius are consistent with the Exclusion Radius used in Ontario mines. In this regard, it is proposed to use the highest value between *ER* and that obtained with the equations presented in Table 13, depending of the seismic mechanism.

6.3. Time of maximum curvature (T_{MC})

The Figure 25 presents the correlation between the time of maximum curvature of the Modified Omori's law and the magnitude of the main event. T_{MC} defines the transition between the highest to lowest rate change (Vallejos & McKinnon, 2010) and is recommended as a preliminary estimate of the time at which it may be considered appropriate to re-enter an area affected by a large magnitude event (Vallejos & McKinnon, 2008, 2010).

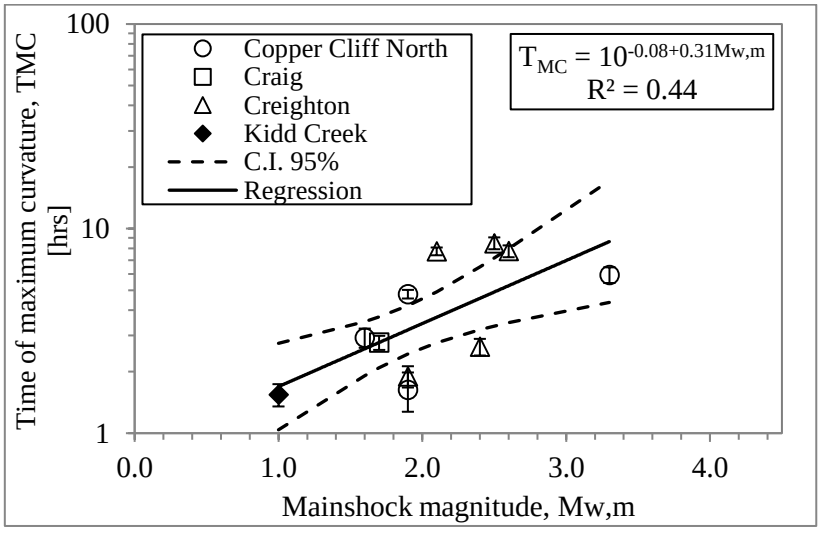

Figure 25. Correlation between the time of maximum curvature, T_{MC}, and the magnitude of the main event. Errors bars were calculated from the MOL's parameters error propagation (Appendix C)

As expected, T_{MC} increases as $M_{w,m}$ increases too, related to a higher seismic activity and the longer time needed to reach the lowest event rate change. To develop a real time re-entry protocol, a series of average MOL curves are defined as a reference to evaluate the actual sequence.

For applying equation (14) to the number of events at time *t* occurring during the last time window Δt it is necessary to consider its integral form for a time interval [T_A, *t*], given by:

$$N_{[t,T_A]} = \int_{T_A}^{t} n(t)dt = \begin{cases} Kln\left(\frac{t+c}{T_A+c}\right) & p = 1 \\ \frac{K}{1-p}[(t+c)^{1-p} - (T_A+c)^{1-p}] & p \neq 1 \end{cases}. \quad (37)$$

By fixing the range of the time interval [T_A, *t*] to a given period Δt:

$$t - T_A = \Delta t \quad (38)$$

and substituting this expression in equation (37), the following is obtained:

$$N_{[t,t-\Delta t]} = \begin{cases} Kln\left(\frac{t+c}{t-\Delta t+c}\right) & p = 1 \\ \frac{K}{1-p}[(t+c)^{1-p} - (t-\Delta t+c)^{1-p}] & p \neq 1 \end{cases} \quad (39)$$

which represents the number of events at time *t* occurring during the previous time window Δt. In this case a value of Δt = *1 hour* is selected. The values of the parameters *p*, *c* and *K* were estimated as explained in section 5.4.

The resulting seismic decay curves are used to provide information on the decay patterns of an on-going sequence. An example is shown with sequence 15 in the Figure 26. In addition, the time of maximum curvature, T_{MC}, and the event rate at T_{MC} are incorporated into the chart. These parameters lead to evaluate a maximum curvature boundary in the event rate diagram that is used to estimate T_{MC} in real time, i.e., when the event rate crosses this boundary the maximum curvature has been reached.

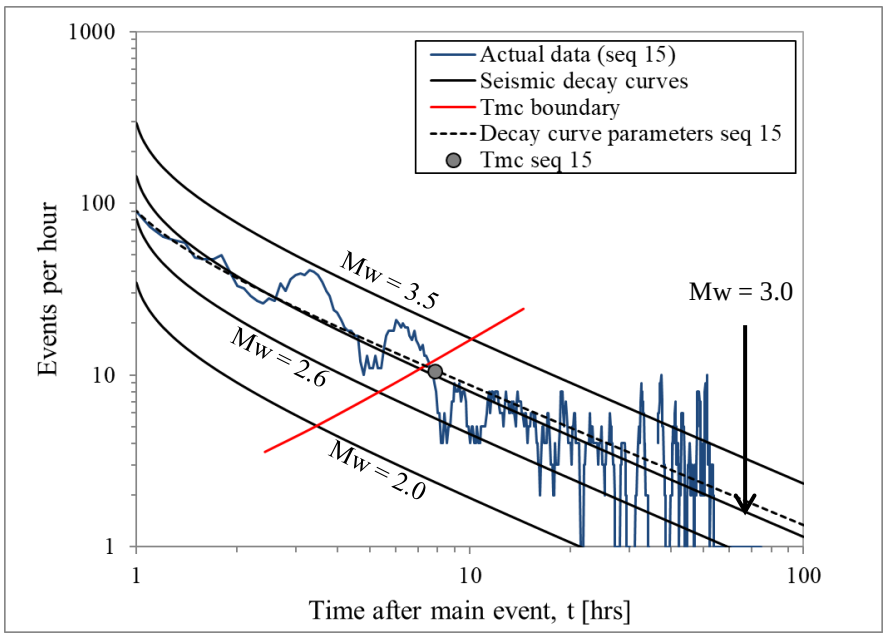

Figure 26. Events per hour as a function of time and magnitude after a main event applied to sequence 15 with $M_{w,m} = 2.6$. Dashed line corresponds to the decay curve calculated with the results obtained in Table 8 (sequence 15). The gray point indicates the value of the T_{MC} for sequence 15.

The dashed line in Figure 26 corresponds to the decay curve of sequence 15, using its own values of *p*, *c* and *K* (see Table 8), which properly follows the actual sequence data. However, the difference between both curves (dashed line and continuous line with $M_{w,m} = 2.6$) is small, where the continuous curve almost perfectly estimates the actual decay curve. This estimation results in that the T_{MC} value corresponds to 7.8 hours.

6.4. Largest aftershock probability

In this section, an application of the Reasenberg – Jones model was made, considering the values of *a'*, *b*, *c* and *p* explained in section 5.4. Also, the difference $M_{w,m} - M_1$ (equation (25)) was considered as $M_{w,m} - M^*$.

As explained in section 5.4, the dependences of Gutenberg – Richter and Omori's parameters with main shock magnitudes were used to plot the fitted Reasenberg – Jones probability curve line (Figure 27). Also, this curve is compared with the curve proposed by Reasenberg & Jones (1989, 1994) and with those obtained for each sequence.

In the Figure 27 it can be observed how the curve associated to the methodology proposed by Reasenberg – Jones, (using the average values of the parameters of the aftershock sequences) underestimates the results obtained in each one of the Ontario sequences.

On the other hand, the methodology proposed in this study, overestimates these curves. This is mainly due to the value of *a'* (equation (23)), which greatly influences the behavior of the probability curve, as shown in Figure 27. In this case, considering the induced seismicity in Canada mines, the adjusted curve best represents the behavior of the probability of occurrence of a seismic event with the magnitude that complies with the expected Bath law for each sequence ($\Delta M^* = 1{,}5$).

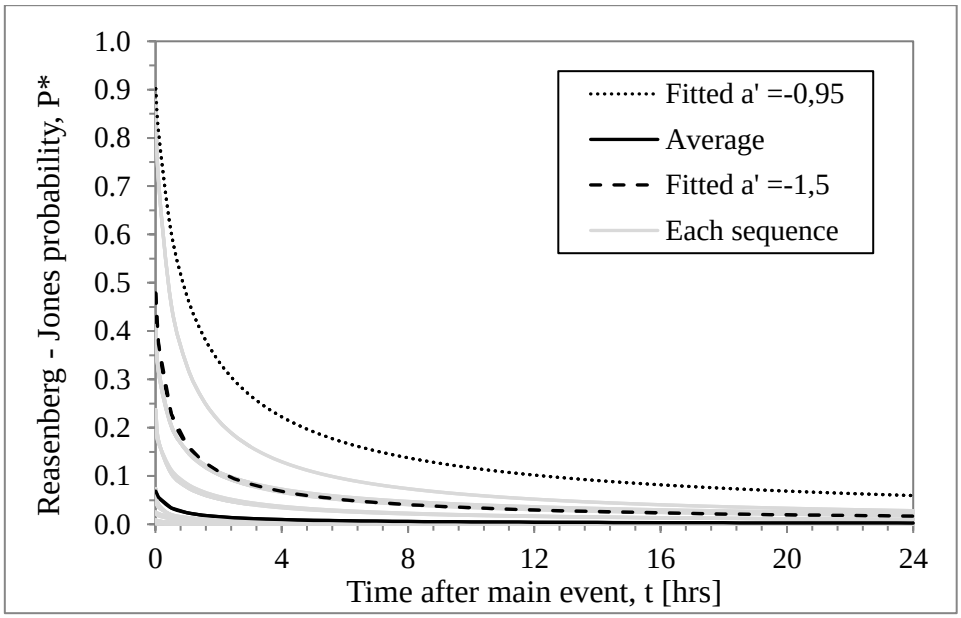

Figure 27. Application of Reasenberg – Jones probability model (equation (25)), considering the values of the parameters of each sequence (gray lines); the average value of the parameters as proposed by Reasenberg & Jones (1989, 1994) (continuous black line): *a' = -3.60, b = 1.39, c = 0.08, p = 0.83*; the values estimated using the methodology proposed in this study with *a' = -0.95* (dotted line) and with *a' = -1.50* (dashed line).

7. Space – Time clustering in mining – induced seismicity application

Different methodologies have been developed and applied to understand the phenomenon and behavior of seismicity, especially at a local, regional and global tectonic level. In mining, the analyzes of induced seismicity are limited to deterministic seismic risk assessments, using seismic indicators with which it is expected to understand the behavior of the rock mass when it is performed the mining production process.

Because of this, a space – time clustering was used, to incorporate the variable time in the analysis of micro – seismicity. This type of clustering allows to define a seismic sequence if each event within this sequence fulfills the condition $d_{ST} \leq D$, where D is the maximum space - time separation distance and $d_{ST} = \sqrt{(d^2 + C^2T^2)}$, which relates the distance (d) and the time (T) between the seismic events related by the value of C (section 2.4).

In this chapter it is propose a new methodology to determine the constants C and D, finding the best fit of the Gutenberg – Richter's law for the clustered and non – clustered seismicity by the Akaike methodology. With this procedure we will be able to define if the induced seismicity has a mayor space or time influence during the process of rupture of the rock mass and how d_{ST} behaves in time previous and after the main shock.

These results were presented in the 9th International Symposium on Rockbursts and Seismicity in Mines, RaSiM 2017 (Estay & Vallejos, 2017).

7.1. Seismic data

The seismic data corresponds to 115,550 mining induced seismicity events of a mine located in Chile from the year 2012. For confidentiality terms no more information about the geology of the mine will be provided.

The Figure 28 presents the frequency – magnitude distribution of the mine induced seismicity. For simplicity, the Magnitude of Completeness (Mc) was defined with the Maximum Curvature procedure (Wiemer & Wyss, 2000; Woessner & Wiemer, 2005). In this case, $Mc=-0.7$.

The maximum magnitude registered in the period was $M_w = 2.2$, but every seismic event with magnitude $Mw \geq 0.6$ is risky for the operation, equipment and people in the mine because of a potential generation of a rockburst.

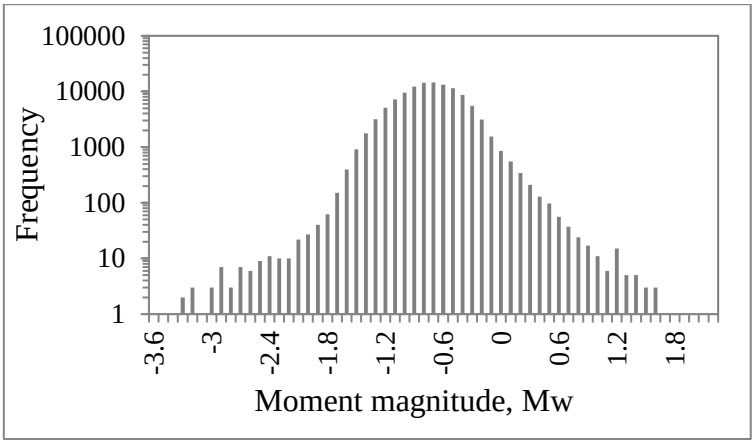

Figure 28. Frequency – magnitude distribution of induced seismicity in the Chilean mine for the year 2012.

7.2. Selection of *C* and *D* values

Frohlich & Davis (1991) and Kijko & Funk (1996) explain that the value of *C* is the mean value of *d/T* ratio for all the events in the catalogue, where *d* is distance between events and *T* the inter – events time. Following this methodology, we estimate the initial value of *C* considering four different moments in time:

(i) Considering only the seismic events previous the largest event ($C_{pre\ Mmax} = 1.7$ *m/hr*).
(ii) Considering the events after the largest event ($C_{post\ Mmax} = 7$ *m/hr*).
(iii) Considering all the events in the catalogue, where *d* and *T*, were calculated with respect of location and time of the largest event ($C_{complete\ Mmax} = 2.8$ *m/hr*).
(iv) The same that in (iii) but with respect to the first event of the year ($C_{complete\ first} = 1$ *m/hr*).

Considering the above, a *C – vector* with values from 0 to 10 in intervals of 0.1 is used in the procedure of cluster selection explained in the next section.

With respect to the selection of the *D – value*, a convenient election, considering the space distribution of the micro seismicity, between 50 and 500 meters with steps of 50 meters was used.

The methodology used to select the optimal *C* and *D* values was:

(i) It was selected a value of C_i ($0 \leq C \leq 10$) and D_j ($50 \leq D \leq 500$). For each combination between *C* and *D:*

   a. For a seismic event *k* ("pivot" event), with time t_k, it was calculated the Space-Time distance, $d_{ST,km}$ with $t_m > t_k$.
   b. A natural cluster is formed by selecting all the events with $d_{ST} \leq D_j$.
   c. For the clustered and non-clustered events (with more than $N = 10$ events), it was calculated the Gutenberg-Richter's law.

i. The value of AIC for clustered events (AIC_c) and for non-clustered events (AIC_{nc}), were calculated.
ii. If $AIC_c + AIC_{nc} \leq AIC_{min}$, we kept the parameters C and D and $AIC_{min} = AIC_c + AIC_{nc}$.

d. $k = k + 1$ and return to *(a)* until the entire seismic catalogue is reviewed.

(ii) Return to *(i)* until finished all the values of C and D.

It is important to note that the space – time distance is calculated between all the events with higher time of occurrence than the "pivot" event.

7.3. Cluster selection and behaviour through time

The Figure 29 shows the results of how the *AICtotal = AICc + AICnc* varies with the different combinations of C and D values. In the figure, just some of the *C – values* are exposed to see the tendency of the results.

The Table 14 shows the parameters of the best and worst result obtained.

As Figure 29 shows, for $C > 1$ the AIC_{total} value tends to stabilize, influenced principally for the reduction in size of the clustered events (the higher the value of C, the lower the number of events in the cluster).

The Figure 30 shows the Gutenberg – Richter's law adjustment to the clustered and non – clustered data, using $C = 0\ m/hr$ and $D = 400\ m$.

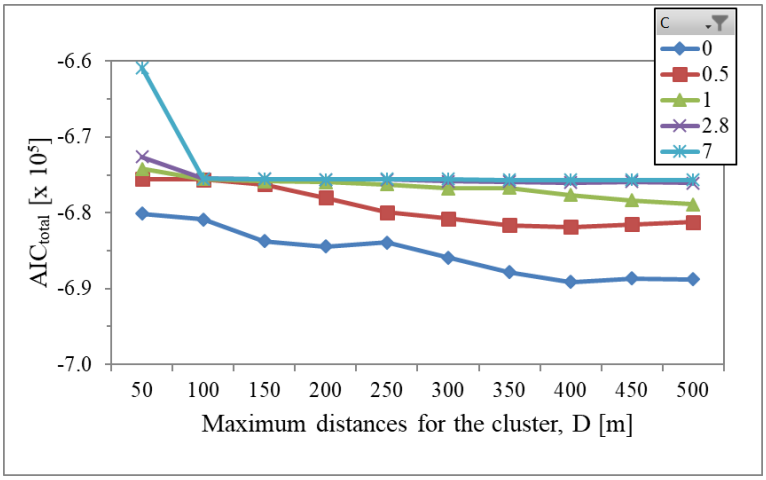

Figure 29. Variations of AIC_{total} for some of the C and D values.

Table 14. Gutenberg – Richter's adjustment for the best and worst results of the Space – time clustering. R^2 corresponds to the coefficient of adjustment of the Gutenberg – Richter's law to the seismic data.

	C = 0 [m/hr] D = 400 [m]		C = 7 [m/hr] D = 450 [m]	
Parameter	Clustered	Not Clustered	Clustered	Not Clustered
N	31,355	28,951	18	60,387
dt	276 days	276 days	1.9 days	277 days
a	3.7	3.9	0.87	4.1
b	1.9	1.4	0.98	1.6
Δb	0.002	0.0009	0.27	0.0008
R^2	0.89	0.86	0.86	0.88
AIC	-412,073.6	-277,040.4	-105.3	-675,554.3
AICtotal	**-689,114**		**-675,659.6**	

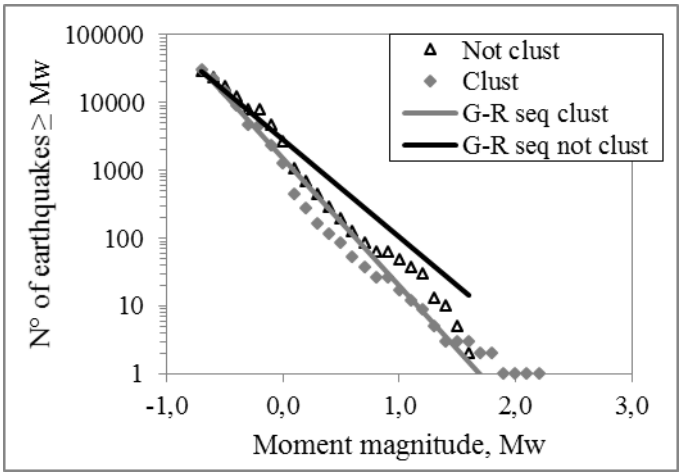

Figure 30. Frequency – magnitude distribution for clustered and not clustered events and *C = 0 [m/hr], D = 400 [m]*. Gray diamonds and gray line correspond to clustered events. Black triangles and black line correspond to the non – clustered events.

The Figure 31 shows how the size of the cluster decreases as the value of *C* increases (even for larger values of *D*). In fact, when *C = 7 m/hr* the clustered seismicity changes the position.

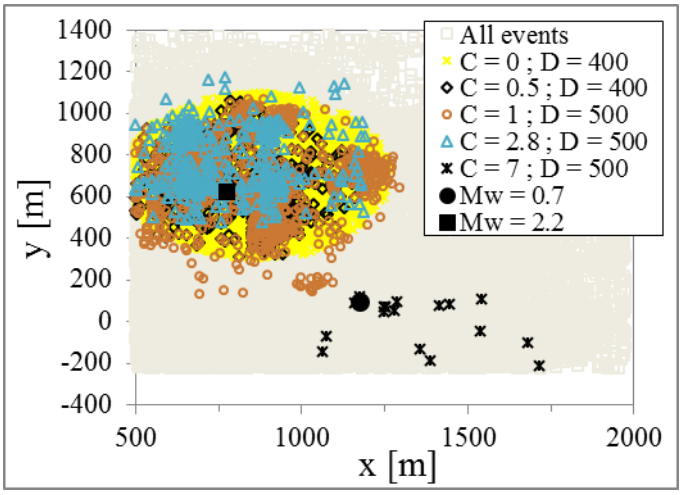

Figure 31. Clustered mining induced seismicity for some values of *C* and *D*. Black dot and square indicate the largest event for extreme cases of *C = 0* and *C = 7 m/hr*.

Finally, the variation of the moving average of dST in time for different values of C and D are plotted in Figure 32. Although the results are not conclusive, a trend can be observed in the results, which show that prior to the main seismic event, the value of dST decreases, to then return to "previous levels" and/or then increase slightly. In first instance, time does not have a greater effect on the behavior of dST with this data, since with C = 0 or C ≠ 0. However, this is not true for the C = 0.5 case in which it seems that the value of dST remains varying between 250 and 300.

Despite the above, this result seems to be in agreement with the results obtained above (Figure 29), where the best value of AIC is obtained with C = 0, which indicates a seismic sequence with a greater spatial dependence than temporary.

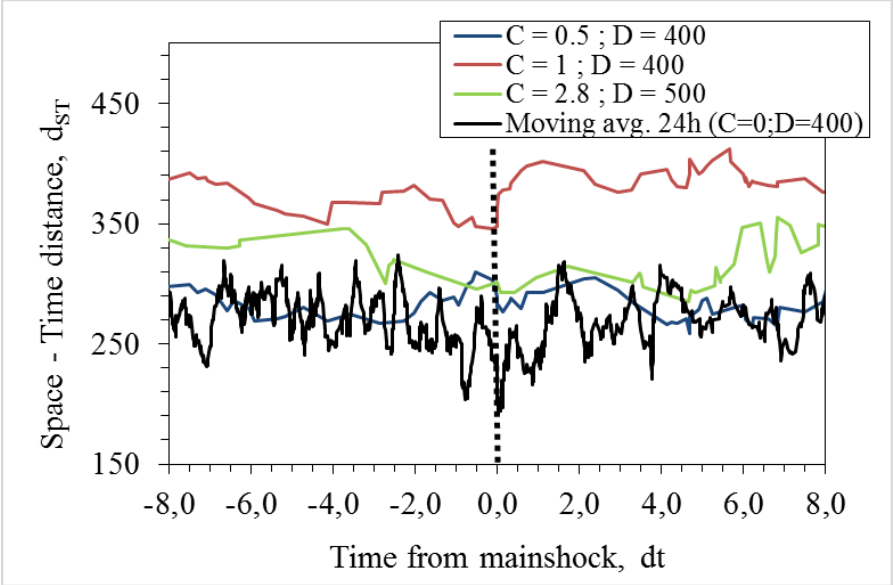

Figure 32. Variation of 8-hours – moving average d_{ST}, 8 hours after and before the main shock (*dt = 0*). Black line corresponds to a moving average of 24-hours.

8. General discussions

For adjusting the parameter *b* of the Gutenberg – Richter's law it is necessary first to confirm that the magnitude distribution can be explained by this scaling relation. Gibowicz & Kijko (1994), explained the bimodal distribution behavior of the mine seismicity, associated to inhomogeneous major geologic features, where low and high energy are released by mining and residual tectonic stress accumulated in the rock mass respectively. In this study, all aftershock sequences have a unimodal frequency – magnitude distribution, which can be correctly explained by the Gutenberg – Richter's law (Figure 14).

The adjusted *b-values* did not present any trend with the main shock magnitude (Figure 15). The mines located in the SIC (Creighton, Craig and Copper Cliff North) have similar *b-values* (except for one sequence from Copper Cliff North). This may represent a type of mechanism and stress conditions in Ontario. Kid Creek mine present a lower *b-value* compared to the Ontario mines, which could indicate a local variation in the type of mechanism of mining induced seismicity.

Linear relationships are adjusted to the MOL's parameters as a function of main shock magnitude. The results presented low correlation values. This is considered as a first approximation to generalize the application of seismic parameters obtained from mining induced seismicity. These relations are more representative to the seismic process generated by mining than using average values or values obtained from tectonic seismicity. Although similar trends and correlations were obtained between the results for the parameters of induced and tectonic seismicity. Then it is advisable to use, at least, the methodologies proposed in this thesis, since it was shown that there may be differences of 0.35 and 0.2 in the case of the *b* and *p* values respectively, being these seismic laws parameters ones of the most used in seismicity research and seismic hazard. The low correlation values can be improved by increasing the number of aftershock sequences used in the analysis.

For applying Båth's law to mining – induced aftershock sequences it is necessary to consider the inferred largest aftershock obtained with the Gutenberg – Richter power law instead of the registered values. The mean value of this scaling relation is $\Delta M_w^* = 1.5 \pm 0.6$, however ΔM_w^* differs from sequence to sequence with variation between 0.44 and 2.70.

This study showed a methodology to define the parameters *C* and *D* associated with space – time distances, d_{ST}, using the statistical criterion of Akaike, which allows a quantitative adjustment criterion.

An interesting behavior in the cluster obtained is the displacement that occurs when $C = 7$ *m/hr*, where a short duration seismic sequence (almost 2 days) with few events ($N = 18$) associated to an event $Mw = 0.7$ is detected. In fact, this micro aftershock sequence is detected using the value of $C_{post,Mmax}$, which is indicative of an aftershock sequence in which the time of

occurrence of seismic events have a greater influence on the process of the rock mass rupture (smaller time differences between events).

In this study the Gutenberg – Richter's law was used to apply the Akaike's criterion, it is possible to use another type of seismic law, such as Omori's law, ETAS in which its parameters can also be obtained through the method of maximum likelihood.

An improvement in the analysis can be carried out considering a greater number of minimum events necessary to be able to make the adjustment of, in this case, Gutenberg – Richter's law.

9. Conclusions

Aftershocks are complex in nature. The statistics present in this thesis are valuable in terms of the behavior of the induced seismic parameters, comparison between induced and tectonic results, development and application of the re-entry protocol.

Correlations between Gutenberg – Richter's *b-value* and the parameters of the modified Omori's law (MOL) with main shock magnitude, $M_{w,m}$, were explored. No significant correlations were obtained, except for the Omori's *c* and *K* values. The opposite occurs if only consider the results of Creighton mine, where high correlations were obtained between *b* and *p* values with the magnitude of the main event. This high correlation may be related to the type of mechanism of the induced seismicity present in the mine. However, the number of sequences is not enough to establish final conclusions. Moreover, a conditional space – time exclusion zone based on spherical radius (R^*), T_{MC}, and its correlation with $M_{w,m}$ have been proposed. Conditionality is obtained by setting the highest value between R^* and *ER*, depending of the mechanism of the induced seismicity.

A maximum expected aftershock magnitude was estimated applying a modified Båth's law to Ontario aftershock sequences. A direct application of Båth's law to induced seismicity data is not recommended. In order to obtain an uncorrelated value of ΔM with $M_{w,m}$, it is necessary to use an inferred largest aftershock, estimated by Gutenberg-Richter's law. Finally, a value of $\Delta M^* = 1.5$ was used in this study.

The concept of seismic decay curves was developed to provide information on the decay patterns of an on-going sequence. With this family of decay-law curves, it is possible to evaluate the path and decay pattern of an induced aftershock sequence after a large magnitude event. Also, considering the T_{MC} it is possible to define a time after which it's safer to return to production in the affected area.

The Reasenberg – Jones probability model was applied to the seismic data, where the methodology proposed in this study presents results that agree with seismicity in Ontario than the methodology proposed by Reasenberg & Jones (1989, 1994).

Based on these main results, this research is a major development of re-entry protocols for mines, in which were considering space – time of the exclusion zone, the magnitude of the expected largest aftershock and its probability to occur.

In case of space – time clustering data used, seismicity has a greater spatial component than a temporal one, which could be affected mainly by the geological conditions of the site and by the fact that seismicity is influenced by mining development. Also, it is found that the Space – Time distance apparently decrease their value before the occurrence of the mainshock to, later, back to its normal value. Nevertheless, it is necessary more evidence to conclude this.

Finally, some future research works are:

- Quantify the effect of space and space – time clustering in the values of the mining – induced seismicity parameters.
- Found some correlations between the mining – induced seismic parameters and the focal mechanism and the type of the source rupture of the induced seismicity.
- Found some "scaling factor" between induced and tectonic seismicity, following, for example, the methodology of Uhl et al (2015).
- Include some mining variables into the analysis, for example, the induced stress and the mining production rate, among others.

Bibliography

1. Akaike, Hirotugu. 1973. Information theory and an extension of the maximum likelihood principle. *In Proceedings of the Second International Symposium on Information Theory*, eds. B.N. Petrov and F. Caski, 267 – 281. Budapest: Akademiai Kiado.
2. Akaike, Hirotugu. 1974. A new look at the statistical model identification, *IEEE Transactions on Automatic Control*, 19, 716 – 723.
3. Aki, Keiiti. 1965. Maximum likelihood estimate of b in the formula *logN = a –bM* and its confidence limits, *Bulletin of Earthquakes Research Institute of Tokyo*, 43, 237 – 239.
4. Aki, K. and Richards, P. 1980. Quantitative seismology, W. H. Freeman, San Francisco
5. Amorèse, Daniel. 2007. Applying a change-point detection method on frequency-magnitude distributions, *Bulletin of the Seismological Society of America*, 91(5), 1694 – 1703. DOI: 10.1785/0120060181.
6. Båth, Markus. 1965. Lateral inhomogeneities in the upper mantle, *Tectonophysics*, 2, 483 – 514. DOI: https://doi.org/10.1016/0040-1951(65)90003-X.
7. Board, M., Brummer, R., and Seldom, S. 2001. Use of numerical modeling for mine design and evaluation, *In Underground Mining Methods: Engineering Fundamentals and International Case Studies*, 483 – 491.
8. Boatwright, J. and Fletcher, J. B. 1984. The partition of radiated energy between P and S waves, *Bulletin of the Seismological Society of America*, 74, 361 – 376.
9. Burnham, K.P. and Anderson, D.R. 2002. Model selection and multimodel inference: A practical information-theoretic approach. New York: Springer-Verlag.
10. Butler, T. G. and Simser, B. P. 2017. Microseismic monitoring strategy and early rockburst experience during the development of Glencore's Nickel Rim Deep and Onaping Depth Projects. *In: 9th International Symposium on Rockbursts and Seismicity in Mines*, eds.: J. Vallejos, Santiago, Chile, 290 – 296.
11. Cao, A. and Gao, S. 2002. Temporal variation of seismic b – values beneath northeastern Japan island arc, *Geophyscal Research Letters*, 29(9), 48-1 – 48-3. DOI: 10.1029/2001GL013775.
12. Chiarabba, C., Jovane, L. & DiStefano, R. 2005. A new view of Italian seismicity using 20 years of instrumental recordings. *Tectonophysics*, 395, 251 – 268. DOI: https://doi.org/10.1016/j.tecto.2004.09.013.
13. Cichowicz, A., Green, R.W.E., Brink, A.v.Z, Grobler, P. and Mountfort, P.I. 1990. The space and time variation of micro-event parameters occurring in front of an active stope. In Proceedings of Rockbursts and Seismicity in Mines. Minneapolis, eds.: C. Fairhurst. Rotterdam: A.A.Balkema, 171 – 175.
14. Console, R., Lombardi, A.M., Murru, M., and Rhoades, D. 2003. Båth's law and the self-similarity of earthquakes, *Journal of Geophysical Research*, 108(B2), 2128 – 2136. DOI: 10.1029/2001JB001651.
15. Cook, N.G.W. 1976. Seismicity associated with mining, *Engineering Geology*, 10(2), 99 – 122.

16. Cornejo, J., Vallejos, J., Emery, X and Rojas, E. 2014. Seismic hazard analysis at the El Teniente Mine using a clustering approach. *In Proceedings of the Third International Congress in Mining of Block and Sublevel Caving, Santiago, Chile*, 5 – 6 June 2014, eds. R. Castro, 575 – 585.
17. Dara, S., Barnes, S-J., Prichard, H. and Fisher, P. 2011. Chalcophile and platinum – group element (PGE) concentrations in the sulfide minerals from the McCreedy East deposit, Sudbury, Canada, and the origin of PGE in pyrite, Miner Deposita 46, 381 – 407. DOI: 10.1007/s00126-011-0336-9
18. Day, W.H.E., and Edelsbrunner, H. 1984. Efficient algorithms for agglomerative hierarchical clustering methods, *Journal of Classification*, 1, 7 – 24. DOI:10.1007/BF01890115.
19. Davis, S.D., and Frohlich, C. 1991. Single – link cluster analysis of earthquake aftershocks: decay laws and regional variations, *Journal of Geophysical Research*, 96, 6335 – 6350. DOI: 10.1029/90JB02634.
20. Dunlop, G., Gaete, S. 1997. Controlling Induced Seismicity at El Teniente Mine: The Sub6 sector case history. Rockbursts and Seismicity in Mines, Gibowicz & Lasocki (eds). Balkema, Rotterdam. Codelco Chile, División El Teniente, Rancagua, Chile, 233 – 235.
21. Duplancic, Paul. 2002. Characterization of caving mechanisms through analysis of stress and seismicity. PhD Thesis. University of Western Australia. Perth, Australia.
22. Eberhart – Phillips, Donna. 1998. Aftershock sequence parameters in New Zealand. *Bulletin of the Seismological Society of America*, 88(4), 1095 – 1097.
23. Enescu, B., and Ito, K. 2003. Values of b and p: their variations and relation to physical processes for earthquakes in Japan. *Annuals of Disaster Prevention Research Institute, Kyoto University*, 46B, 709 – 719.
24. Enescu, B., Mori, J., Miyazawa, M., and Kano, Y. 2009. Omori – Utsu law c – values associated with recent moderate earthquakes in Japan, *Bulletin of the Seismological Society of America*, 99(2A), 884 – 891. DOI: 10.1785/0120080211.
25. Estay, Rodrigo. 2014. Metodología para la evaluación del desempeño de indicadores sísmicos en sismicidad inducida por la minería, Msc. Thesis, Universidad de Chile.
26. Estay, R. and Vallejos, J. 2017. Space or Space – Time clustering? A selection criterion methodology using mining induced seismicity data, In: 9th International Symposium on Rockbursts and Seismicity in Mines, eds.: J. Vallejos, Santiago, Chile, 339 – 343.
27. Estay, R. and Vallejos, J. A comparisson of characteristic parameters of mining induced and tectonic seismic sequences (*in preparation to be published at 2019)*
28. Felzer, K., Becker, T., Abercrombie, R., Ekström, G., and Rice, J. 2002, Triggering of the 1999 M_w 7.1 Hector Mine earthquake by aftershocks of the 1992 M_w 7.3 Landers earthquake, *Journal of Geophysical Research*, 107(B9), 2190 – 2202. DOI: 10.1029/2001JB000911.
29. Felzer, Karen. 2006. Calculating the Gutenberg – Richter b – value. American Geophysical Union Talk. Available on – line.

30. Frohlich, C. and Davis, S. 1985, Identification of aftershocks of deep earthquakes by a new ratios method, *Geophysical Research Letters*, 12(10), 713 – 716. DOI: 10.1029/GL012i010p00713.
31. Frohlich, C., and Davis, S.D. 1990. Single-link cluster analysis as a method to evaluate spatial and temporal properties of earthquake catalogues, *Geophysical Journal International*, 100, 19 – 32. DOI: 10.1111/j.1365-246X.1990.tb04564.x.
32. Gasperini, P. and Lolli, B. 2006. Correlation between the parameters of the aftershock rate equation: implications for the forecasting of rupture sequences, *Physics of the Earth and Planetary Interiors*, 156, 41 – 58. DOI: https://doi.org/10.1016/j.pepi.2006.01.005.
33. Gerstenberger, M. C., Wiemer, S. and Jones, L. M. 2004. Short – term probabilistic aftershock hazard mapping. *Proceedings in the New Zealand Society for Earthquake Engineering* (NZSEE)
34. Gibowitz, Slawomir Jerzy. 1973. Stress drop and aftershocks. *Bulletin of the Seismological Society of America*, 63 (4), 1433 – 1446.
35. Gibson, H., Richardson, D., Hannington, M., Gibbins, S., DeWolfe, M. and Duff, D. 2003, The Kidd Creek volcanogenic massive sulfide deposit: a growing giant, after forty years of mining, exploration and research, In: Ore deposits at depth, Ontario.
36. Guha, S., Rastogi, R. and Shim, K. 1998. CURE: An efficient clustering algorithm for large database. In: Proceedings of the ACM SIGMOD Conference, Seattle, USA.
37. Guo, Z., and Ogata, Y. 1995. Correlation between characteristics parameters of aftershock distribution in time, space and magnitude, *Geophysical Research Letter*, 22, 993 – 996. DOI: 10.1029/95GL00707.
38. Gutenberg, B. & Richter, C. F. 1944. Frequency of earthquakes in California. *Bulletin of the Seismological Society of America*, 34(4), 185 – 188.
39. Hanks, T. C. and Kanamori, H. 1979. A moment tensor magnitude scale. *Journal of Geophysical Research*, 84, 2348 – 2350.
40. Hamaguchi, H., and Hasegawa, A. 1970. An investigation on the aftershocks of the Tokachi-oki earthquake of 1968, (2) Statistical study on time distribution, *Science Reports of the Tohoku University. Series 5, Geophysics*, 20 (3), 119 – 133.
41. Hartigan, John. 1975. Clustering algorithms (Probability & Mathematical Statistics), John Wiley & Sons Inc., New York; London.
42. Hudyma, M and Potvin, Y. 2004. Mining-Induced Seismicity in Underground, Mechanised, Hardrock Mines – Results of a World-Wide Survey. Australian Centre for Geomechanics Research Report.
43. Hudyma, M., and Potvin, Y. 2009. An engineering approach to seismic risk management in hard rock mines, *Rock Mechanics and Rock Engineering*, 43, 891 – 906. DOI: 10.1007/s00603-009-0070-0.
44. Kagan, Y., and Houston, H. 2005. Relation between mainshock rupture process and Omori's law for aftershock moment release rate, *Geophysical Journal International*, 163, 1039 – 1048. DOI: 10.1111/j.1365-246X.2005.02772.x.

45. Kaiser, P. K., McCreath, D. R. and Tannant, D. D. 1996. Canadian Rockburst Support Handbook. 324 pp.
46. Kijko, A. and Funk. C. W. 1996. Space – time interaction amongst clusters of mining induced seismicity, *Pure and Applied Geophysics*, 100 (2), 277 – 288. DOI: https://doi.org/10.1007/BF00877483.
47. Kisslinger, C. & Jones, L. 1991. Properties of aftershock sequences in Southern California, *Journal of Geophysical Research*, 96, 11947 – 11958. DOI: https://doi.org/10.1029/91JB01200.
48. Lasocki, S., Orlecka – Sikora, B., Mutke, G., Pytel, W., Rudzinski, L., Markowski, P. and Piasecki, P. 2017. Invited lecture: A catastrophic event in Rudna copper – ore mine in Poland on 29th November 2016: what, how and why. In: 9th International Symposium on Rockbursts and Seismicity in Mines, eds.: J. Vallejos, Santiago, Chile, 316 – 324.
49. Ling, Robert. 1973. A probability theory of cluster analysis, *Journal of the American Statistical Association*, 68, 159 – 196. DOI: 10.2307/2284161.
50. Lolli, B. & Gasperini, P. 2006. Comparing different models of aftershock rate decay: the role of catalog incompleteness in the first times after mainshock. *Tectonophysics*, 423, 43 – 59. DOI: https://doi.org/10.1016/j.tecto.2006.03.025.
51. Lombardi, Anna Maria. 2002. Probabilistic interpretation of Båth's law, *Annals of Geophysics*, 45(3/4), 455 – 472. DOI: 10.1.1.518.8016.
52. Malek, F., Suorineni, F.T. and Vasak, P. 2009. Geomechanics strategies for rockburst management at Vale Inco Creighton Mine. In: Rock Engineering in Difficult Conditions.
53. McQuitty, Louis. 1957. Elementary linkage analysis for isolating orthogonal and oblique types and typal relevancies, *Educational and Psychological Measurments*, 17, 207 – 229.
54. Mignan, A., Werner, M. J., Wiemer, S., Chen, C.-C., and Wu, Y.-M. 2011. Bayesian estimation of the spatially varying completeness magnitude of earthquake catalogs, *Bulletin of the Seismological Society of America*, 101, 1371 – 1385. DOI: 10.1785/0120100223.
55. Mignan, A. and Woessner, J. 2012. Estimating the magnitude of completeness for earthquake catalogs, Community Online Resource for Statistical Seismicity Analysis. DOI:10.5078/corssa-00180805. Available at http://www.corssa.org
56. Mikumo, T., and Miyatake, T. 1979. Earthquake sequences on a frictional fault model with non-uniform stregths and relaxation times, *Geophysical Journal of Royal Astronomical Society*, 59, 497 – 522. DOI: 10.1111/j.1365-246X.1979.tb02569.x.
57. Mogi, Kiyoo. 1962. Study of elastic shocks caused by the fracture of heterogeneous materials and its relations to earthquake phenomena. *Bulletin of the Earthquake Research Institute, Tokyo*, 40, 125 – 173.
58. Mogi, Kiyoo. 1967. Earthquakes and fractures, *Tectonophysics*, 5, 35 – 55. DOI: https://doi.org/10.1016/0040-1951(67)90043-1.

59. Mori, J., and Abercrombie, R. 1997. Depth dependence of earthquake frequency-magnitude distribution in California: implications for rupture initiation, *Journal of Geophysical Research*, 102(B7), 15081 – 15090. DOI: 10.1029/97JB01356.
60. Mukwakwami, J., Lfrance, B. and Lesher, C. 2011, Back – thrusting and overturning of the southern margin of the 1,85 Ga Sudbury Igneous Complex at the Garson mine, Sudbury, Ontario, *Precambrian Research 196 – 197*, 81 – 105. DOI: 10.1016/j.precamres.2011.10.020.
61. Nanjo, K. Z., Enescu, B., Shcherbakov, R., Turcotte, D. L., Iwata, T. & Ogata, Y. 2007. Decay of aftershock activity for Japanese earthquakes. *Journal of Geophysical Research, 112*. DOI: https://doi.org/10.1029/2006JB004754.
62. Narteau, C., Shebalin, P., and Holschneider, M. 2002. Temporal limits of the power law aftershock decay rate, *Journal of Geophysical Research*, 107(B12), 2359 – 2372. DOI: 10.1029/2002JB001868.
63. Natural Resources Canada and Ontario Geological Survey. 2015. Copper Cliff, Greater Sudbury: A driving tour of Greater Sudbury's mining industry; GeoTours Northern Ontario series.
64. Newman, M. E. J. 2005. Power law, pareto distributions and Zipf's law, *Comtemporary Physics*, 46 (5), 323 – 351.
65. Nishikawa, T., and Ide S. 2015. Background seismicity rate at subduction zones linked to slab-bending-related hydration, *Geophysical Research Letters*, 42, 7081–7089. DOI:10.1002/2015GL064578.
66. Nuannin, P., Kulhanek, O., Persson, L., and Tillman, K. 2002. Forecasting of increasing induced seismicity in the Zinkgruvan mine, Sweden, by using temporal variations of *b*-values, *Acta Montana*, *Series A*, 21, 13 – 25.
67. Nur, A. & Booker, J. R. 1972. Aftershocks caused by pore fluid flow?, *Science*, 175, 885 – 887. DOI: https://doi.org/10.1126/science.175.4024.885.
68. Nuttli, O.W. 1973, Seismic wave attenuation and magnitude relations for Eastern North America, *Journal of Geophysical Research*, 78, 876 – 885. DOI: 10.1029/JB078i005p00876.
69. Nyffeneger, P. and Frohlich, C. 2000. Aftershock occurrence rate decay properties for intermediate and deep earthquake sequences, *Geophysical Research Letter*, 27(8), 1215 – 1218. DOI: 10.1029/1998GL010371.
70. Obert, L and Duval, W. 1967. Rock mechanics and the design of structures in rock, chapter 19; John Wiley & Sons, INC. 650 p.
71. Ogata, Yosihiko. 1983. Estimation of the parameters in the modified Omori formula for aftershock frequencies by the maximum likelihood procedure, *Journal of Physics of the Earth*, 31, 115 – 124. DOI: http://doi.org/10.4294/jpe1952.31.115.
72. Ogata, Y. and Katsura, K. 1993. Analysis of the temporal and spatial heterogeneity of magnitude frequency distribution inferred from earthquake catalogues, *Geophysical Journal International*, 113, 727 – 738. DOI: https://doi.org/10.1111/j.1365-246X.1993.tb04663.x.

73. Okada, Masami. 1979). Statistical distribution of the difference in magnitude between the main shock and its largest aftershock, *Journal of the Seismological Society of Japan*, 32 (4), 462 – 476. DOI: https://doi.org/10.4294/zisin1948.32.4_463
74. Omori, Fusakishi. 1894a. On after – shocks, *Rep. Imp. Earthq. Inv. Corn.*, 2, 103 – 138 (in Japanese).
75. Omori, Fusakishi. 1894b. On after – shocks of earthquakes, *J. Coll. Sci. Imp. Univ. Tokyo*, 7, 111 – 200.
76. Ortlepp, W.D. 1992. Invited Lecture: The design of support for the containment of rockburst damage in tunnels – An engineering approach. Proceedings of Rock Support and Underground Construction, (editors: P.K. Kaiser and D.R. McCreath), Rotterdam: Balkema, 593 – 609.
77. Ouillon, G. & Sornette, D. 2005. Magnitude – dependent Omori law: theory and empirical study. *Journal of Geophysical Research*, 110(B4), DOI: https://doi.org/10.1029/2004JB003311.
78. Pastén, D., Estay, R., Comte, D. and Vallejos, J. 2015. Multifractal análisis in mine microseismicity and its application to seismic hazard in mine. *International Journal of Rock Mechanics and Mining Sciences, 78, 74 – 78.* DOI: http://dx.doi.org/10.1016/j.ijrmms.2015.04.020
79. Purcaru, G. 1974. On the statistical interpretation on the Båth's law and some relations in aftershock statistics. *Geol. Inst. Technic. And Ec. Study Geophys. Prosp.*, 10, 35 – 84.
80. Reasenberg, P., and Jones, L. 1989. Earthquake hazard after a main shock in California, *Science*, 24, 1173 – 1176. DOI: 10.1126/science.243.4895.1173
81. Reasenberg, P., and Jones, L. 1994. Earthquake aftershocks: Update, *Science*, 265, 1251 – 1252. DOI: 10.1126/science.265.5176.1251.
82. Rebuli, D.B., and S. J. Kohler. 2014. Using clustering algorithms to assist short-term seismic hazard analysis in deep South African mines. In Proceedings of the Seventh Iinternational Conference on Deep and High Stress Mining, Sudbury, 16 – 18 September 2014, eds. M. Hudyma and Y. Potvin, 699 – 708.
83. Richter, Charles. 1935. An instrumental earthquake magnitude scale. *Bulletin of the Seismological Society of America*, 25, 1 – 32.
84. Richter, Charles. 1958. Elementary Seismology, W. H. Freeman, San Francisco.
85. Rojas, E. and Balboa, S. 2017. Keynote lecture: Management of seismic hazard in high stress conditions, El Teniente Mine. In: 9th International Symposium on Rockbursts and Seismicity in Mines, eds.: J. Vallejos, Santiago, Chile, 280 – 289.
86. Rydelek, P.A. and Sacks, I.S. 1989. Testing the completeness of earthquake catalogues and the hypothesis of self – similarity, *Nature*, 337, 251 – 253. DOI: 10.1038/337251a0.
87. Scholz, Christopher. 1968. The frequency-magnitude relation of microfracturing in rock and its relation to earthquakes, *Bulletin of the Seismological Society of America*, 58(1), 399 – 415.
88. Schorlemmer, D., Wiemer, S. and Wyss, M. 2005. Variations in earthquake – size distribution across different stress regimes, *Nature Letters*, 437, 539 – 542. DOI:10.1038/nature04094.

89. Shcherbakov, R., and Turcotte, D. 2004. A modified form of Båth's law, *Bulletin of the Seismological Society of America*, 94, 1968 – 1975. DOI: 10.1785/012003162.
90. Shi, Y. and Bolt, B. 1982. The standard error of the magnitude – frequency b value, *Bulletin of the Seismological Society of America*, 72(5), 1677 – 1687.
91. Sneath, Peter. 1957. The application of computers to taxonomy, *Journal of General Microbiology*, 17, 201 – 226. DOI: 10.1099/00221287-17-1-201.
92. Sonley, E., and Atkinson, G. M. 2005. Empirical relationship between Moment magnitude and Nuttli magnitude for small – magnitude earthquakes in Southeastern Canada, *Seismological Research Letter*, 76, 752 – 755. DOI: 10.1785/gssrl.76.6.752.
93. Stirling, M., McVerry, G. & Berryman, K. 2002. A new seismic hazard model for New Zealand, *Bulletin of the Seismological Society of America, 92*(5), 1878 – 1903. https://doi.org/10.1785/0120010156.
94. Tahir, Mohammad. 2011. Aftershock properties and its triggering mechanism. PhD Thesis, Grenoble's University, Grenoble, France, 207 p.
95. Tahir, M., Grasso, J. – R. and Amorèse, D. 2012. The largest aftershock: How strong, how far away, how delayed? *Geophysical Research Letters*, 39, L04301, 1 – 5. DOI: 10.1029/2011GL050604.
96. Therriault, A., Fowler, A. and Grieve, R. 2002. The Sudbury Igneous Complex: A differentiated impact melt sheet. Econ. Geol. 97 (7), 1521 – 1540. DOI: 10.2113/gsecongeo.97.7.1521.
97. Tsapanos, Theodoros. 1990. Spatial distribution of the difference between the magnitudes of the main shock and the largest aftershock in the circum-pacific belt, *Bulletin of the Seismological Society of America*, 80, 1180 – 1189.
98. Uhl, J., Pathak, S., Schorlemmer, D., Liu, X., Swindeman, R., Brinkman, B., LeBlanc, M., Tsekenis, G., Friedman, N., Behringers, R., Denisov, D., Schall, P., Gu, X., Wright, W., Hufnagel, T., Jennings, A., Greer, J., Liaw, P., Becker, T., Dresen, G., and Karin A. Dahmen, K. 2015. Universal quake statistics: from compressed nanocrystals to earthquakes, *Nature Scientific Reports*, 5, 16493, DOI: 10.1038/srep16493
99. Urbancic, T.I., Young, R.P., Bird, S. and Bawden, W. 1992, Microseismic source parameters and their use in characterizing rock mass behaviour: considerations from Strathcona mine. In Proceedings of 94th Annual General Meeting of the CIM: Rock Mechanics and Strata Control Sessions, Montreal, 26 – 30.
100. Utsu, Tokuji. 1961. A statistical study of the occurrence of aftershocks, *Geophysical Magazine*, 30, 521 – 605.
101. Utsu, Tokuji. 1969. Aftershock and earthquake statistics (1). Some parameters which characterize an aftershock sequence and their interactions. *Journal of the Faculty of Science, Hokkaido University Series VII (Geophysics), 3*(3), 129 – 195.
102. Utsu, Tokuji. 1970. Aftershock and earthquake statistics (2). Further investigation of aftershocks and other earthquake sequences based on a new classification of earthquake sequences, *Journal of the Faculty of Science, Hokkaido University Series VII (Geophysics), 3*(4), 197 – 266.

103. Utsu, T., Ogata, Y., and Matsu'ura, R. 1995. The centenary of the Omori formula for a decay law of aftershock activity, *Journal of Physics of the Earth*, 43, 1 – 33. DOI: http://doi.org/10.4294/jpe1952.43.1
104. Utsu, Tokuji. 2002. Statistical features of seismicity, International Handbook of Earthquake and Engineering Seismology part A, chapter 43. Eds.: W. Lee, H. Kanamori, P. Jennings and C. Kisslinger. 719 – 724.
105. Vallejos, J.A. 2010. Analysis of seismicity in mines and development of re-entry protocols, Ph.D. Thesis, Queen's University, Canada.
106. Vallejos, J.A., and McKinnon, S.D. 2008, Guidelines for development of re-entry protocols in seismically active mines, *Proceedings of the 42nd US Rock mechanics symposium, San Francisco, California, ARMA/USRMS*.
107. Vallejos, J.A., and McKinnon, S.D. 2009a, Re – entry protocols for seismically active mines using statistical analysis of aftershock sequences. Rock Engineering in Difficult Conditions, Proceedings of the 3rd CANUS Rock Mechanics Symposium, Toronto, Canada.
108. Vallejos, J. A., and McKinnon, S.D. 2009b, Scaling laws and their implications for re – entry protocol development, *The 7th International Symposum on Rockburst and Seismicity in Mines, Dalian, China*.
109. Vallejos, J.A., and McKinnon, S.D. 2010, Omori's law applied to mining-induced seismicity and re-entry protocol development, *Pure and Applied Geophysics*, 167, 91 – 106. DOI: 10.1007/s00024-009-0010-7.
110. Vallejos, J. & Estay, R. 2017. Seismic Parameters of Mining-Induced Aftershock Sequences for Re – entry Protocol, *Pure and Applied Geophysics*. DOI: https://doi.org/0.1007/s00024-017-1709-5.
111. Vere – Jones, David. 1969. A note on the statistical interpretation of Båth's law, *Bulletin of the Seismological Society of America*, 59, 1535 – 1541.
112. Villaescusa, E., Simser, B., and Carlisle, S. 2007. Stress measurements at great depth at Craig – Onaping Mines, Sudbury, Canada, Rock Engineering in Difficult Conditions, *Proceedings of the 3rd CANUS Rock Mechanics Symposium, Toronto, Canada*.
113. Wagenmakers E. – J. and Farrel, S. 2004. AIC model selection using Akaike weights. *Psychonomic Bulletin & Review*, 11 (1), 192 – 196.
114. Wang, Jeen – Hwa. 1994. On the correlation of observed Gutenberg – Richter's b value and Omori's p value for aftershocks, *Bulletin of the Seismological Society of America*, 84, 2008 – 2011.
115. Warren, N., and Latham, G. 1970. An experiment study of thermal induced microfracturing and its relation to volcanic seismicity, *Journal of Geophysical Research*, 75, 4455 – 4464. DOI: 10.1029/JB075i023p04455.
116. Wiemer, S. & Katsumata, K. 1999. Spatial variability of seismicity parameters in aftershock zones. *Journal of Geophysical Research, 104*(B6), 13135 – 13151. DOI: https://doi.org/10.1029/1999JB900032.

117. Wiemer, S., and Wyss, M. 2000. Minimum magnitude of complete reporting in earthquake catalogs: examples from Alaska, the Western United States, and Japan, *Bulletin of the Seismological Society of America*, 90, 859 – 869. DOI: 10.1785/0119990114.
118. Wiemer, S., Gerstenberger, M. and Hauksson, E. 2002. Properties of the aftershock sequence of the 1999 M_w 7,1 Hector Mine earthquake: Implications for aftershock hazard, *Bulletin of the Seismological Society of America*, 92(4), 1227 – 1240. DOI: https://doi.org/10.1029/2001JB000911.
119. Woessner, J., and Wiemer, S. 2005. Assessing the quality of earthquake catalogues: estimating the magnitude of completeness and its uncertainty, *Bulletin of the Seismological Society of America*, 95, 684 – 698. DOI: 10.1785/0120040007.
120. Yamakawa, Norio. 1968. Foreshocks, aftershocks and earthquakes swarms (IV) – Frequency decrease of aftershocks in its initial and later stages, *Papers in Meteorology and Geophysics*, 19, 109 – 119.

Appendix A - Fisher information matrix

In this section, it is developed each term of the Fisher's information matrix proposed by Ogata (1983). Each term of the matrix is defined as J_{ij}, where the pair ij corresponds to the row i and column j.

First, the integral in equation (40) is resolved by parts.

$$\int_S^T \frac{\ln(t+c)}{(t+c)^a}\,dt \tag{40}$$

$$u = \ln(t+c) \rightarrow du = \frac{dt}{t+c}$$

$$dv = \frac{dt}{(t+c)^a} \rightarrow v = \frac{1}{(1-a)(t+c)^{a-1}}$$

$$\int_S^T \frac{\ln(t+c)}{(t+c)^a}\,dt = \frac{\ln(t+c)}{(1-a)(t+c)^{a-1}}\Bigg|_S^T - \int_S^T \frac{dt}{(1-a)(t+c)^a} \tag{41}$$

$$\begin{aligned}\int_S^T \frac{\ln(t+c)}{(t+c)^a}\,dt = {} & \frac{\ln(T+c)}{(1-a)(T+c)^{a-1}} - \frac{\ln(S+c)}{(1-a)(S+c)^{a-1}} \\ & - \frac{1}{(1-a)^2}\left[\frac{1}{(T+c)^{a-1}} - \frac{1}{(S+c)^{a-1}}\right]\end{aligned} \tag{42}$$

$$\begin{aligned}\int_S^T \frac{\ln(t+c)}{(t+c)^a}\,dt = {} & \frac{1}{(1-a)(T+c)^{a-1}}\left[\ln(T+c) - \frac{1}{(1-a)}\right] \\ & - \frac{1}{(1-a)(S+c)^{a-1}}\left[\ln(S+c) - \frac{1}{(1-a)}\right]\end{aligned} \tag{43}$$

The elements of the diagonal of the Fisher's information matrix, J_{11}, J_{22} and J_{33}, were calculated as follows:

$$J_{11} = \int_S^T \frac{\mathrm{dt}}{K(t+c)^p} = \frac{1}{K}\left[\frac{(t+c)^{-p+1}}{1-p}\right]_S^T = \frac{(T+c)^{1-p} - (S+c)^{1-p}}{K(1-p)} \tag{44}$$

$$J_{22} = \int_S^T \frac{\mathrm{K}p^2 \mathrm{dt}}{(t+c)^{p+2}} = \mathrm{K}p^2 \left[-\frac{(t+c)^{-p-1}}{p+1} \right]_S^T = \frac{\mathrm{K}p^2}{p+1} \left[-(T+c)^{-p-1} + (S+c)^{-p-1} \right] \tag{45}$$

$$J_{33} = K \int_S^T \frac{\{\ln(t+c)\}^2}{(t+c)^p} dt \tag{46}$$

$$u = \{\ln(t+c)\}^2 \rightarrow du = \frac{2\ln(t+c)\, dt}{t+c}$$
$$dv = \frac{dt}{(t+c)^p} \rightarrow v = \frac{1}{(1-p)(t+c)^{p-1}}$$

$$K \int_S^T \frac{\{\ln(t+c)\}^2}{(t+c)^p} dt = K \left\{ \left[\frac{\{\ln(t+c)\}^2}{(1-p)(t+c)^{p-1}} \right]_S^T - \frac{2}{(1-p)} \int_S^T \frac{\ln(t+c)}{(t+c)^p} dt \right\} \tag{47}$$

$$= K \left\{ \frac{\{\ln(T+c)\}^2}{(1-p)(T+c)^{p-1}} - \frac{\{\ln(S+c)\}^2}{(1-p)(S+c)^{p-1}} - \frac{2}{(1-p)} \left[\frac{1}{(1-p)} \left\{ \frac{\ln(T+c)-1}{(T+c)^{p-1}} - \frac{\ln(S+c)-1}{(S+c)^{p-1}} \right\} \right] \right\} \tag{48}$$

$$J_{33} = K \left\{ \frac{1}{(1-p)} \left[\frac{\{\ln(T+c)\}^2}{(T+c)^{p-1}} - \frac{\{\ln(S+c)\}^2}{(S+c)^{p-1}} \right] - \frac{2}{(1-p)^2} \left\{ \frac{1}{(T+c)^{p-1}} \left[\ln(T+c) - \frac{1}{1-p} \right] - \frac{1}{(S+c)^{p-1}} \left[\ln(S+c) - \frac{1}{1-p} \right] \right\} \right\} \tag{49}$$

Equations (50), (52) and (55) show the results of the rest of the elements of the matrix:

$$J_{12} = J_{21} = -p \int_S^T \frac{\mathrm{dt}}{(t+c)^{p+1}} = \left[(t+c)^{-p} \right]_S^T = (T+c)^{-p} - (S+c)^{-p} \tag{50}$$

$$J_{13} = J_{31} = -\int_{S}^{T} \frac{\ln(t+c)}{(t+c)^{p}}\,dt \tag{51}$$

$$J_{13} = \frac{1}{(p-1)(T+c)^{p-1}}\left[\ln(T+c) - \frac{1}{(1-p)}\right] - \frac{1}{(p-1)(S+c)^{p-1}}\left[\ln(S+c) - \frac{1}{(1-p)}\right] \tag{52}$$

$$J_{23} = J_{32} = Kp\int_{S}^{T} \frac{\ln(t+c)}{(t+c)^{p+1}}\,dt \tag{53}$$

$$J_{23} = Kp\left\{-\frac{1}{p(T+c)^{p}}\left[\ln(T+c) + \frac{1}{p}\right] + \frac{1}{p(S+c)^{p}}\left[\ln(S+c) + \frac{1}{p}\right]\right\} \tag{54}$$

$$J_{23} = -\frac{K}{(T+c)^{p}}\left[\ln(T+c) + \frac{1}{p}\right] + \frac{K}{(S+c)^{p}}\left[\ln(S+c) + \frac{1}{p}\right] \tag{55}$$

Appendix B – Clustered seismicity per sequence

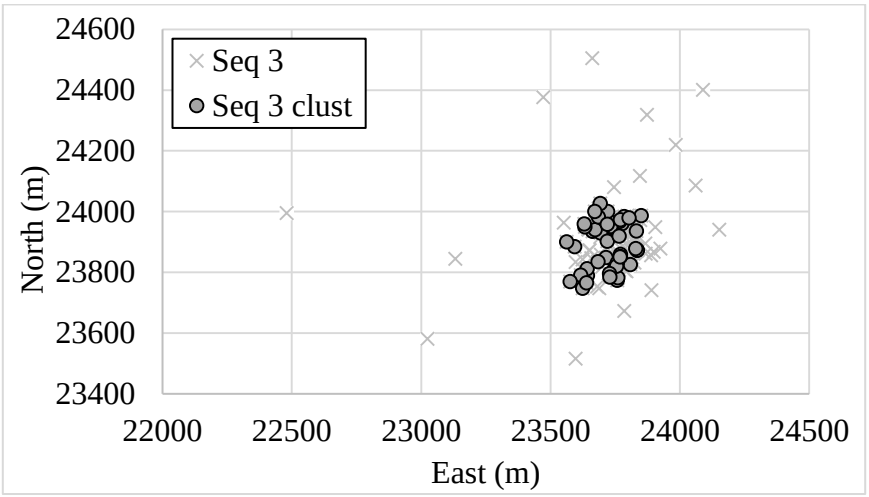

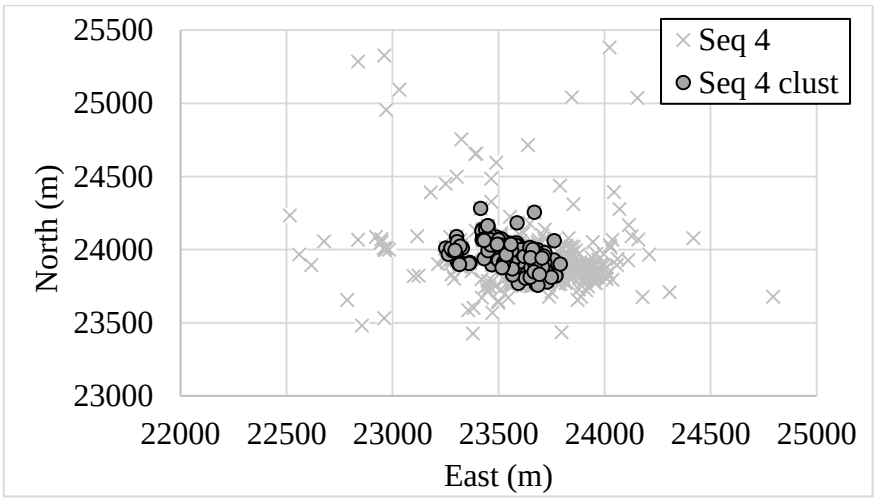

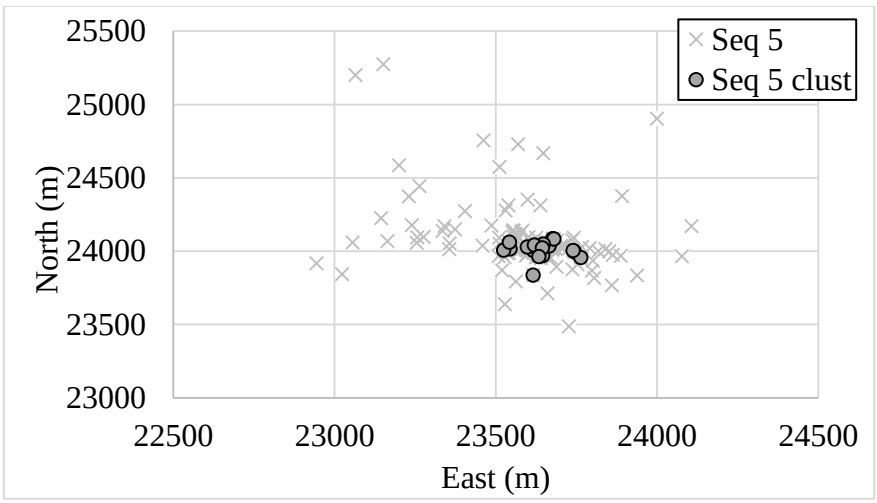

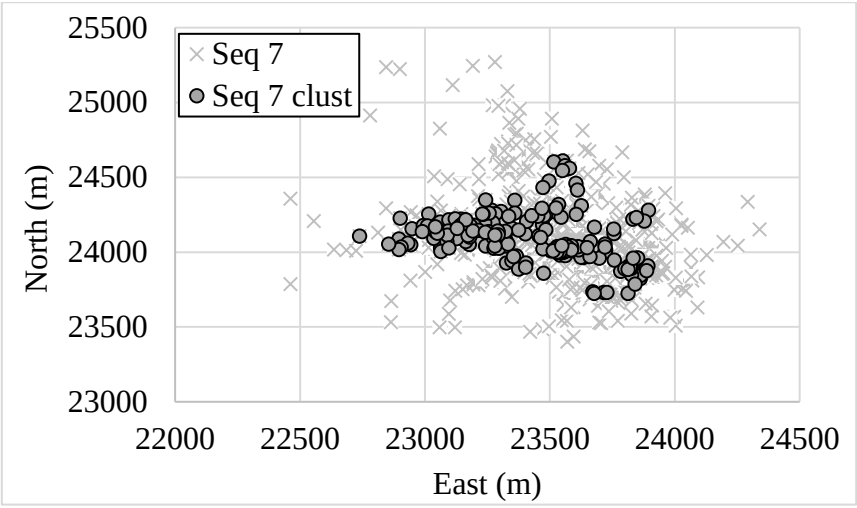
Seq 7
Seq 7 clust
North (m)
East (m)
25500
25000
24500
24000
23500
23000
22000
22500
23000
23500
24000
24500

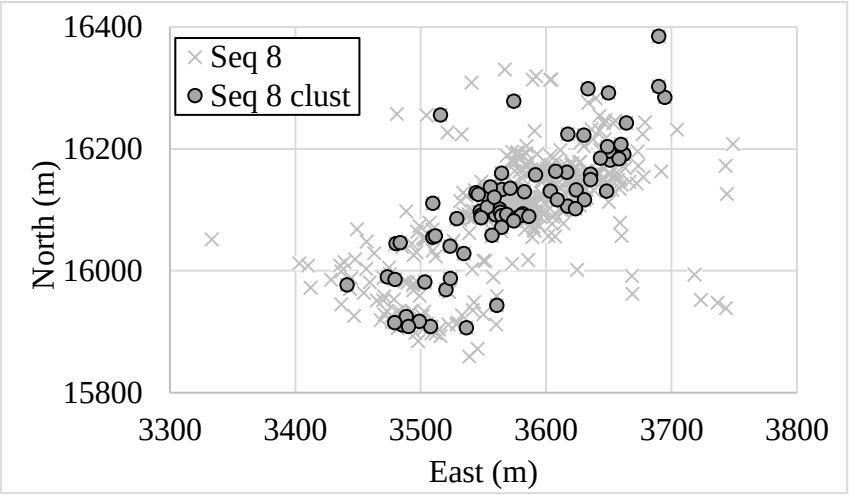
Seq 8
Seq 8 clust
North (m)
East (m)
16400
16200
16000
15800
3300
3400
3500
3600
3700
3800

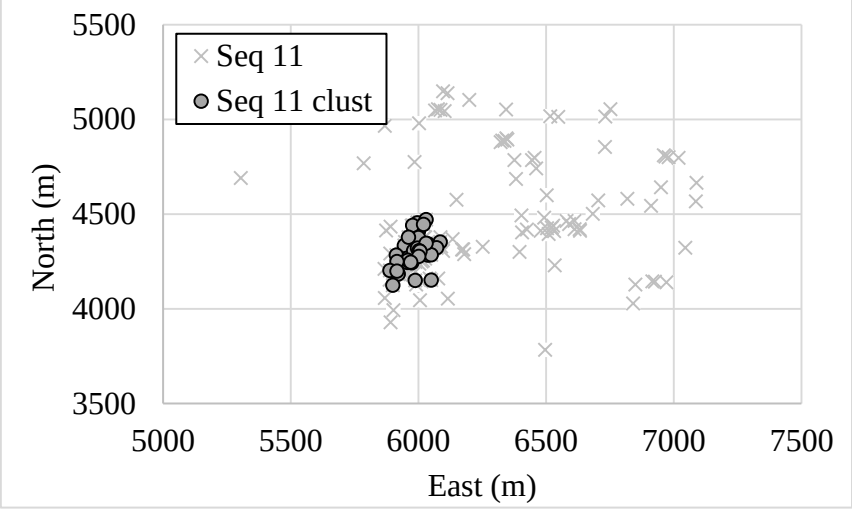
Seq 11
Seq 11 clust
North (m)
East (m)
5500
5000
4500
4000
3500
5000
5500
6000
6500
7000
7500

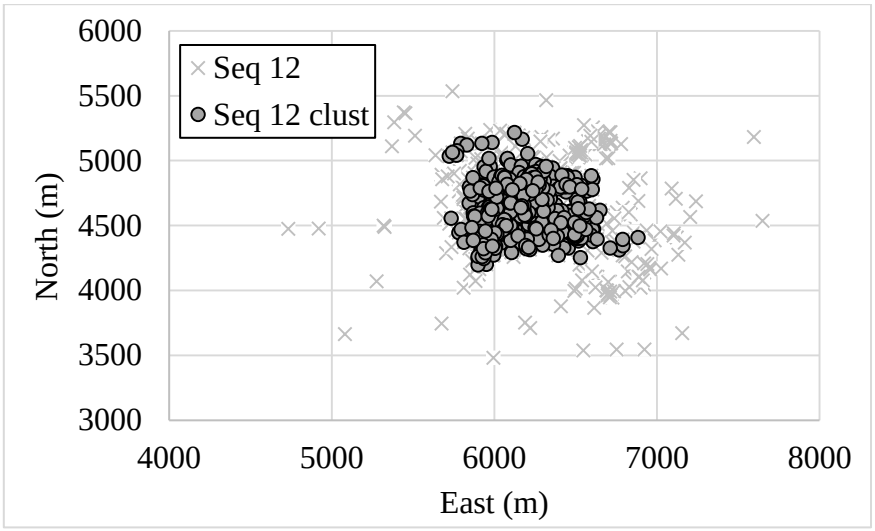
Seq 12
Seq 12 clust
North (m)
East (m)
6000
5500
5000
4500
4000
3500
3000
4000
5000
6000
7000
8000

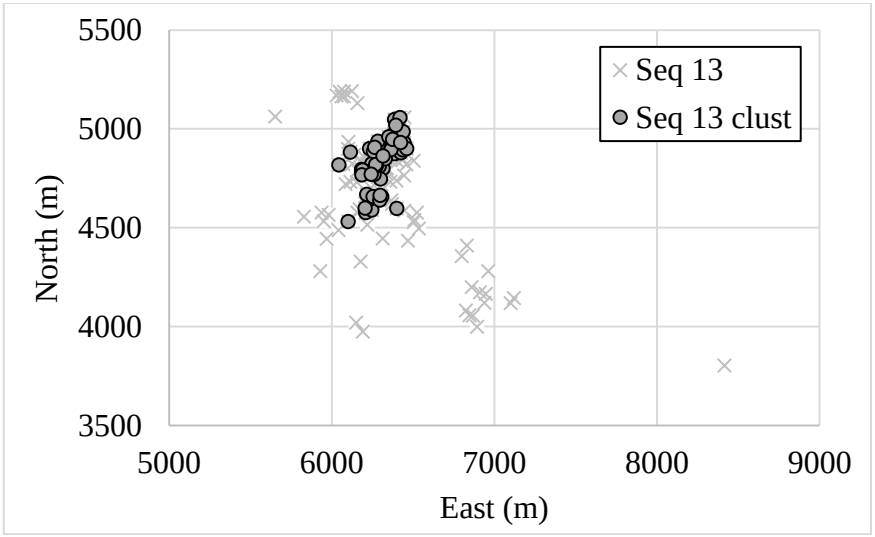
Seq 13
Seq 13 clust
North (m)
East (m)
5500
5000
4500
4000
3500
5000
6000
7000
8000
9000

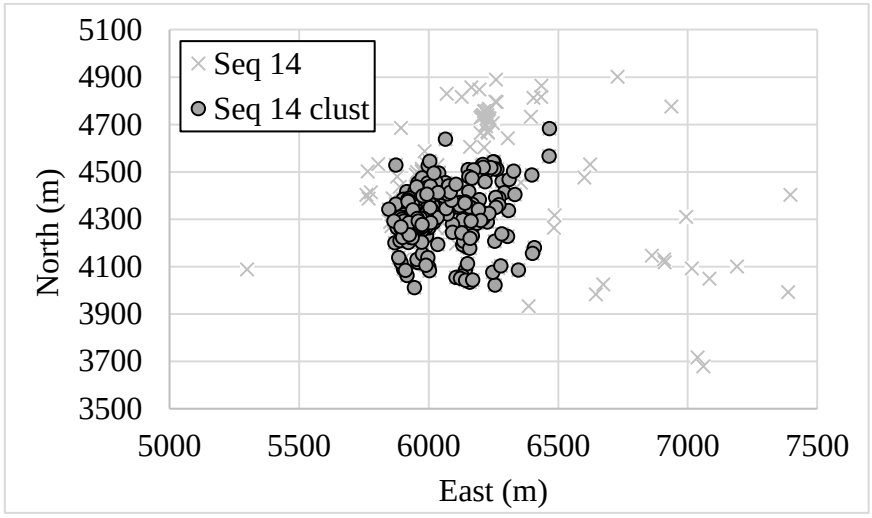
Seq 14
Seq 14 clust
North (m)
East (m)
5100
4900
4700
4500
4300
4100
3900
3700
3500
5000
5500
6000
6500
7000
7500

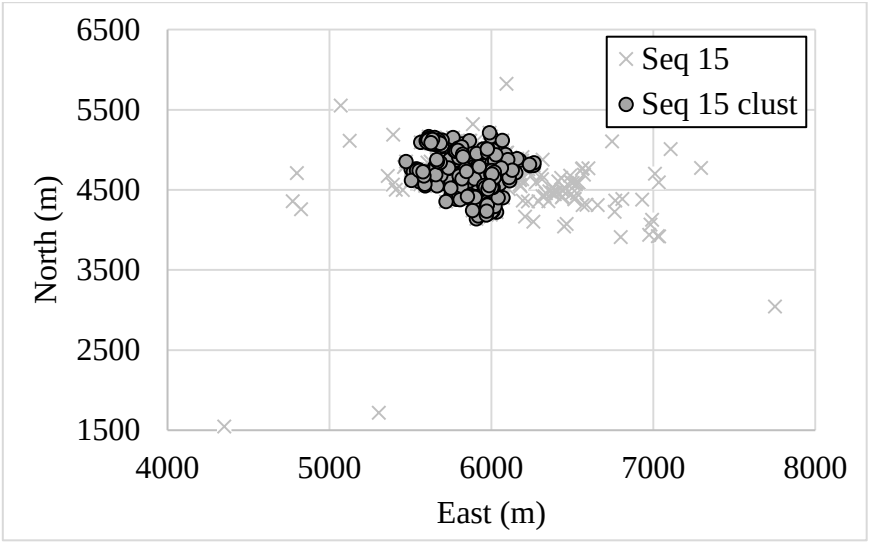
6500
5500
4500
3500
2500
1500
North (m)
4000
5000
6000
7000
8000
East (m)
Seq 15
Seq 15 clust

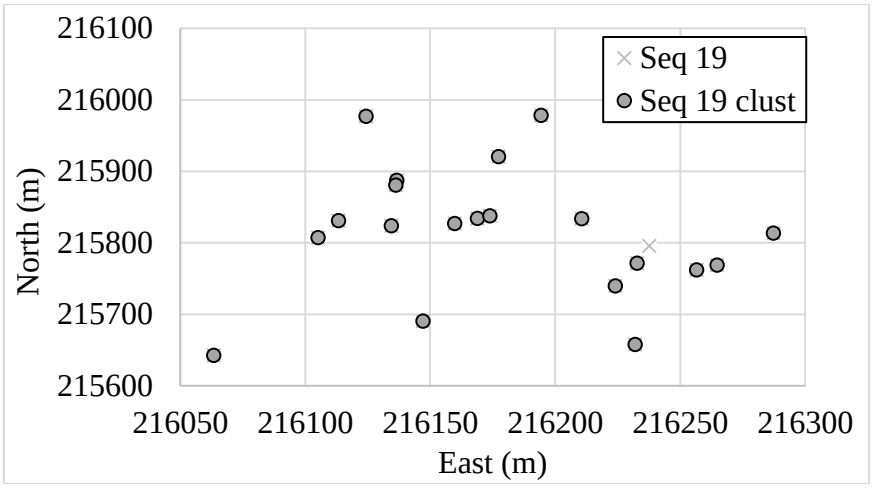
216100
216000
215900
215800
215700
215600
North (m)
216050
216100
216150
216200
216250
216300
East (m)
Seq 19
Seq 19 clust

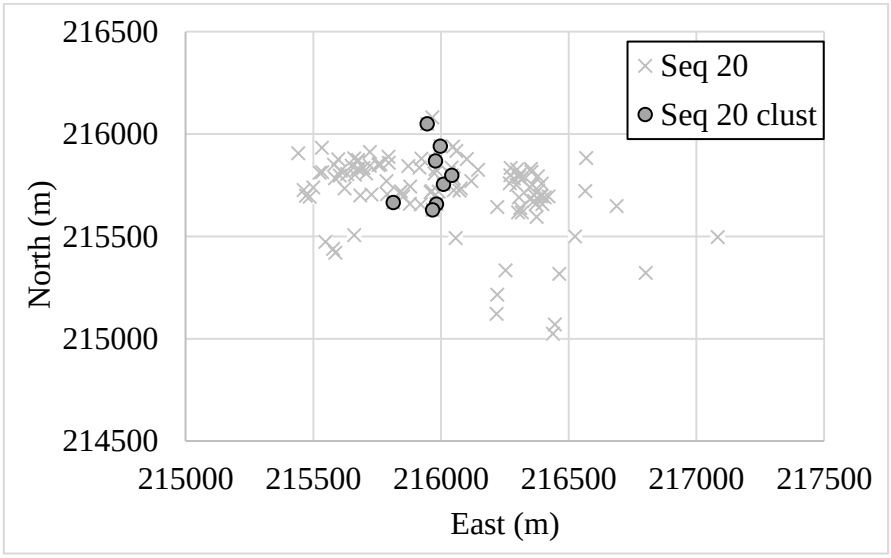
216500
216000
215500
215000
214500
North (m)
215000
215500
216000
216500
217000
217500
East (m)
Seq 20
Seq 20 clust

Appendix C – Error propagation

The general rule for the error propagation is defined by:

$$\Delta f(x,y,z) = \left|\frac{\partial f}{\partial x}\right| \Delta x + \left|\frac{\partial f}{\partial y}\right| \Delta y + \left|\frac{\partial f}{\partial z}\right| \Delta z. \quad (56)$$

Considering that, for the different mathematical operations, the total errors are calculated as follow:

- Addition/Substraction

Assume the function $f = a + b + \ldots + c - x - y - \ldots - z$, each value with its respective measurement of the error, Δa, Δb, etc.:

$$\Delta f = \Delta a + \Delta b + \cdots + \Delta c + \Delta x + \Delta y + \cdots + \Delta z. \quad (57)$$

- Multiplication/Quotient

Assume the function $f = \frac{a \times b \times \ldots \times c}{x \times y \times \ldots \times z}$, each value with its respective measurement of the error Δa, Δb, etc.:

$$\frac{\Delta f}{|f|} = \frac{\Delta a}{|a|} + \frac{\Delta b}{|b|} + \cdots + \frac{\Delta c}{|c|} + \frac{\Delta x}{|x|} + \frac{\Delta y}{|y|} + \cdots + \frac{\Delta z}{|z|}. \quad (58)$$

- Power function

Considering the function $f = x^n$:

$$\frac{\Delta f}{f} = |n| \frac{\Delta x}{|x|}. \quad (59)$$

- Logarithm

Considering the function $f = ln(x)$:

$$\Delta f = \frac{\Delta x}{|x|}. \quad (60)$$

- Exponential

Considering the function $f = exp(x)$

$$\frac{\Delta f}{f} = \Delta x. \quad (61)$$

Despite the above, if the original uncertainties associated with the measurement quantities are independent and random, these rule swill produce values of uncertainty that are unnecessarily large.

If the errors in measurement are normal distributed and that measured quantities are independent of each other, the method called *adding in quadrature*, provides the following rules for computing uncertainty in *f*, for addition/subtraction (equation (62)) and for multiplication/quotient (equation (63)):

$$\Delta f = \sqrt{(\Delta a)^2 + (\Delta b)^2 + \cdots + (\Delta c)^2 + (\Delta x)^2 + (\Delta y)^2 + \cdots + (\Delta z)^2} \tag{62}$$

$$\frac{\Delta f}{f} = \sqrt{\left(\frac{\Delta a}{|a|}\right)^2 + \left(\frac{\Delta b}{|b|}\right)^2 + \cdots + \left(\frac{\Delta c}{|c|}\right)^2 + \left(\frac{\Delta x}{|x|}\right)^2 + \left(\frac{\Delta y}{|y|}\right)^2 + \cdots + \left(\frac{\Delta z}{|z|}\right)^2} \tag{63}$$

C.1. T_{MC} estimation error propagation

The error associated a T_{MC}, can be estimated, following this procedure. Equation (18) can be written as:

$$T_{MC} = exp\left\{\frac{1}{1+p} ln\left(Kp\sqrt{\frac{2p+1}{p+2}}\right)\right\} - c. \tag{64}$$

Expanding the natural logarithm, equation (64) is rewritten as:

$$T_{MC} = exp\left\{\frac{1}{1+p}[ln(K) + \ln(p) + 0.5\ln(2p+1) - 0.5\ln(p+2)]\right\} - c. \tag{65}$$

For shorten written, considering the argument of the exponential function as the symbol %. Then, it is calculated each partial derivative:

$$\frac{\partial T_{MC}}{\partial c} = -1, \tag{66}$$

$$\frac{\partial T_{MC}}{\partial K} = \exp\{\%\}\frac{1}{1+p}\frac{1}{K}, \tag{67}$$

$$\frac{\partial T_{MC}}{\partial p} = \exp\{\%\}ABCD \tag{68}$$

where:

$$A = \frac{\partial}{\partial p}\left(\frac{lnK}{1+p}\right) = -\frac{lnK}{(1+p)^2}, \tag{69}$$

$$B = \frac{\partial}{\partial p}\left(\frac{\ln(p)}{1+p}\right) = \frac{1/p(1+p) - \ln(p)}{(1+p)^2} = \frac{(1+p) - p\ln(p)}{p(1+p)^2}, \tag{70}$$

$$C = \frac{\partial}{\partial p}\left(\frac{\ln(2p+1)}{2(1+p)}\right) = \frac{{}^{2}/_{2(p+1)}{}^{2(1+p)-2\ln(2p+1)}}{4(1+p)^2} = \frac{2(1+p)-(2p+1)\ln(2p+1)}{2(2p+1)(1+p)^2}, \tag{71}$$

$$D = \frac{\partial}{\partial p}\left(\frac{\ln(p+2)}{2(1+p)}\right) = \frac{{}^{1}/_{(p+2)}\,2(1+p)-2\ln(p+2)}{4(1+p)^2} = \frac{(1+p)-(p+2)\ln(p+2)}{2(p+2)(1+p)^2}. \tag{72}$$

Finally, the total error of T_{MC} is:

$$dT_{MC} = \frac{\partial T_{MC}}{\partial c}dc + \frac{\partial T_{MC}}{\partial K}dK + \frac{\partial T_{MC}}{\partial p}dp. \tag{73}$$